Engineering | Lancaster University

Design of the High Luminosity Large Hadron Collider Crab Cavity Support System

MSc by Research

Lancaster University Engineering Department

Author: Thomas Joseph Jones BEng CEng MIMechE

Awarding University: Lancaster University

Thesis Submission Date: March 2020

Supervisor: Prof. Graeme Burt (Lancaster University)

Science & Technology Facilities Council

CERN

Lancaster University

Faculty of Science and Technology

Engineering Department

Signed Declaration on the submission of a thesis

I declare that this project/thesis is my own work and has not been submitted in substantially the same form towards the award of a degree or other qualification.
Acknowledgement is made in the text of assistance received and all major sources of information are properly referenced. I confirm that I have read and understood the publication *Guidance on Writing Technical Reports* published by the Department.

I would like to thank my supervisor Professor Graeme Burt for his guidance and advice.

Signed   ……Thomas Jones……………………………………………………..

Date   ………March 2020………………………………………………….

Abstract

Title: Design of the High Luminosity Large Hadron Collider Crab Cavity Support System

Degree Award: MSc by Research

Author: Thomas Joseph Jones BEng CEng MIMechE

Thesis Submission Date: March 2020

This thesis describes the development of the High Luminosity Large Hadron Collider (HL-LHC) Crab Cavity Support System, including a preliminary options study, conceptual design and analysis, leading to the detailed design, testing and operation of the complete system.

Superconducting Crab Cavities are an essential part of the High Luminosity upgrade of the Large Hadron Collider at CERN. The cavities are used to rotate bunches of hadrons (Protons or Lead ions) prior to collision in order to reduce their crossing angle. This provides a higher probability of individual hadron-hadron interaction which leads to increased scientific output of the machine. The cavities function at 2 Kelvin, and therefore require a controlled cryogenic environment in which to operate. The cavities are powered by radio waves (RF), and the operating RF frequency is controlled by a mechanical tuner. The complete suite of components required for operational cavities is known as a Cryomodule. A critical aspect of cavity performance is how they are supported within the cryomodule. Correct design of these support structures ensures the cavities are aligned to the rest of the machine and that they operate at the RF frequency expected. The structures are required to be as stiff as possible whilst minimising 'heat leak' from the outside world at 300 Kelvin to the cavities operating at 2 Kelvin. The support system also needs to allow the cavities to contract as they cool, such that stress is minimised to acceptable levels within each sub-system of the cryomodule. The unique form of the Crab Cavities for LHC together with constraints from the RF input coupler required a novel cavity support system to be developed. The new concept of a cavity 'Blade' support produced by the author, in addition to the author's work on design optimisation of the cavity tuning device, contributed significantly to the success of the Prototype DQW Cryomodule. This was tested with beam on the Super Proton Synchrotron, achieving the world's first crabbing of a proton bunch.

Contents

i. List of Figures

ii. List of Tables

1. Introduction

1.1. CERN

"CERN, the European Organisation for Nuclear Research, operates the world's leading laboratory for particle physics" (CERN, 2016a). CERN is an acronym for the "Conseil Européen pour la Recherche Nucléaire" which was "a provisional body founded in 1952 with the mandate of establishing a world-class fundamental physics research organisation in Europe." (CERN, 2017a). The mission of CERN is to answer fundamental questions about the Universe and it uses "the world's largest and most complex scientific instruments to study the basic constituents of matter – the fundamental particles." (CERN, 2017a). CERN has an annual budget of approximately 1100Million CHF (CERN, 2017b). This is comprised of contributions from 22 full member states, of which the UK provides approximately 170Million CHF (CERN, 2017c) per year. This funding is used to support a broad range of particle physics experiments. One of the earliest accelerators built at CERN was the Proton Synchrotron, the PS, which first accelerated protons on 24th November 1959. This machine is still operational today and is one of the earliest stages of acceleration feeding the flagship experiment at CERN, the Large Hadron Collider (see Figure 1).
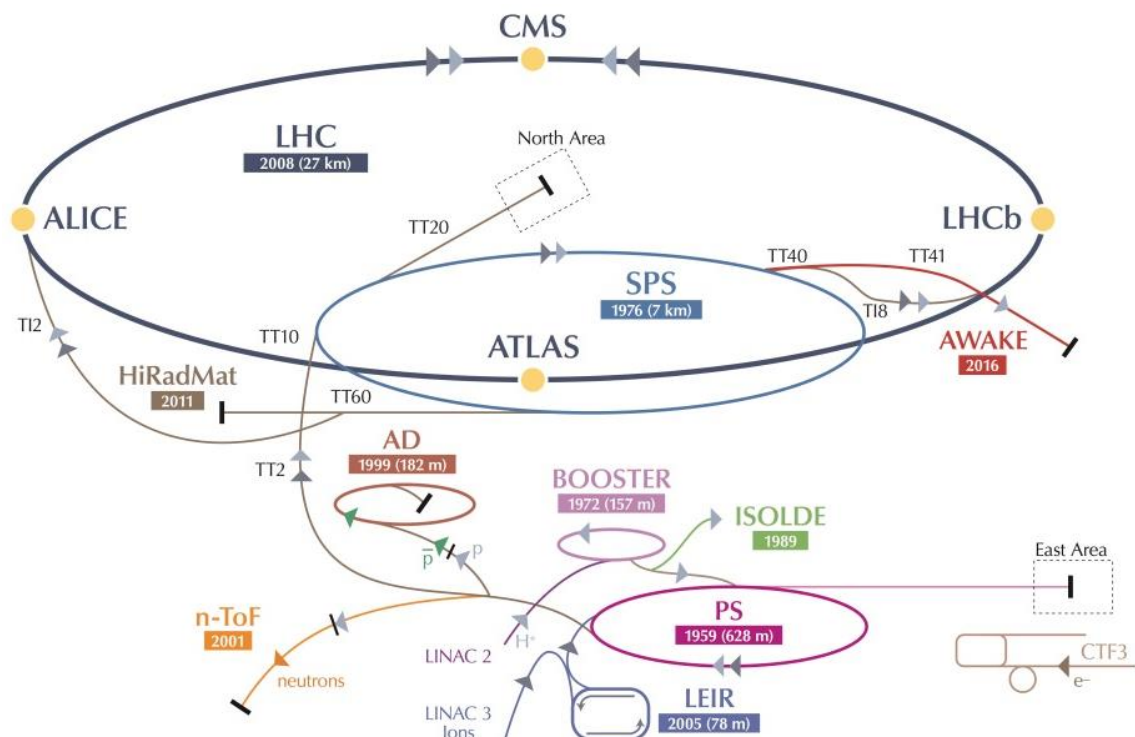
Figure 1. Accelerator Complex at CERN (CERN, 2017d)

1.2. The Large Hadron Collider

The LHC is the largest and most powerful particle accelerator ever built, with a circumference of 27km and currently running at 13TeV (Table 1), with a design energy of 14TeV. It is also the largest vacuum system ever built, with 2 beams being accelerated adjacent to each other making the total length of the vacuum system 54km. The 2 beams can be comprised of protons or Lead ions. These are accelerated through a complex of accelerator systems prior to reaching the LHC as can be observed in Figure 1. The 2 accelerated beams are collided in several locations about the circumference of the machine where there are large and complex detectors designed to find any generated particles. The LHC aims to answer the following questions (CERN, 2017d);

- What is the origin of mass? In July 2012 this question was answered, with the LHC providing the evidence to prove the existence of the Higgs Boson, leading to a Nobel prize for François Englert and Peter W. Higgs.
- Will we discover evidence for supersymmetry?
- What are dark matter and dark energy?
- Why is there far more matter than antimatter in the universe?
- How does the quark-gluon plasma give rise to the particles that constitute the matter of our Universe?
- Plus the capability to provide more knowledge of particles we are already aware of.

Table 1. LHC Run 2 Parameters (CERN, 2017d)

Circumference	26 659 m
Dipole operating temperature	1.9 K (-271.3°C)
Number of magnets	9593
Number of main dipoles	1232
Number of main quadrupoles	392
Number of RF cavities	8 per beam
Nominal energy, protons	6.5 TeV
Nominal energy, ions	2.56 TeV/u (energy per nucleon)
Nominal energy, protons collisions	13 TeV
No. of bunches per proton beam	2808
No. of protons per bunch (at start)	1.2 x 1011

Number of turns per second	11245
Number of collisions per second	1 billion
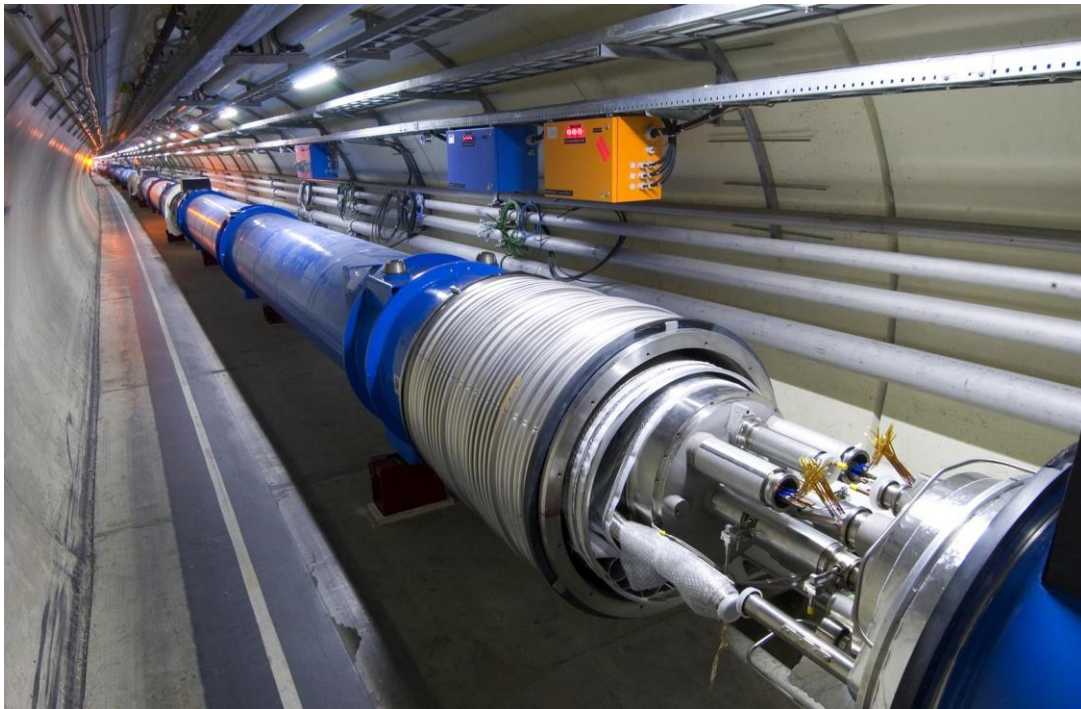
Figure 2. LHC Tunnel

The LHC uses superconducting magnets and Radio Frequency wave (RF) powered systems. For the electrical conductors to have negligible resistance these devices operate at temperatures as low as 1.9K (-271.25°C). Without superconductivity the LHC ring would have needed to be even larger, as an 8.3 Tesla magnetic field is required in the Dipoles to contain the 7TeV beams within the 8.6km diameter tunnel. Achieving such high fields could only be realised through the use of superconductivity. At the time of the initial LHC planning, achieving these high gradients was only demonstrated on a small scale, and certainly not over the length of that required for an LHC style module (10m+). The LHC was a significant driving factor in the development and innovation of superconducting technology which has many benefits outside particle physics, for example in medical applications with MRI scanners and Liquid Natural Gas storage (Cryogenic Society of America, 2018). The magnet and RF systems are cooled using large re-circulating liquid helium plants. The blue tanks that are common in photographs of the LHC are in fact insulating vacuum vessels, required to keep the magnets at their operational temperature. Along with all the internal

components this device is known as a cryostat, these vary in length in the machine up to 12m. In Figure 2 one can see an intersection of the machine where two cryostats meet. Surrounding the intersection is a large outer bellows (which is slid back in the photograph), and within this are interconnects for the current leads and beam vacuum chambers. A combination of design error and quality assurance of the electrical joints led to an explosion in 2008 (CERN, 2008), which contaminated a significant portion of the machine and led to over 1 years downtime of the machine. This highlights the need for a robust design and thorough testing of every component, sub-system and system in the machine. In addition to the current leads are the beam vacuum vessels with both beam vacuum vessels passing through each magnet. Within the vacuum vessel is a beam screen, designed to shield the cold magnets from heat generated by the beam. The cryostats are in a tunnel ~100m below ground. They are installed via large ~20m diameter vertical bore holes at various locations about the 27km circumference of the machine.

Dipole magnets in the machine are used to steer the beam, whereas quadrupole magnets are used to focus the beam. The beams are made up of bunches of ions with the same charge, therefore they want to spread out or 'blow-up', hence the need for the high levels of magnetic field to focus them. In the case of Proton-Proton collisions, at the interaction point these bunches are focused to a 16µm x 16µm section, and each bunch contains 1.15×10^{11} protons (CERN, 2010). The bunches travel in straight lines tangent to the two final arcs, therefore they collide at an angle, θ_c, known as the Collision Angle. The larger this angle the lower the probability of Proton-Proton interactions. With the current beam properties of the LHC the probability of any two protons colliding is $\sim 4 \times 10^{-21}$. However, with 1.15×10^{11} protons per bunch the number of effective interactions per bunch is predicted to be ~20 (CERN, 2010) . The average number of bunches per beam is 2808, and the number of beam rotations per second is 11245, therefore there are 32 million bunch crosses every second. With 20 interactions per bunch this gives 600 million collisions per second. As one can imagine, the data produced by the LHC is huge, and there is supercomputing distributed around the world dedicated to post-processing the 25GB/s data coming from the machine (CERN, 2017e). Luminosity is a measurement of the number of potential collisions in the machine per cross sectional area of the bunch and per second. Luminosity is therefore proportional to the rate of the collisions in the machine.
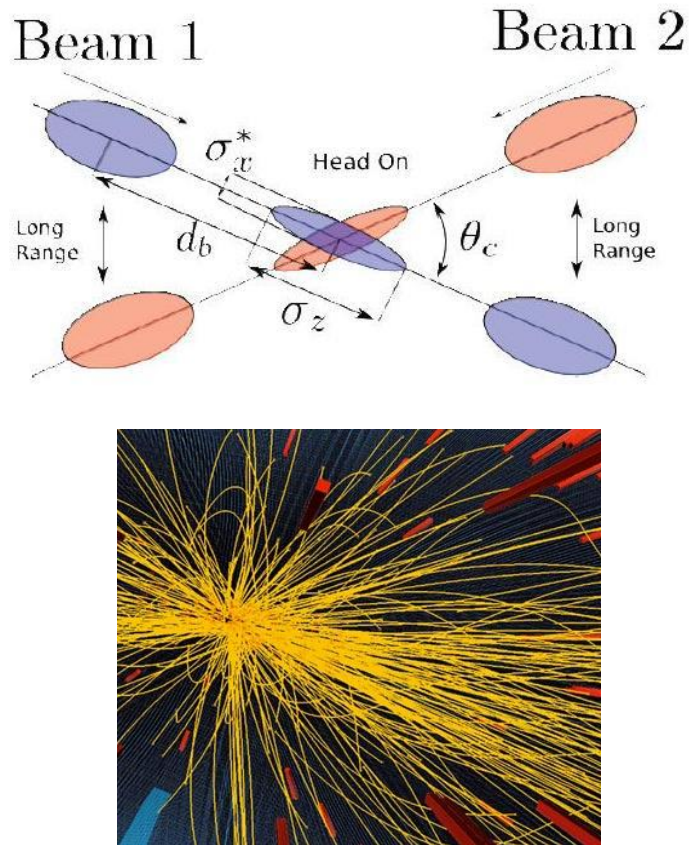
Figure 3. LHC Collision Angle (left) A 7 TeV Proton-Proton Collision Yielding 100 charged particles (Right) (CERN, 2010)

1.3. The High Luminosity Upgrade Project

"The full exploitation of the LHC is the highest priority in the European Strategy for Particle Physics, adopted by the CERN Council and integrated into the ESFRI Roadmap. The HL-LHC project funding was approved by the CERN Council in June 2014." (CERN, 2016b). The schedule for HL-LHC is shown in Figure 4. The aim of the High Luminosity upgrade to the LHC, or HL-LHC, is to increase the machine luminosity by a factor of 10 over the original design value. There are several activities to be performed in parallel in order to achieve this aim, including;

- Improvements and optimisation of the collision angle – This will be achieved predominantly by SRF Crab Cavities which can rotate the Proton bunches and therefore decrease the effective crossing angle. For the shorter bunch lengths of HL-LHC crabbing becomes a critical aspect of machine operation to ensure overlap of the beams. Also involved in this work package is computational simulation of the interaction region, to identify how best to exploit the crab cavities (Brett, 2014).

- Upgrades to the injector system – As discussed previously, parts of the injector chain date back to the 1950's, therefore, upgrades are required to improve and ensure reliability of these machines (Coupard, 2016).

- A tighter focus and steering of the beam – Cutting edge technology now allows higher strength 11 Tesla magnets, allowing better steering and focusing of the beam (Willering, 2019).

- Increasing the number of bunches in the beam at any one time – This is currently limited by secondary electron emission, an effect whereby an electron cloud is liberated from the LHC beam screens (primary electrons) by the accelerated ions and when passing through a dipole field the liberated electrons collide back into the beam screen walls, which then produces even more electrons, known as secondary electrons. The electron cloud has a detrimental effect on the ion beam and the collisions back into the beam screen increase the heat load on the cryogenic system. Clearly if more secondary electrons are generated there is also an avalanche type effect in the machine. It is therefore imperative to reduce the Secondary Electron Yield, SEY to <1. The SEY is the rate of secondary electron produced per primary electron. There are 2 methods being investigated to achieve this; Carbon Coating (Vallgren, 2011) and Laser Engineered Surface Structures (Sitko, 2018).

- Upgraded diagnostics – The beam loss monitors will be upgraded to allow safe and reliable operation at higher luminosity. The Beam Position Monitors will also be upgraded to allow significant improvements on beam profiling. (Jones R. , 2015)

- Upgraded detectors and computer systems to handle the increased data – The increased luminosity will lead to even more data generated. Current predictions are that a total of ~400Pb of data will have been stored by the end of Run 4 (Krzewicki, 2014).

- Novel methods of cold powering the magnets - In its present configuration, current is supplied to the LHC magnets at room temperature from the surface, with local power converters and cryostats located in the accelerator tunnel used to achieve the required supply. It would be beneficial to remove the need for the local services, to prevent radiation damage, allow ease of maintenance and to create space in the LHC tunnel. To achieve this, novel high temperature superconducting links are required to transfer the current over relatively long distances, with cable lengths up to 500m (Ballarino, 2014).
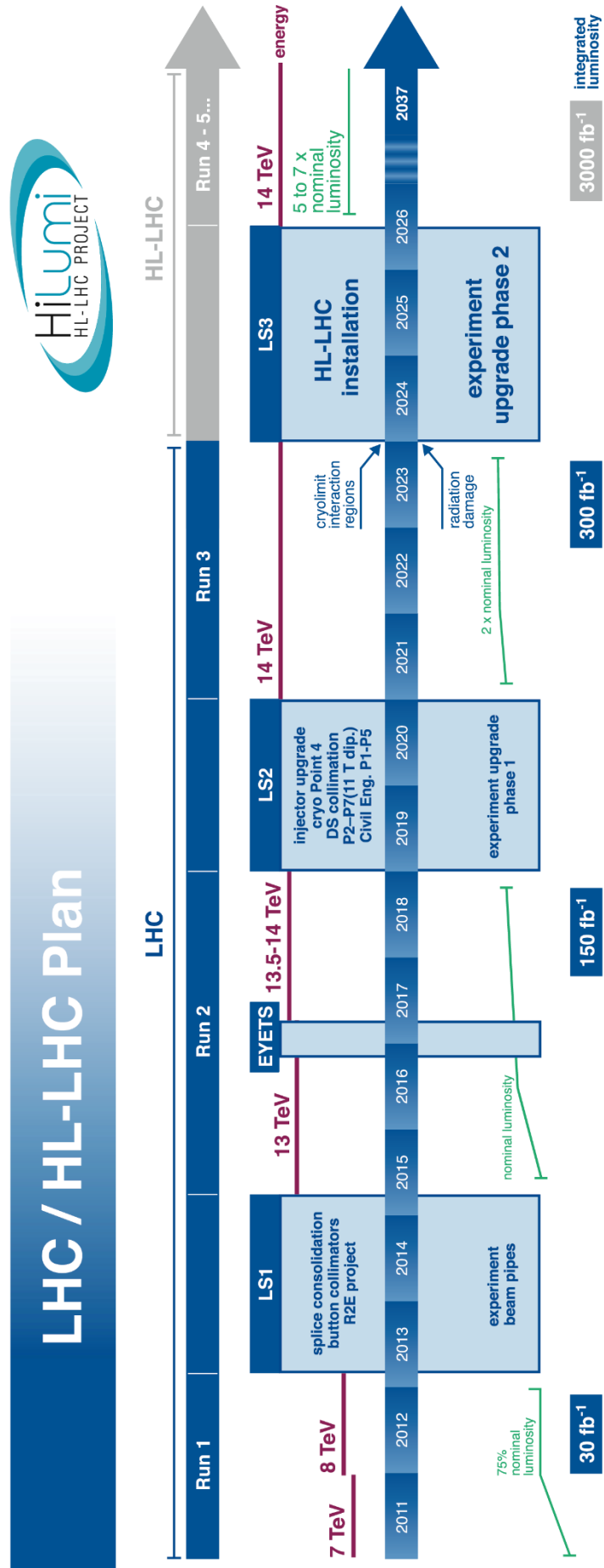
Figure 4. HL-LHC Schedule (CERN, 2016b)

1.4. SRF Compact Crab Cavities

These cavities rotate or 'crab' the beam, hence the name Crab Cavities. This rotation can be used to effectively reduce the crossing angle to zero as can be observed in Figure 5. They are compact as they need to fit into the space between the vacuum beam pipes in the LHC which is 194mm (Verdú-Andrés S. , 2013). Without this restriction the cavity geometry could have been a large but comparably simple elliptical cavity, however, this spatial constraint requires the complex geometry of the Compact Crab Cavities. The cavities run a continuous wave (CW) configuration, as opposed to a pulsed configuration. The required RF deflecting mode frequency is 400.8 MHz and the minimum required deflecting voltage is 3.4MV (CERN, 2018a). The power required to drive the cavity must be within the capabilities of the RF power amplifiers which can provide 40kW to 80kW, therefore to achieve the duty cycle and deflecting voltage the cavity must be made superconducting, with a surface resistance <20nΩ (Xiao, 2013). Therefore these crab cavities are made from high-purity Niobium, which is cooled to ~2K.
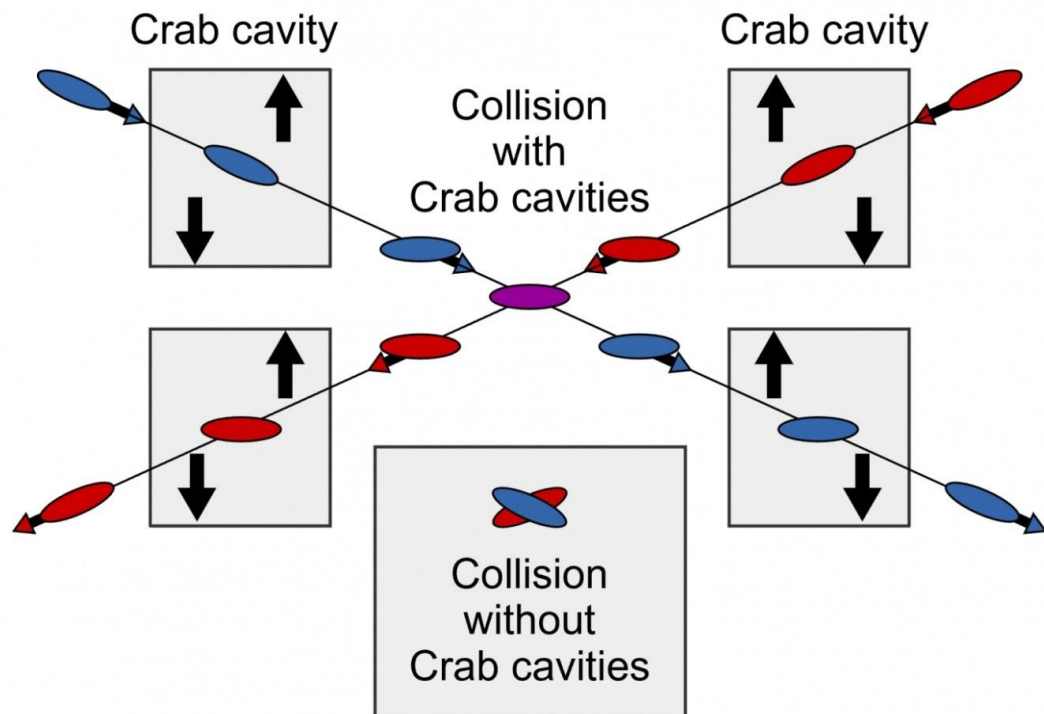
Figure 5. Crab Cavity crossing angle (Raynova, 2017)

There are currently 2 crab cavity designs envisaged for the HL-LHC upgrade. These are the Double Quarter Wave Resonator (DQW) and the RF Dipole (RFD), the designs for which are shown in Figure 6. The design of the DQW RF structure has been led by Brookhaven National Laboratory, the RFD by Old Dominion University. Each cavity type has a different deflecting plane, the DQW rotates bunches vertically, whereas the RFD deflects bunches horizontally. The performance requirements of the cavities are shown in Table 2. As crabbing of a proton beam has never previous been demonstrated, testing on a similar high power proton machine was required before the technology would be accepted for use within the LHC. The Super Proton Synchrotron (SPS) as CERN was selected as the test bed, in a location where the cavities could be moved in and out of the beam dependant on the operational scenario of the SPS, i.e. when the SPS was in use as an injector to the LHC, the crab cavities would be moved out of the beam.
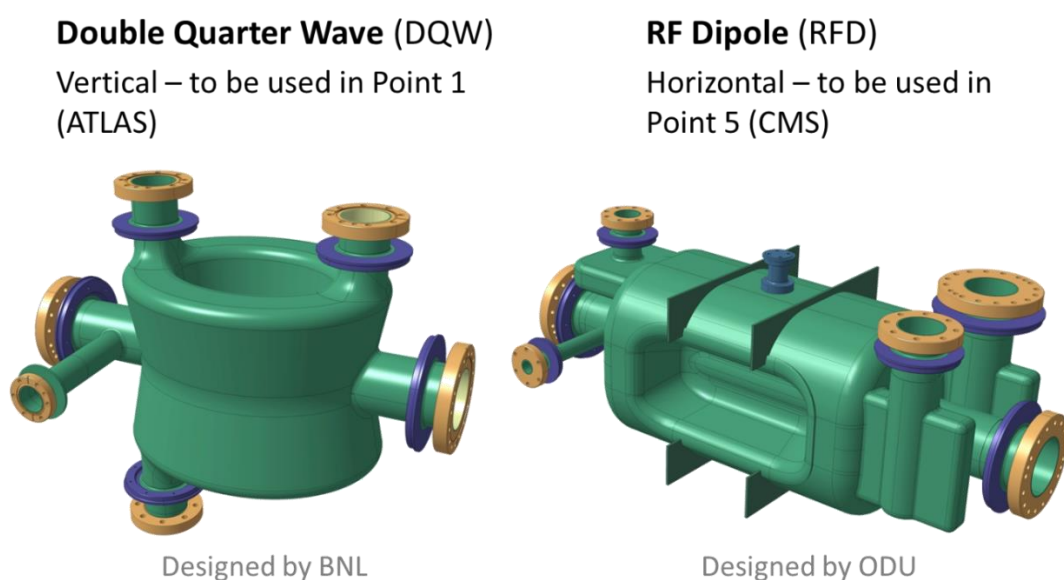
Figure 6. SRF Compact Crab Cavity Designs for HL-LHC

Table 2. Crab Cavity RF and Performance Requirements (CERN, 2018a)

RF and Performance Requirements	Units	DQW	RFD
F (Resonant Frequency at 2 K) [1]	MHz	400.79 ± 0.15	
Elastic tuning range	kHz	± 150	± 150
VT (Deflecting Voltage)[2] at 2 K	MV	≥ 4.1	
P_{dyn} (Dynamic Heat Load per cavity at 2 K and 4.1 MV) [1, 3]	W	≤ 10	

RF and Performance Requirements	Units	DQW	RFD
LFD (Lorentz Force Detuning Coefficient)	Hz/MV2	< 400	≤ 865
dF/dp (Sensitivity to LHe pressure fluctuations)	Hz/mbar	≤ 300	
Pole Symmetry (Electrical Centre deviation)	mm	≤ 0.8 [7]	
Field Non-linearity (b_3) [4, 5]		< 1500 (TBC[6])	
Q_{ext}	-	$5 \cdot 10^5$	
RF Power	kW - CW	40 (80 peak)	
Beam Clearance	mm	84 ± 3 mm	

[1] with all coupler ancillaries
[2] nominal 3.4 MV
[3] Q_0 (at 2 K and 3.4 MV) calculated from P_{dyn} (with R/Q$_{(DQW)}$ = 430 Ω and R/Q$_{(RFD)}$ = 429.7 Ω) ≥ 5.4 x10^9
[4] preliminary value, which will be confirmed by ongoing studies
[5] measured using bead pull or wire method
[6] normalized to 10 MV
[7] clarification pending

The cavities sit within a Grade 2 Titanium liquid helium tank. This material is chosen as it has an almost identical co-efficient of thermal expansion to the Niobium cavity. Within the helium vessel is an internal cold magnetic shield used to minimise external magnetic fields to <1µT at the cavity surface. The shield has an extremely high magnetic permeability, effectively acting as a sponge for magnetic flux. This is critical for superconducting operation, where higher than 1µT fields can increase the risk that a portion of the cavity would become normal conducting, which would give resistive heating, and this heat would then cause adjacent parts of the cavity to be normal conducting which gives increased resistive heating and so on, in an avalanche effect known as a 'Cavity Quench'. Conflat (CF) vacuum sealing flanges have been chosen as the connection for all components. The power is delivered to the cavity via the Fundamental Power Coupler (FPC) which is connected via a DN63 CF connection on the top of each cavity. There are additional CF ports on the cavities for the attachment of High Order Mode Suppressors (HOMS), these are used to couple to and remove unwanted RF resonances in the structure. There is an additional CF port for an RF probe used to measure cavity parameters during operation. The end CF ports are for connection of the cavities to the rest of the beam line. There are mechanical interfaces

on the cavity for connection to the Cavity Tuner. This tuner allows for the precise RF tuning of the cavity. These components combined form what is known as the 'Dressed Cavity'. The Bare Cavity is simply the cavity without helium vessel or any peripheral components. The dressed cavity components and beamline connections are made in an ISO Class 4 Cleanroom environment, this is critical to achieving cavity performance. The inner surfaces of the cavities are acid etched in a process known as Buffered Chemical Polishing (BCP) to remove superficial materials in the cavity surface and surface defects (Jones T. , 2017). This process has been shown through empirical methods to dramatically improve cavity performance.
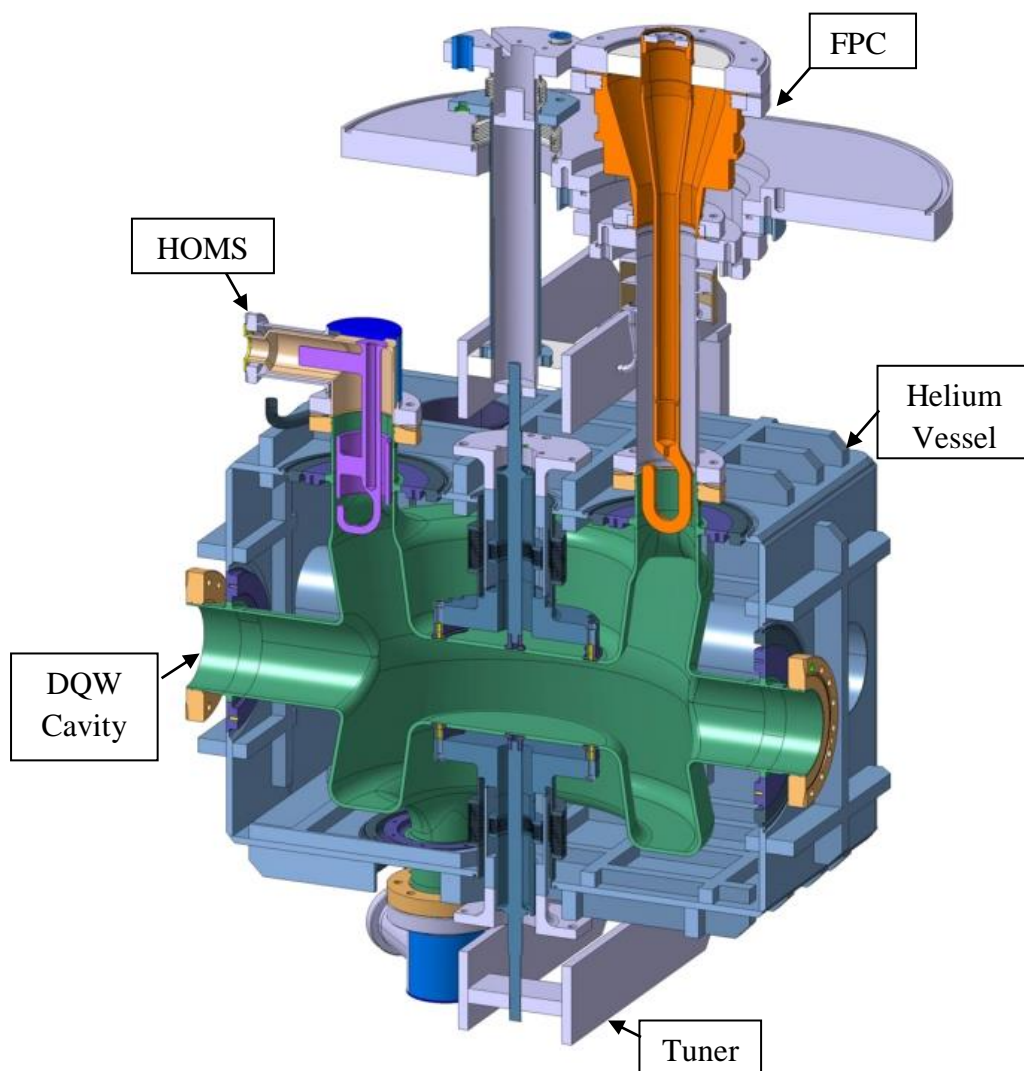
Figure 7. Dressed DQW Cavity Design (Capatina, 2014)

1.5. HL-LHC Crab Cavity Cryomodule design for the SPS

Crabbing of a Proton beam using SRF Cavities had never previously been demonstrated anywhere in the world. The risk of installing unqualified cavities into the LHC was deemed unacceptable; therefore a test of 2 DQW cavities in the Super Proton Synchrotron was planned and performed in 2018, demonstrating this technology for the first time (CERN, 2018c). The dressed cavities require many ancillary components to allow them to function. This overall system is known as a 'Cryomodule', the Crab Cavity SPS Cryomodule is shown in Figure 8. The Cryomodule consists of several sub-systems including;

- The Outer Vacuum Chamber (OVC) – This provides an insulating vacuum around the cavity in order to maintain the operating temperature of 2K. It also forms the rigid foundation of the support system.

- Thermal Shield – The thermal shield is cooled with gaseous helium at 50K-70K. Radiative heat from the OVC can pass through the insulating vacuum, and the thermal shield absorbs this instead of the liquid helium tanks.

- Multi-Layer-Insulation (MLI) – This works in addition to the thermal shield to insulate the cavities, it is alternate layers of low emissivity material interlaced with a low thermal conductivity material.

- Magnetic Shielding – There is both a warm external magnetic field and individual cold shields for the cavities; these are required to reduce external magnetic fields to <1µT at the cavity surface.

- Fundamental Power Coupler (FPC) – These are used to feed ~50kW CW power into each cavity. The FPC is also part of the supporting system in the case of the Crab Cavities.

- Cavity Support and alignment system – This is required to hold the cavities in position during cool-down and operation, and also allows external manipulation for cavity alignment.

- Cavity Tuner – This is comprised of a tuning frame around the cavity at cryogenic temperatures, and a warm part of the tuner outside the OVC. The warm part contains all the motion and control equipment, allowing exchange for maintenance.

- HOMS RF Lines – These connect the HOMS to water cooled loads external to the module.

- Frequency Scanning Interferometry (FSI) System – This is used to monitor the cavity position within the Cryomodule (Sosin, 2016).
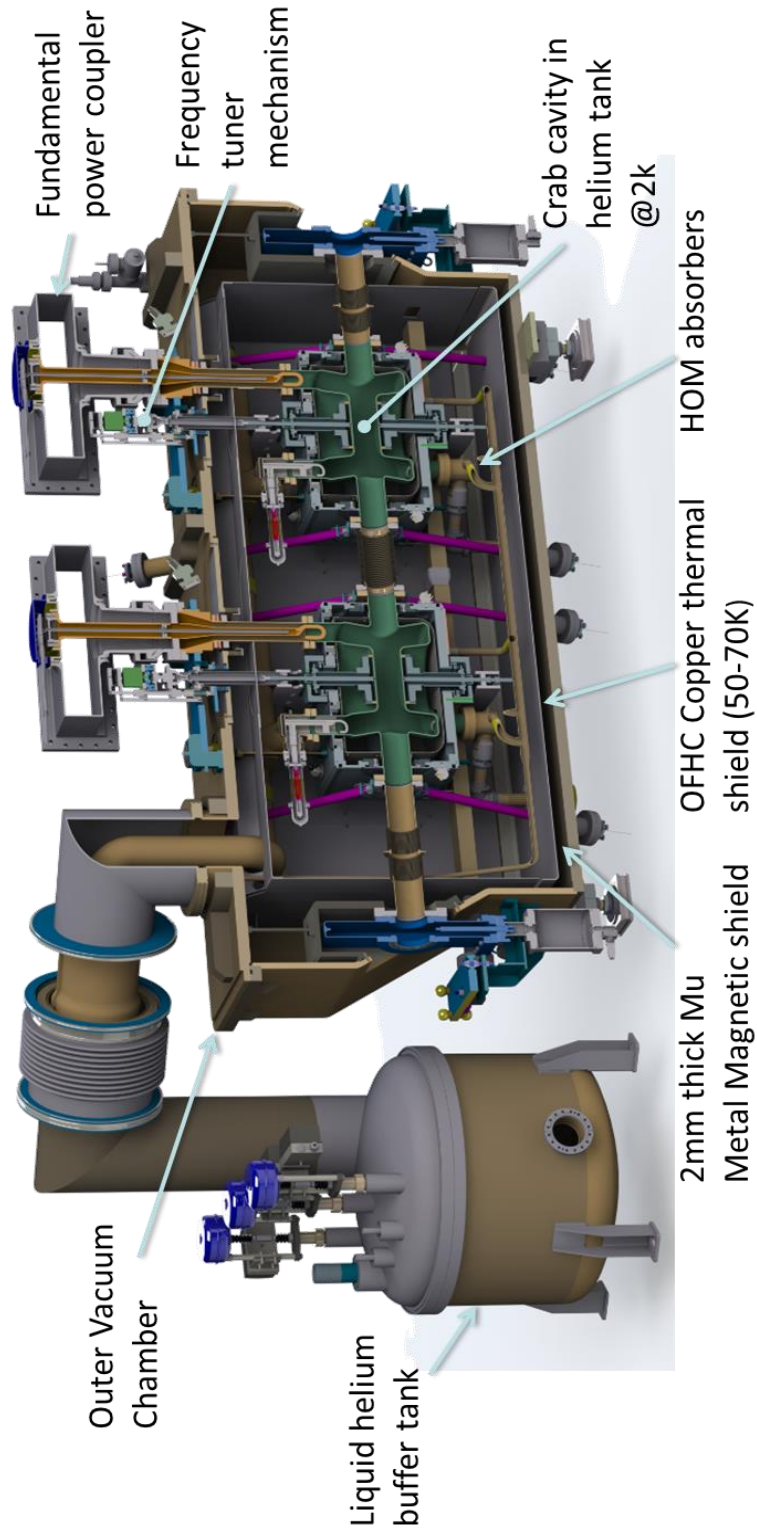
Figure 8. DQW Crab Cavity Cryomodule cross section view

1.6. SRF Cavity Support Systems

The SRF Cavity Support System is a key sub-assembly of all cryomodules. It is the primary connection between the cavities and the outside world, which means it affects many aspects of cavity assembly, alignment, handling, transportation and operation. The primary function of the system is to secure the cavities within the module without any yielding and with a suitable factor of safety for a broad series of load conditions, some examples to consider are given below;

- The load of the self-weight of the cavities, beam line components and any other ancillaries supported by the system.

- Maximum possible loads induced during alignment.

- The deformation due to cavity cool-down to 2 Kelvin, with the base connection of the support system to the outside world at room temperature.

- Handling and transportation loads typically 1G static in all directions (Department for Transport, 2002) but higher factors to be considered for conditions such as international transportation (by air or sea), handling by outside organisations etc.

SRF Cavities operate at a specified RF frequency and a designed accelerating or deflecting voltage. Deformation of the cavity leads to detuning of the resonant frequency of the cavity, yet RF power is still required at the operating frequency. This means that a relative increase in RF power is required to maintain a specified voltage within a detuned cavity. The Cavity Support System should minimise deformation of the cavity under all operating conditions, to a specification agreed for the specific cryomodule. The deformation caused to the cavity via mechanical vibration is known as Microphonics (Doolittle, 1989). These vibrations are transmitted to the cavity predominantly via the rigid connection of the support system. The stiffness of the support system determines the modes of vibration of the system and therefore the level of coupling to external sources. For some cryomodules this issue can be mitigated via the installation of a fast acting tuner system to counter act the vibration and therefore keep the cavities on tune. For cryomodules such as the Crab Cavity Cryomodule, which do not have a fast acting tuner mechanism, the consideration of microphonics is

essential. The TESLA and ILC Cryomodule report states within a table of Key Functional requirements for cryomodules "As for any SRF cavity support structure, minimize cavity vibration and coupling of external sources to cavities. This is addressed by means of providing a stiff support system" (Peterson, 2000). The description of the requirements, justification and analysis of microphonics is a key part of this thesis and discussed at length throughout.

The support system is a key contributor to the static heat transferred to the 2 Kelvin liquid Helium cooling system for the cavities. The mode of heat transfer is via conduction, within the cryomodule community this is known as 'heat leak'. Conduction is governed by Fourier's equation of heat conduction which is provided and discussed in Sub-Section 2.2 of this thesis. To minimise heat leak the ideal support system would be manufactured from a low conductivity material, with a low cross sectional area and long aspect ratio. A long and thin structure, however, is certainly not ideal for the mechanical requirements of the system. In addition the system is required to allow for several millimetres of cavity string thermal contraction, which can lead to complex support systems with many components. The number of components in the system can itself be an issue, adding to complexity in assembly and alignment, and introducing issues with thermal contraction of components within the support structure itself, leading to loss of pre-load and fasteners coming loose (Arkan, 2018).

The earliest cryomodules were developed in the 1980's. Several solutions were employed to meet the requirements outlined above. KEK developed a complex system utilising G10, a low thermal conductivity fibre glass material, in a series of sliding supports (shown in Figure 9), with two central fixed supports adjacent to the power couplers, the overall cryomodule layout is shown in Figure 10. These supports were rigid, yet with the cost of a high heat leak providing a significant contribution to the 30W static heat leak to the cavity liquid helium system (Mitsunobu, 1989). Around a similar time it was common for cavities, or a string of cavities and their ancillary components, to be suspended on an arrangement of tensioned low cross section rods from the insulation vacuum chamber to the helium tanks of the cavity, as shown in Figure 11. This system provides a very low conductive path, with heat leak values as low as 0.15W for the suspension rod system (Buhler, 93). The down side of the support rod system is the relatively low fundamental modes of vibration which couple to large amplitudes of ground vibration and cause microphonics issues (see Sub-Section 2.1).
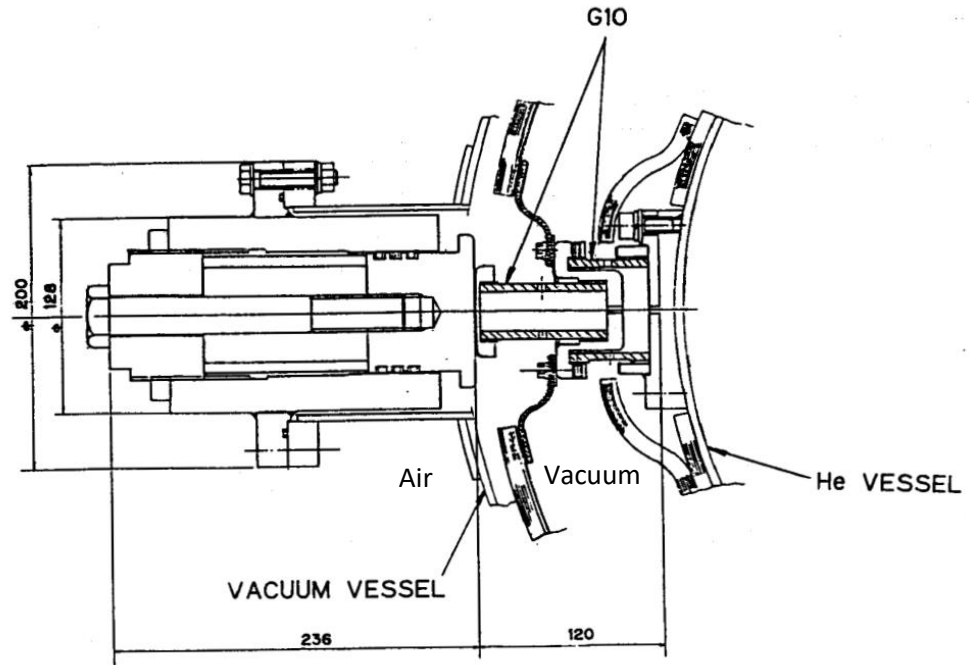
Figure 9. KEK Cavity support system for TRISTAN Cryostat (Mitsunobu, 1989)
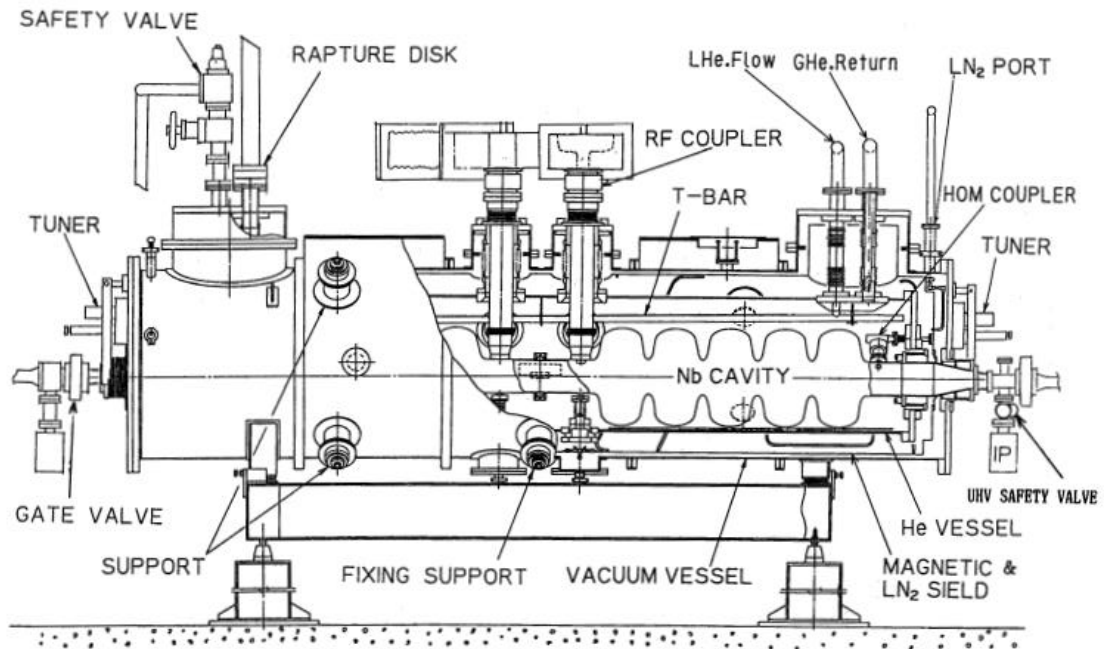
Figure 10. TRISTAN 'Superconducting Cavity Cryostat' developed by KEK
(Mitsunobu, 1989)
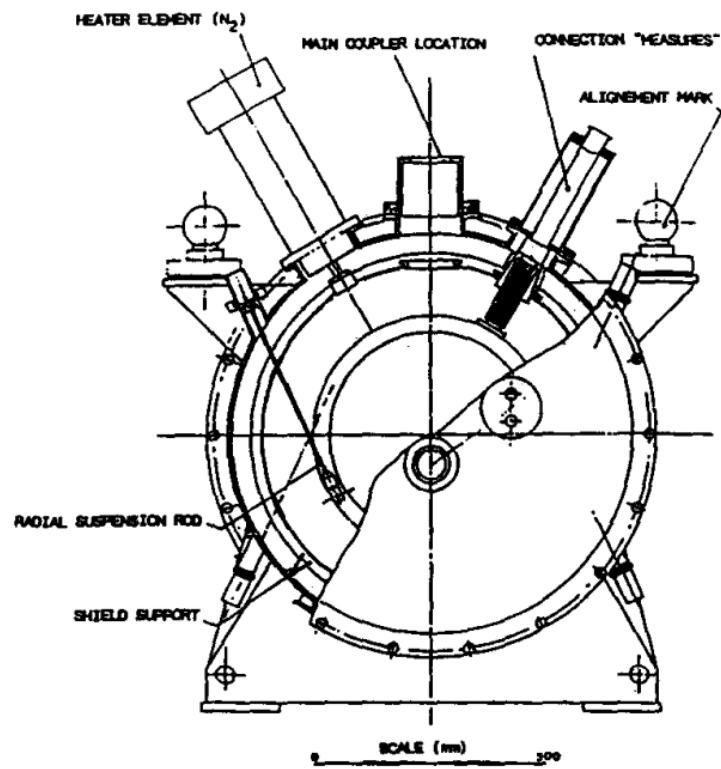
Figure 11. MACSE Cryomodule developed at IPN Orsay Laboratory (Buhler, 93)
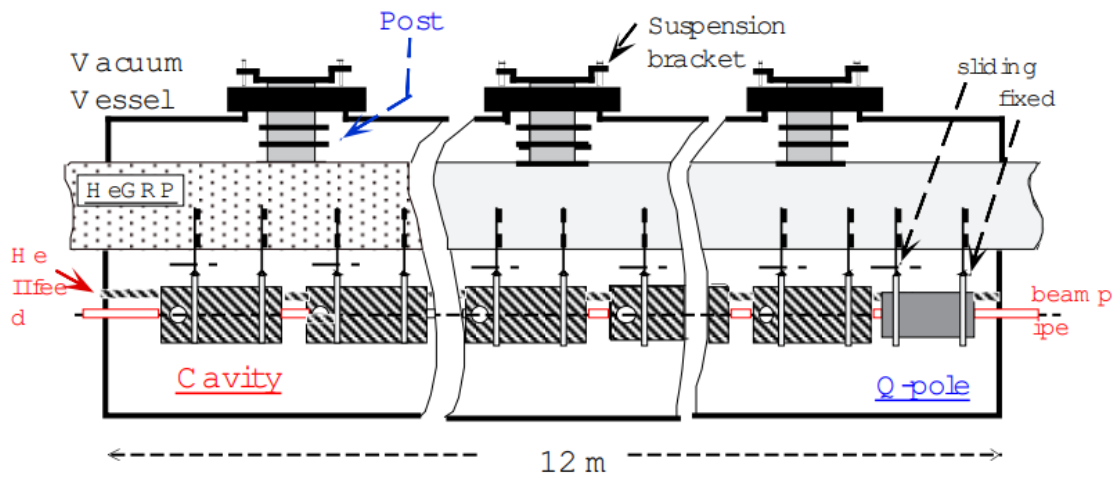
Figure 12. TESLA Test Facility Linac schematic (Edwards, 1995)
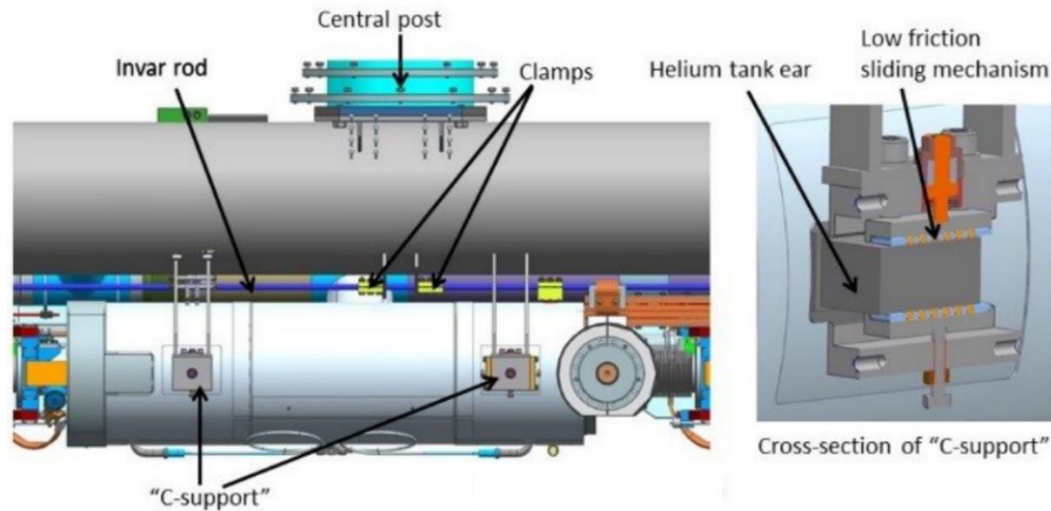
Figure 13. TESLA style "C-Support" system (Peterson, 2000)

A considerable design effort was made to balance thermal constraints with increasing mechanical stiffness for the Tesla Test Facility Linac (Edwards, 1995). A system was developed whereby a limited number (3 over the 12m length) of G10 support posts with intermediate passively cooled temperature intercepts were fixed to the large diameter gas return line of the liquid helium system. The cavities below were then suspended off this rigid pipe via a fixed support end and a supported end with bearings to allow the cavities to slide as they are cooled, known as the "C-Support" mechanism, as shown in Figure 13 (Peterson, 2000). The aim of the design was to have a support system with a natural frequency of >25Hz, to avoid coupling to the repetition rate of 10Hz at which the particle bunches were fired. Aiming for this higher value had the added advantage of avoiding large displacements in ground vibration. Such was the success of this design that is was used for all 103 XFEL Cryomodules (Berry, 2016) as well as several other cryomodules, including CW Cornell Injector Cryomodule (Medjidzade, 2005) and the LCLS-II cryomodule (Galayda, 2018).

It was stated in the Tesla Test Facility Linac report that this type of support system "has the disadvantage of requiring the cavity input couplers to be flexible", "however, preliminary data on flexible couplers designed at FNAL and DESY have not so far evidenced any serious problem in making them perform to specification" (Edwards, 1995). Unfortunately several of these input coupler bellows failed in the transportation of the LCLS-II modules from Fermilab in Illinois to Stanford Linear Accelerator in California (Huque, 2019) and shown in Figure 20. The failure mode was

identified as fatigue, due to many cycles of bellows expansion as they coupled to vibration induced by road noise. These bellows have also been reported to generate copper flakes, as the coating can be damaged in bellows movement (Popielarski, 2013). These copper flakes can be hugely detrimental to the cleanliness and therefore performance of the cavities. These issues can be mitigated through appropriate transport restraints, transportation frame design, handling and testing. However, in the case of the SPL cryomodule it was decided to remove the bellows from the coupler all together, and to have this as part of the support structure itself (Parma, 2013). As shown in Figure 14 the cavity string is supported by the "Double-Walled Tube" which is the outer conductor of a rigid power coupler. The name 'double-walled' comes from the fact that this tube is actually two tightly fitting tubes, with cooling channels machined onto the surface of the inner tube, used to remove heat from the component. Between each cavity is a sliding "Inter-Cavity Support" which ensures that the coupler support is not cantilevered. The idea of supporting the cavities via the fundamental power coupler is the starting point for the Crab Cavity support structure design. The requirements of which are discussed in the following section.
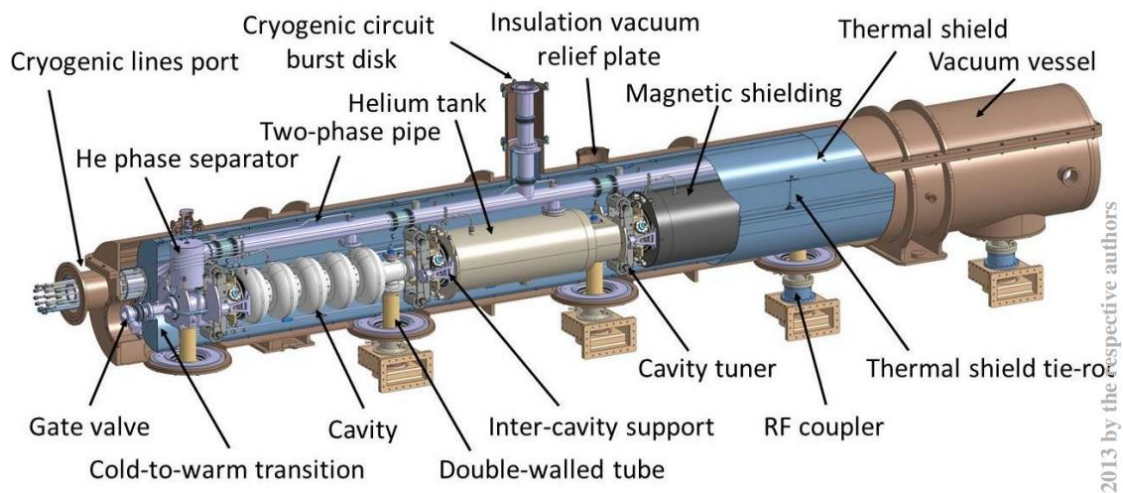
Figure 14. SPL Cryomodule Design (Parma, 2013)

2. HL-LHC SRF Crab Cavity Support System Design

2.1. Support System Requirements

The cavity support system is to be capable of supporting the ~250Kg dressed cavity, yet with low cross section in order to minimise conductive heat losses into the 2K cryogenic system. The support system should allow for thermal contraction of the 2K components so that there are no stresses above the respective material yield, and in the cavity the stresses should be as low as possible. In addition, cavity RF frequency detuning due to vibration (microphonics) is to be minimised to as low as reasonably practicable and should be less than 1/4 of the single sided cavity bandwidth (which is 400Hz) therefore less than 100Hz (Baudrenghien, 2013). The sensitivity of the cavity in the central tuning region is 372kHz/mm (Verdu-Andres, 2015), this is the shift in RF frequency per mm of movement of the capacitive plates. To achieve 100Hz stability the plates need to see dynamic movement less than 300nm. Microphonics can be compensated for through the use of a fast acting Piezo tuner, however, it is believed that through careful design this should not be required for the HL-LHC Crab Cavities. The choice of operating below the lambda point of helium, i.e. the operation at 2K, is partially driven by this desire to minimise microphonics as in this superfluid state helium should not boil (Carra F. , 2015).

The reasoning behind minimising microphonic detuning is that if the cavity is not on resonance more RF power is required to drive the desired operational RF frequency. The equation below describes the relationship between microphonics ($\Delta\omega$) and RF Power Coupler Power (Burt, 2019)

$$ P_+ = \frac{V_c{}^2 \left(1+\beta\right)^2}{8R\beta} \left(1 + 4Q_L{}^2 \frac{\Delta\omega^2}{\omega^2} \right) \qquad [Eq.\ 1] $$

Where P_+ is RF Power, V_c is cavity voltage, β is the coupling factor (i.e. the ratio of power loss in the external circuit to losses in the cavity), R is the shunt impedance, Q_L is the loaded quality factor, $\Delta\omega$ is the change in RF frequency due to microphonics and ω is the operating RF frequency.

The DQW Crab Cavity has an operating frequency of 400.79MHz, the minimum voltage requirement was 3.4MV for SPS, however, up to 5MV has been

observed in vertical test cryostats and is therefore desirable. The Q_L is ~5x10^5, β can be calculated by Q_0 (1x10^{10}) divided by Q_{EXT} (5x10^5) giving a value of ~20000, (CERN, 2018a). Figure 15 shows a plot of the calculated power ratio increase for a given level of microphonic detuning. At the level of ~100Hz detuning the additional power requirement is 6.25%, this rises to 25% additional power required for 200Hz detuning and 100% additional power required for detuning of 400Hz. The power coupler is limited to ~40kW continuous wave, the detuning of 400Hz takes the coupler outside of its maximum power rating at the desirable 5MV target. Ideally the cavity will be driven at its operating voltage of 3.4MV for the minimum amount of RF power possible. This puts a lower heat load into the cryogenic system and a lower load on the sensitive ceramic and coatings of the coupler.
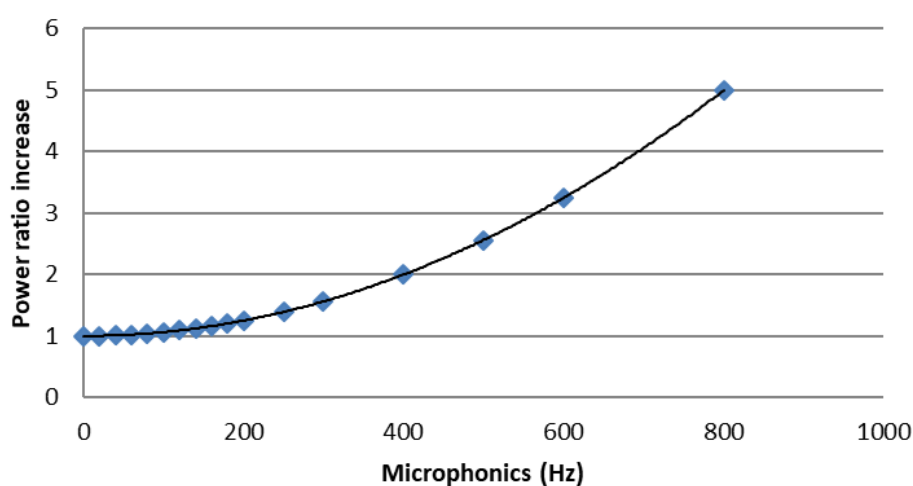
Figure 15. Power required for varying levels of microphonic detuning

Studies were performed as part of this thesis to assess and minimise Microphonics to acceptable levels. From experience gained from within the accelerator community it is understood that there are certain frequencies that should be 'avoided' in a typical ground (or base excitation) spectra, for example the rise in integrated displacement at 50Hz observed in the SPS ground data (Figure 17) is common to almost all facilities. What was seemingly less understood was how far from this value modes should be tuned in order to minimise the amplification to an acceptable level. All the mechanical frequencies of the cavity will interact with all base excitation frequencies to some degree, and this needed to be reflected in any transmission calculations. If the natural frequency of a system is the same as the driving frequency i.e. a ω/ω_n ratio of 1, then the amplification of the input is only limited by the damping in the system, for low damping levels the amplification (or transmissibility) can be >100x the input.

Should a system be made stiffer and the natural frequency is higher than the driving frequency, i.e. a ω/ω_n <1, the transmissibility tends towards 1 as can be observed in Figure 16 (Sharma, 2005). In this case a supported mass will follow the input frequency. For modes lower than the input driving frequency, the transmissibility can decrease below 1, and therefore isolate from higher frequencies.
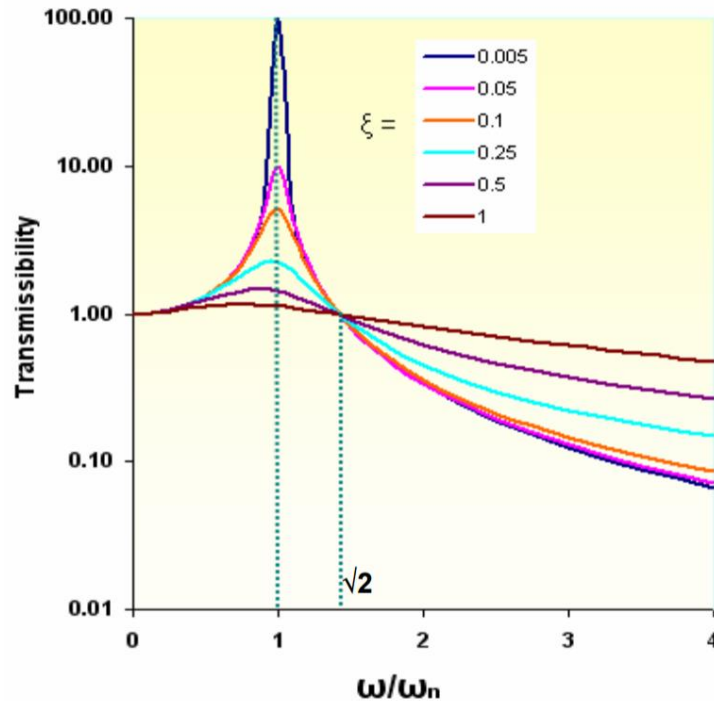
Figure 16. Transmissibility - Ground vibration to system oscillation amplitude (Sharma, 2005)

Ground vibration amplitudes tend to increase to the 4th power with decreasing frequency, due to the amount of energy involved in the processes driving these frequencies, for example tidal noise. Within the accelerator community it is therefore best practice to increase the stiffness of a supporting system and build the entire accelerator upon a floor with as low as reasonably practicable background noise, rather than to try to employ a system of 'soft supports'. This is to ensure alignment of the accelerator components. The integrated RMS, equal to the Root of the Sum of Squared values (RSS), of all modes should be kept as low as reasonably practicable. The accelerator facilities at CERN, being deep underground, typically have very low background noise. Measured data received from CERN for the ground within the SPS tunnel had an integrated RMS vertical ground motion value of less than 4.6nm taking data from 1Hz to 100Hz (Ziemianski, 2014). For comparison, data obtained for the Diamond Light Source (DLS) facility has an integrated RMS value of 20nm for vertical

motion (Huang, 2006). The SPS data will be referred to as 'quiet' due to the fact that the data was measured in a region of the machine with no cryogenic or vacuum pumps running, and it is understood that the environment in which the cryomodule will be installed will likely have a higher background vibration level. The DLS data is taken in a relatively noisy environment.

To assess the expected level of microphonics, the first 10 vibration modes were calculated using Finite Element Analysis (FEA) and a transmission matrix was developed to determine mode deflections for both sets of ground data (SPS and DLS), in order to have 'best case' and 'worst case' scenarios. For all results a conservative value of 0.001 for the fraction of critical damping was used. This would be the value for a completely solid steel system (Sharma, 2005). For a system with bolted connections such as this the damping in reality could be up to a factor 10 higher. For certain modes, such as the vibration of the tuner mechanism which is mechanically coupled to the cavity, the level of RF detuning is estimated. This is achieved by calculating modal values, using the transmission matrix to find peak amplitudes of oscillations, calculating cavity deflection due to mode deflection and comparing this to RF parameter studies which provide RF detuning per mm movement of the cavity tuning plates. The transmission matrix generated offers a detailed and efficient solver for vibration amplitudes when compared to FEA random vibration solvers. The design and analysis performed in this section had a direct bearing on the mechanical design of the overall Cryomodule, one of the critical systems within the HL-LHC upgrade.
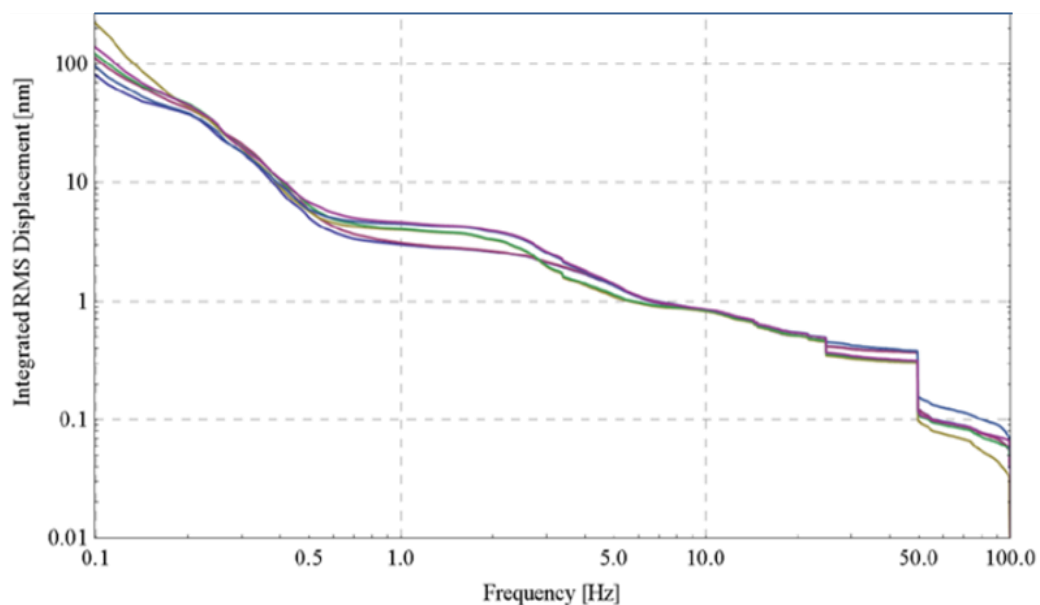
Figure 17. SPS Vertical Integrated RMS displacement in several locations (Ziemianski, 2014)

It was decided that for ease of alignment the cavity should be supported, along with the mechanical tuning mechanism, via a common support plate which itself is mounted to the upper vacuum flange of the outer vacuum vessel of the cryomodule, (initial concept shown in Figure 19). The allowable tolerances on the alignment of the cavities relative to each other and the beam axis are as follows (CERN, 2015);

1. The rotation of each cavity in Rz (beam axis), from Figure 18, should be < 0.3° (at 3x standard deviation (3σ)).
2. The rotation of each cavity with respect to Rx and Ry from Figure 18 should be less than 1 mrad (at 3σ).
3. The transverse misalignment of one cavity with respect to the other i.e. the intra-cavity alignment in the transverse plane with respect to the cryomodule axis should not exceed a 0.5mm (3σ) tolerance.
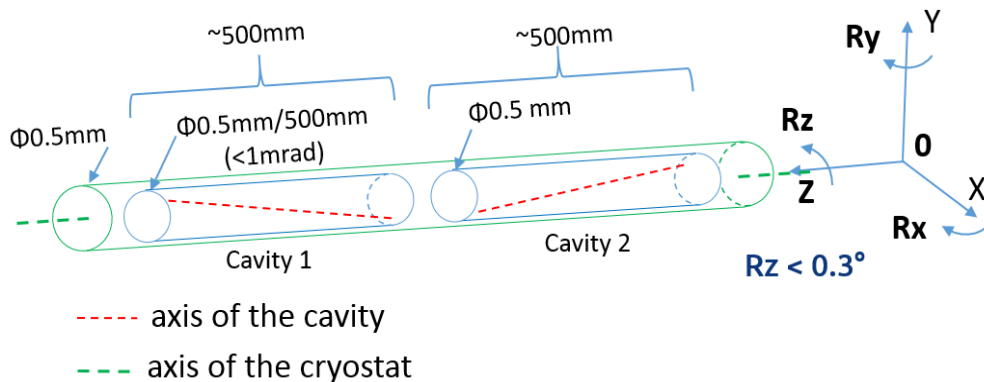
Figure 18. Crab Cavity alignment tolerances
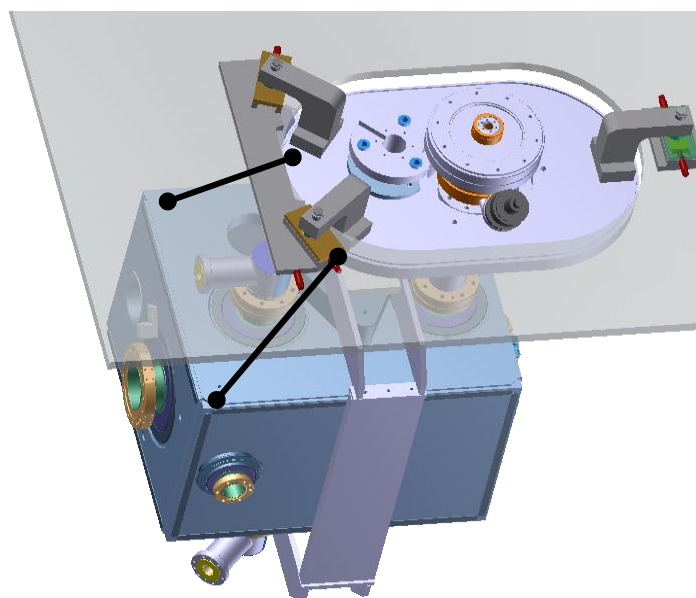
Figure 19. Cavity suspended from common support plate

33

To remove the necessity for bellows in the design of the Fundamental Power Coupler (FPC) it was determined that this would be the main support for the cavity, similar to the technique used in the SPL Cryomodule (Parma, 2013). Stainless Steel bellows in the RF line require copper coating and there is a risk of this copper coating flaking off and contaminating the coupler or cavity (Popielarski, 2013). It has also been observed that bellows in the RF input coupler line can fail due to fatigue, when the bellows couples with vibration induced through transportation loads (Huque, 2019). The failure is considered as catastrophic as the beam vacuum is then vented to atmosphere and contamincated with particulates, requiring a complete strip down and rebuild of the cryomodule. Removing the bellows from the FPC eliminates the risk of copper flaking and bellows damage.
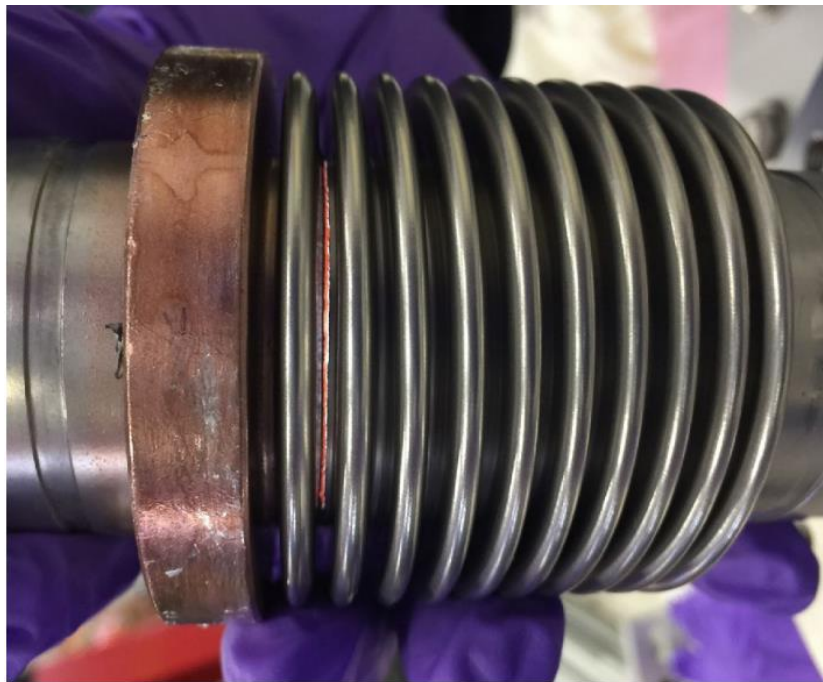
Figure 20. Catastrophic cyclic failure of an LCLS-II coupler bellows (Huque, 2019)

The use of the FPC as a primary support also has the advantage of reducing the static heat leak to the cavity by minimising the number of rigid support structures. The total heat leak specification for any additional support structures (over the FPC) was originally to be less than 0.8W at 2K. However, this was later relaxed to up to 2W (Carra F. , 2017) allowing an improvement in the ridgidity of the system due to increased width and thickness of the support flexures.

2.2. Cavity support flexure design

It was the suggestion of the author of this thesis that the use of flexural blades as the supplementary support to the fundamental power coupler could dramatically improve the performance of the cavity support system. It was proposed that such an arrangement would act to rigidify the system yet remain flexible in the direction of thermal contraction, minimising stress in the cavity and coupler on cool-down. This is a technique based on components previously designed and used successfully by the author in an STFC project for the SPICE instrument thermal testing enclosure shown in Figure 21 (Jones T. , 2013). The novel element of this work was incorporating support flexures as an SRF cavity support mechanism.
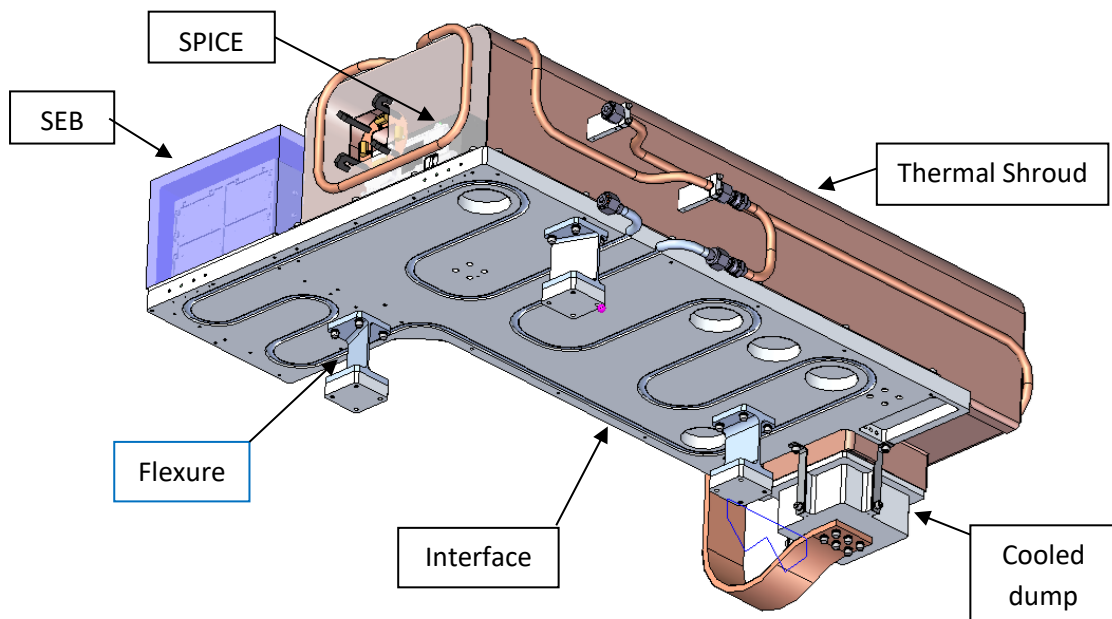
Figure 21. SPICE instrument thermal testing environment
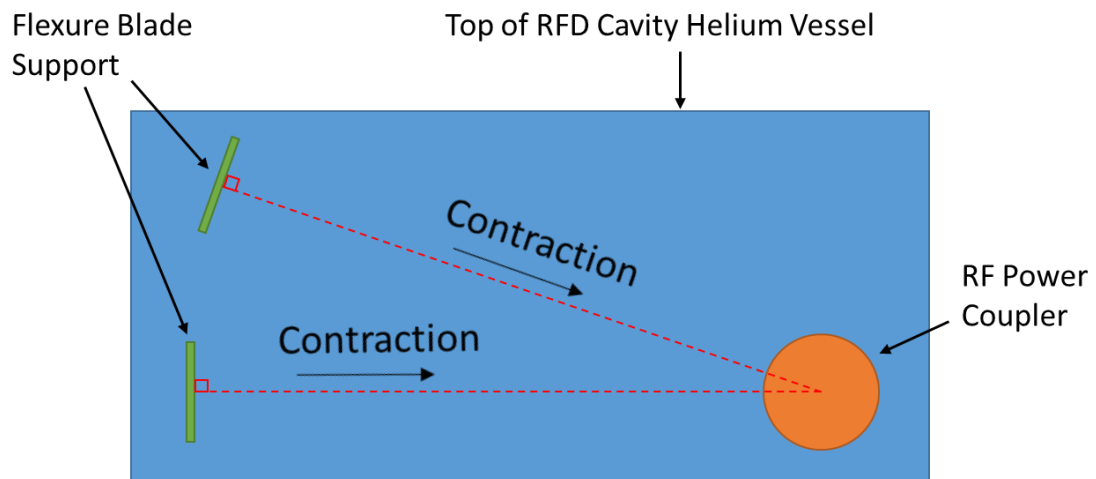
Figure 22. Sketch of RFD Cavity Support System (plan view)

35
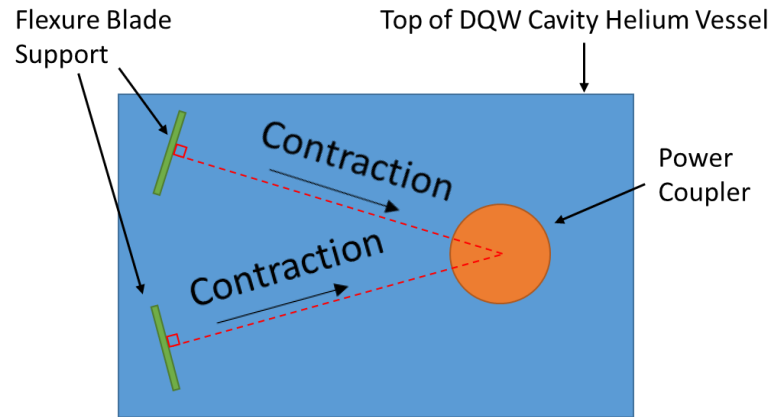
Figure 23. Sketch of DQW Cavity Support System (plan view)
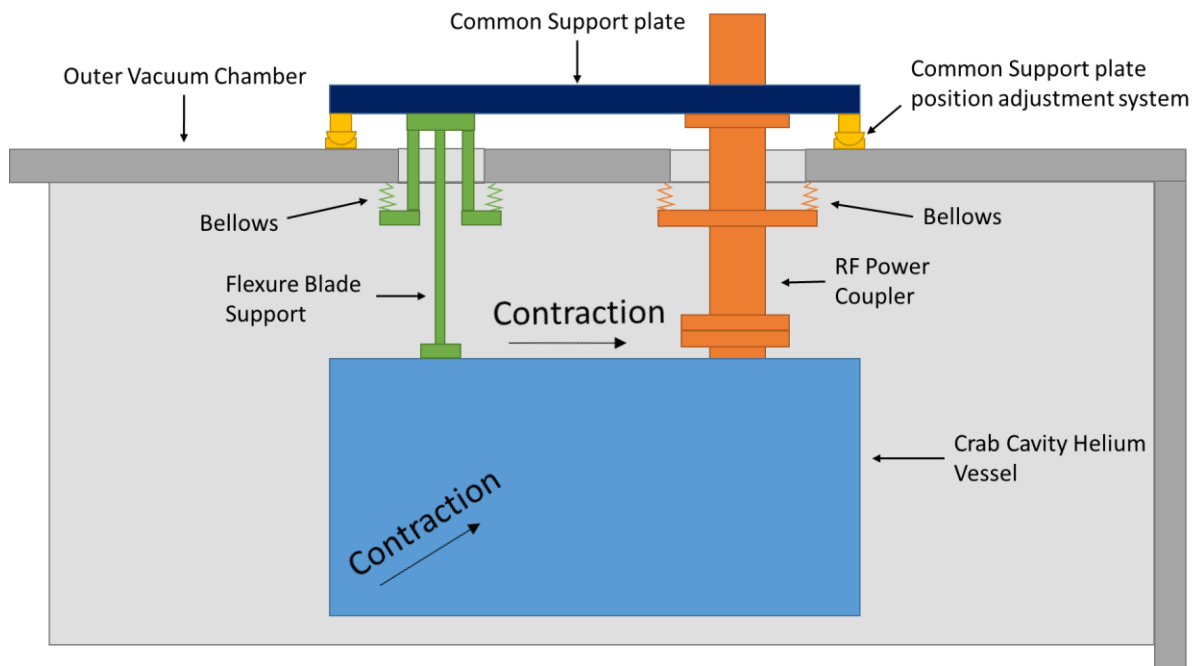
Figure 24. Sketch of typical crab cavity support system (side view)

The blades are designed such that the flexural bending plane is tangential to the cylindrical surface of the Fundamental Power Coupler (FPC) which acts as the fixed point (as is shown in Figure 22 and Figure 23). This allows for thermal contraction towards the FPC, whilst the system remains comparatively rigid in all other directions. For the design of such flexures first one must consider the amount of thermal contraction of the helium vessel. This is calculated using the following formula when using integrated thermal contraction values;

$$\Delta L = L_i \times \int_2^{293} \lambda_t \times dT \quad [Eq.\,2]$$

(Barron, 1985)

Where, ΔL is the change in length, L_i is initial length and λ_t is the integrated thermal contraction value from room temperature at 293K to the final temperature of the operational helium vessel which is 2K (Barron, 1985). For Grade 2 Titanium this λ_t value is 7e-6 (FERMILAB, 2013). The distance from the coupler to the flexures can be optimised but was initially set to 650mm. This gives a contraction of 1.3mm, therefore the flexures must deform by this amount. Taking this value one can calculate the required geometry of the flexure using the following formulae;

$$S = \frac{W}{Z}\left(\frac{1}{2}l - x\right) \quad [Eq.\,3]$$

$$y = \frac{Wx^2}{12EI}(3l - 2x) \quad [Eq.\,4]$$

Where, S is the stress at a given location x from the 'moving' end, W is the force acting perpendicular to the flexure, l is the flexure length, E is the Young's modulus of the flexure material, I is the second moment of area of the flexure geometry and Z is the section modulus. The deflection of the flexure is denoted by y which in this case is known. Therefore one can re-arrange Equation 4 and solve for W. Then by using W in Equation 3 one can obtain the maximum stresses in the structure, which are equal and opposite and found at the support ends. To do this the I and Z values are required which are given by;

$$I = \frac{bd^3}{12} \quad [Eq.\,5]$$

$$Z = \frac{bd^2}{6} \quad [Eq.\,6]$$

Where b is the width of the flexure, d is the thickness. By observing the formulae it can be found that increasing the width of the flexure increases the force required to deflect it, however, does not increase the stress in the flexure. Therefore the width can be increased up to the limit imposed by the thermal conductance limit which is set by the cryogenic capacity at 2K.

The flexure will be manufactured from 316L Stainless Steel to give similar vertical thermal contraction to the fundamental power coupler. To minimise the heat leak to the 2K system the flexure will need to be intercepted by a passive cooling strap (cooling the mounting region to ~80K) to provide a thermal profile similar to that of the fundamental power coupler (Figure 25).
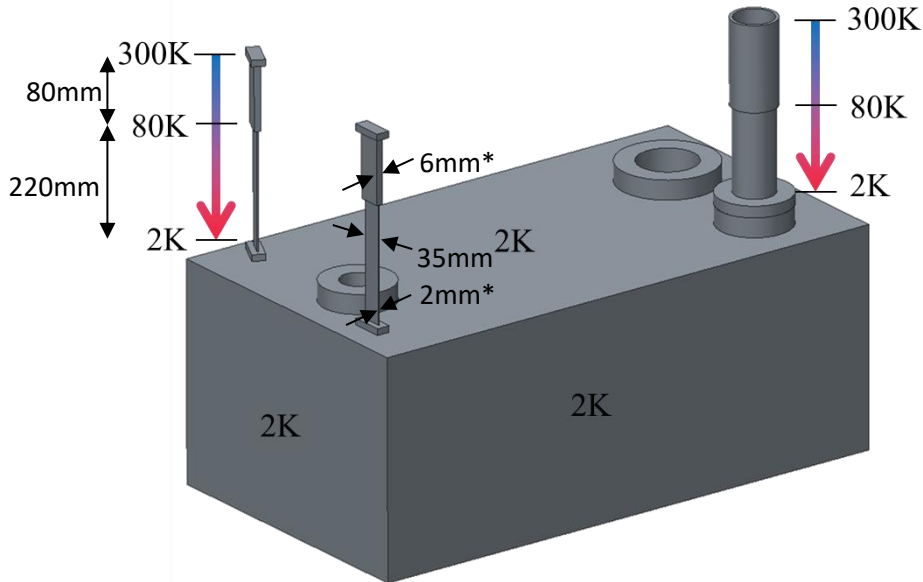
Figure 25. Blade thermal profile (*initial values)

Thermal conductivity data has been measured and integrated (Barron, 1985), these values can be seen in Table 3. These values can be used in combination with the geometry of the blades to calculate the heat leak to each of the cooling circuits using the Fourier rate equation;

$$\dot{Q} = (K_h - K_c)\left(\frac{A}{L}\right) \ [Eq.\,7]$$

Where;

$$K = \int_{4K}^{T_h} k_t \, dT \ [Eq.\,8]$$

K_h is the thermal conductivity integral value at the higher temperature, K_c that of the lower temperature. A is the cross sectional area of the blade, where L is the length between the two temperatures.

Table 3. Thermal conductivity integrals for Stainless Steel (Barron, 1985)

Temperature (K)	4	10	30	50	80	120	160	250	300
Conductivity Integral, K (W/m)	0	3	42	135	349	726	1170	2340	3060

Integrating from 2K instead of 4K provides almost identical values, therefore it is a fair assumption to use the same values for 2K. If one calculates $\dot{Q}$ based upon the geometry shown in Figure 25 the values are 7.12W at 80K and 0.11W at 2K per flexure. A blade width sweep is performed later in this section showing $\dot{Q}$ at 2K with increasing width calculated using Equation 7.

2.3. Concept comparison

2.3.1. Structural model boundary conditions and assumptions

A heavily simplified version of the RFD cavity was used initially for the options analysis as it is both the heavier of the 2 cavity types and has the most cantilevered support, therefore representing the 'worst case' of the 2 cavity types. The mass used was approximate, but was valid for these comparative purposes, in addition the exact mass of the helium vessel was not yet fixed at that point in time. An acceleration of 9.81m/s^2 was applied to the model to represent standard earth gravity. The power coupler, rods and flexures were all fully fixed at the location of the common support plate, therefore assuming that this plate is infinitely rigid. This was deemed an acceptable assumption for this options analysis. Static total deformation, maximum von-Mises Stress and the first 4 mechanical vibration modes were obtained for each option shown in Figure 26. The same 1.5mm element size was used for all supports in each analysis (Figure 27), with 10mm elements on the rigid cavity body. The non-linear material properties used were provided by Fermilab (FERMILAB, 2013).
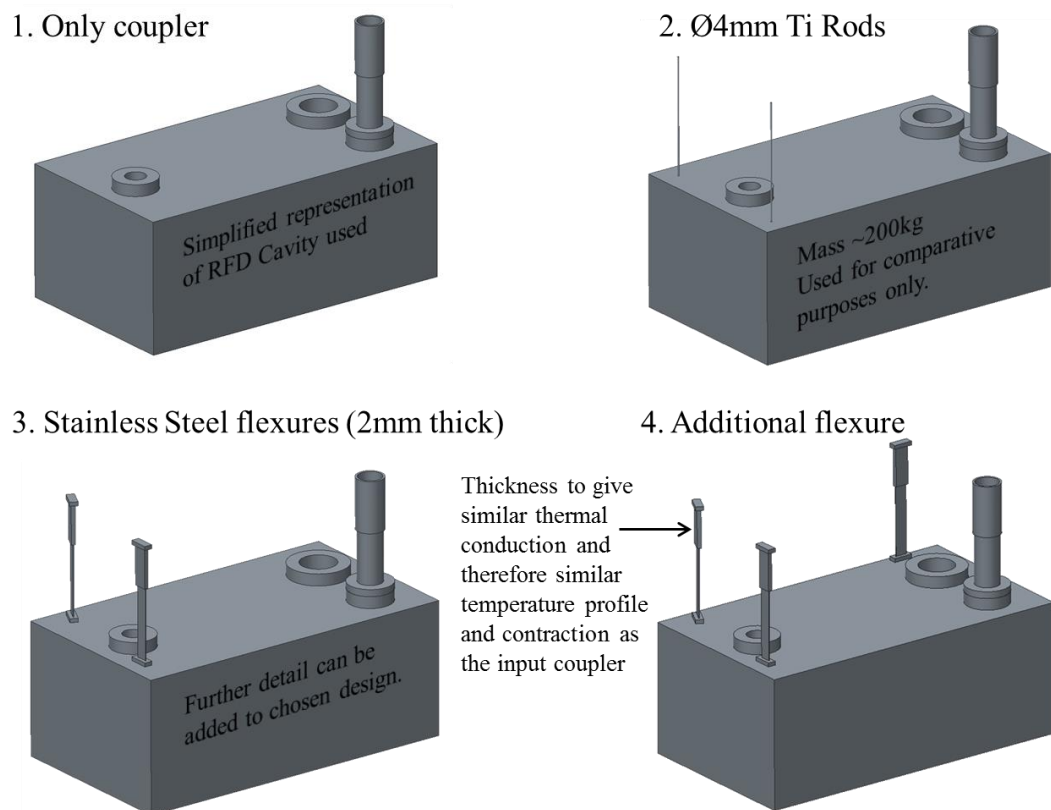
Figure 26. Cavity support options
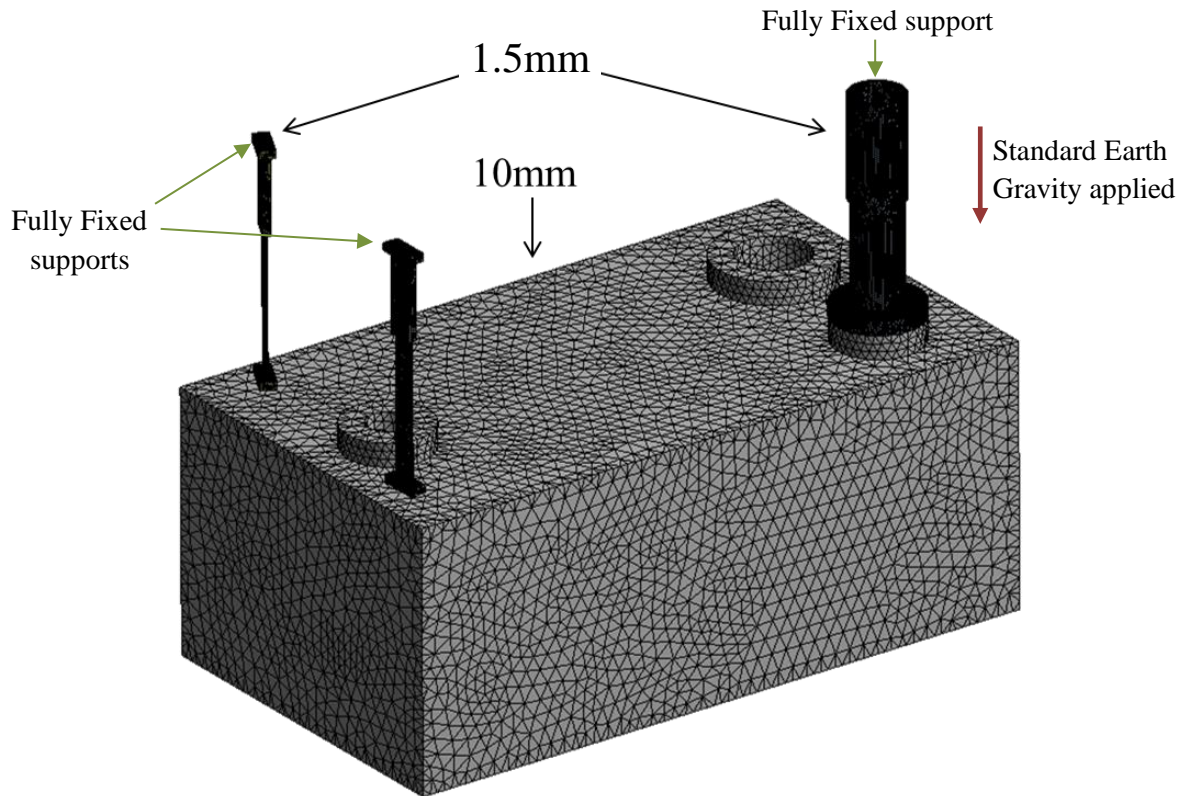
Figure 27. Typical support option mesh, boundary conditions and load

2.3.2. Structural analysis results

As can be observed in Table 4, the performance of the flexural blade type supports is significantly greater than that of a rod type arrangement. The static deformation is reduced by a factor of 10. First order vibration modes increased by greater than a factor of 3. A thorough study of rod configurations was completed by CERN (Zanoni, 2015), which compared various rod angles and pre-tension values. Even with increasing the rod thickness within the allowable heat leak limit, the results showed no particular improvement over the 4mm vertical rods (concept 2) used for this comparison. The 3 blades provide optimimum performance, however, also give increased heat leak and increased integration complexity within the module. Therefore it was decided to proceed with the coupler as the main support and to have 2 stainless steel support blades.

FEA First mode @ 7.7 Hz
Mostly rotation about coupler axis
but with some vertical bending.
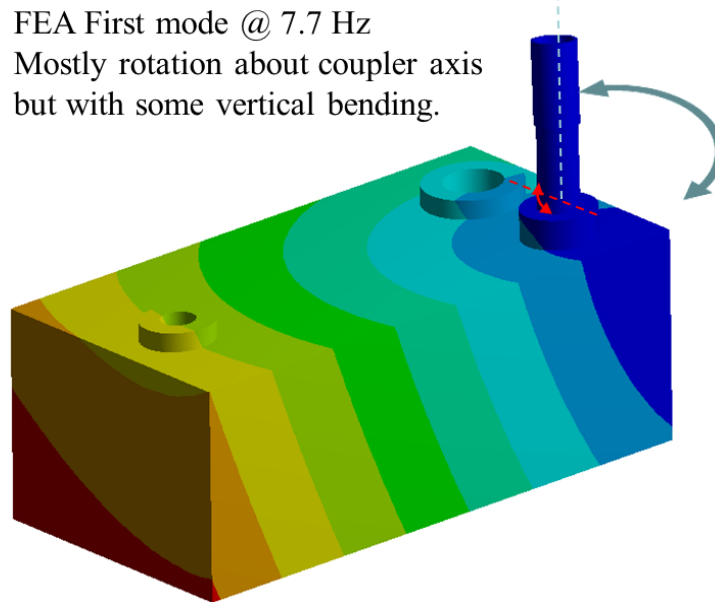
Figure 28. Option 1, Mode 1 deflection

Table 4. Cavity support options results

Analysis	Max Static Deformation (mm)	Max von-Mises stress (MPa)	Mode 1 Frequency (Hz)	Mode 2 Frequency (Hz)	Mode 3 Frequency (Hz)	Mode 4 Frequency (Hz)
1	3.9	183	7.7	8.3	16.1	61.1
2	0.24	65.2	8.5	25.3	38.3	70.9
3	0.025	15.3	25.1	48.3	56.5	122
4	0.01	10.5	27.2	50.15	66.9	174

2.3.3. Analysis validation

In order to validate the finite element model used in this analysis Equation 9 was used to calculate the fundamental mechanical vibration mode for option 1 (Figure 28). The result gives a natural frequency of 9.1Hz. The FEA result is at 7.7Hz. The difference of 17% is most likely due to the fact that the FEA includes sag of the FPC which the empirical calculation does not.

$$\omega_n = \sqrt{\frac{\frac{\pi G d^4}{32l}}{J_0}} \quad \left(\frac{rad}{sec}\right) \quad OR \quad f_n = \frac{1}{2\pi}\sqrt{\frac{\frac{\pi G d^4}{32l}}{J_0}} \quad \left(\frac{cycle}{sec}\right) \quad [Eq.\ 9]$$

2.3.4. Thermally neutral inter-cavity support structures

It was envisaged that some form of inter-cavity support could assist in stiffening the cavity string assembly, similar to the SPL Cryomodule (Parma, 2013). A novel thermally neutral inter-cavity support system was developed (as part of this research) which relied upon the differences in thermal contraction of materials from room temperature to 2K to provide a structure that maintains the same length before and after cool-down. This has the significant advantage over other similar systems in that is has no moving parts, i.e. bearings which can potentially lose pre-load on cool-down.
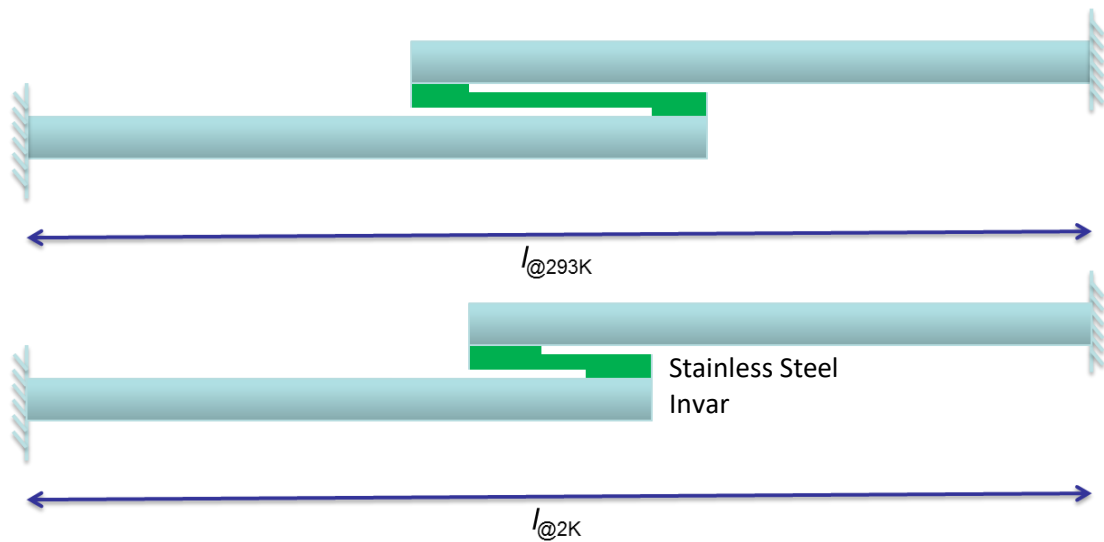
Figure 29. Thermally neutral inter-cavity supports (all 3 components are shorter in the lower image, yet the overall length is the same.

A set of simultaneous equations were derived using Equation 2 and appropriate boundary conditions, assuming the plates were mounted in line with the power coupler, i.e. the fixed point. L_i is the length of Invar at Room Temperature required. L_{ss} is the length of Stainless Steel at Room Temperature required.

Invar integrated contraction from room temperature to 2K is L_i x (0.037/100)

304 Stainless steel contraction from room temperature to 2K is L_{ss} x (0.306/100)

Therefore;

$$2L_i \text{ x } (0.037/100) = L_{ss} \text{ x } (0.306/100)$$

$$2L_i - L_{ss} = 1032mm \text{ (distance between fixed points)}$$

Therefore 2Li x (0.037/100) = (2Li – 1032) x (0.306/100)

Solving the simultaneous equation gives L_i = 587mm and L_{ss} = 142mm

2.3.5. Inter-cavity support options

Similar to the cavity support options analysis performed earlier, several configurations of inter-cavity support were considered and are shown in Figure 30.
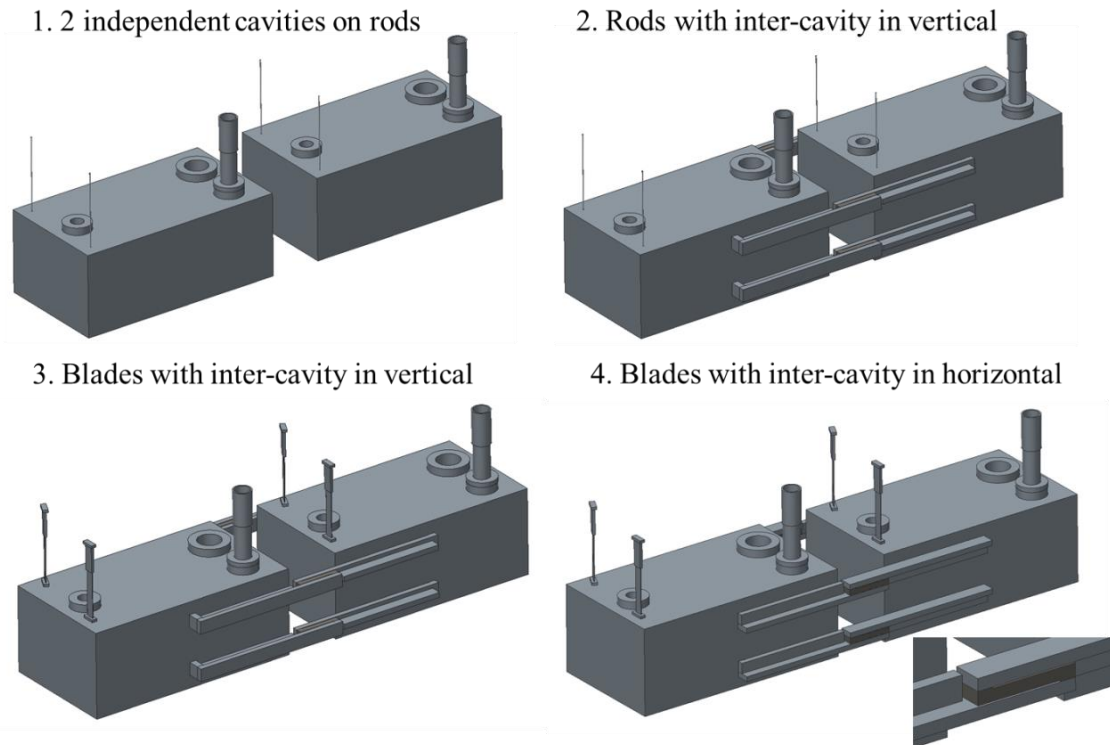
Figure 30. Inter-cavity support options

By using Finite Element Analysis it was shown that the use of the inter-cavity support in conjunction with the blade flexure supports offered improved performance over using a rod type support. However, there was no significant improvement over the individual blade supports described previously, some modes were even lowered due to the increased mass, as shown in Table 5. Note that cavity deflection for options 3 and 4 was ~0.026mm, shown in Figure 31, the maximum deflection was in the inter-cavity support itself. Invar, a strongly magnetic material, was used in the XFEL Cryomodule Cavity Support System with no detrimental effect on cavity performance (Petersen, 2008), however, it was still believed to be a risk to include in the cryomodule, adjacent to the cavities. The inter-cavity supports also prevent any relative motion between the cavities which may be a desirable feature. It was therefore decided to not implement this option within the cryomodule, but it may be useful in future cryogenic system applications.

Table 5. Inter-cavity support options

Analysis	Max Static Deformation (mm)	Max von-Mises stress (MPa)	Mode 1 Frequency (Hz)	Mode 2 Frequency (Hz)	Mode 3 Frequency (Hz)	Mode 4 Frequency (Hz)
1	0.24	65.2	8.5	25.3	38.3	70.9
2	0.43	61.8	12.6	20	27.5	34.3
3	0.063*	18.2	26.4	40.5	44.7	55
4	0.068*	24	26.1	40.9	44.9	55.1

*deformation of the inter-cavity supports.
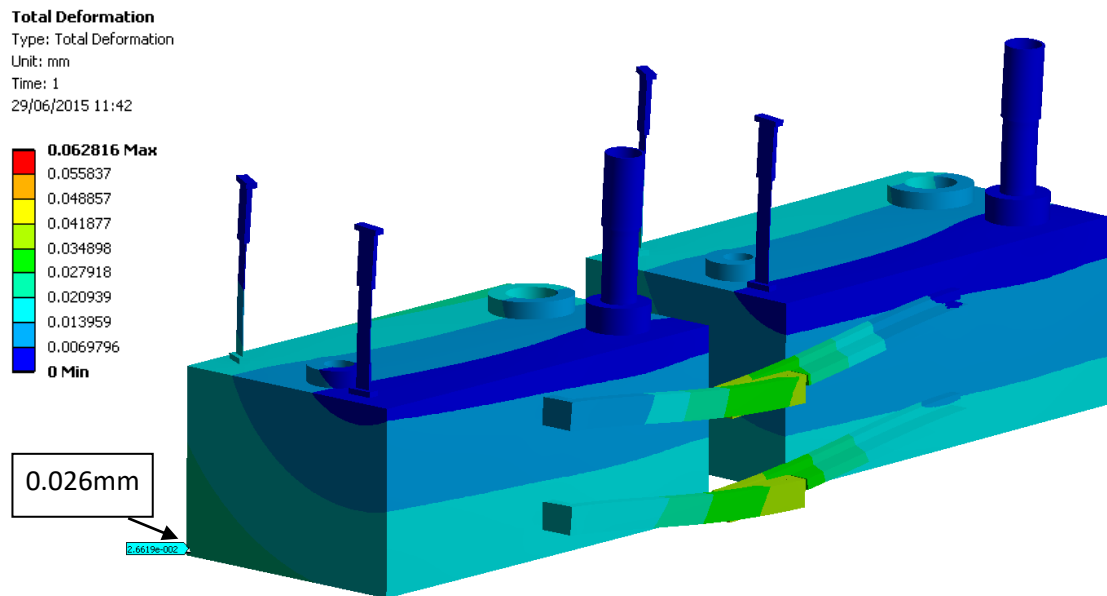
Figure 31. Deflection of inter-cavity supports

2.3.6. Support distance sweep

A parameterised analysis was performed without the inter-cavity support system to find the optimum distance from the coupler to the flexure supports, the results of which are shown in Figure 32. The flexures were moved closer to input coupler in steps of 50mm from 700mm to 400mm. It was found that deformation and stress reduce the further the blades are from the coupler. Due to the increased stiffness of the system, the modes of vibration increase the further the blades are positioned from the coupler. Therefore it was recommended that the blades be as far into the corners of the vessel as practicable.
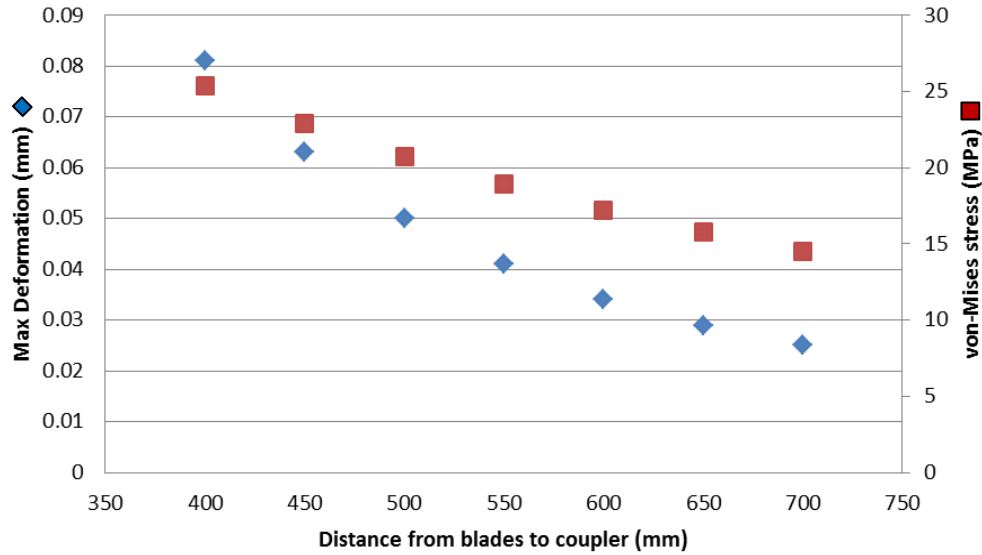
Figure 32. Deformation and stress vs. blade position

2.3.7. Blade width sweep

The width of the blade flexure was varied from 20mm to 60mm with the thickness maintained at 2mm. As expected the system stiffness increases (Figure 33). The negative is that heat leak to 2K increases at approximately the same rate. Therefore the overall cryogenic budget must be considered before increasing this width. Caution is also required here as the fundamental vibration mode approaches 50Hz. At this frequency the amplitude of ground vibrations is relatively high, as can be observed in Figure 17, (Ziemiański, 2014). Care should be taken to ensure the system is suitable stiff but avoids high peaks in the ground vibration spectrum. It was determined that a more detailed model of the dressed cavity and support system be analysed to gain an accurate estimate of the vibration modes.
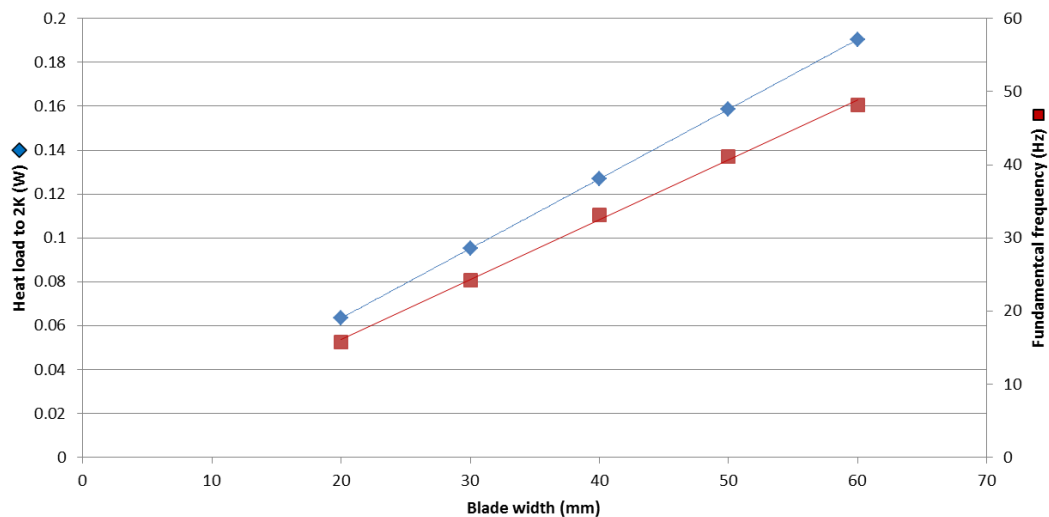
Figure 33. The effect of blade width on mechanical and thermal performance

2.3.8. Options analysis with DQW cavity

For completeness the options analyses were performed again with the DQW geometry and approximate mass at the time (the complete mass of the final dressed cavity design was ~250Kg). There is a requirement for a helium buffer tank above the main helium tank which limits the space available for the blade supports. Option 4 shown in Figure 34 represented the likely position of the blades in the final configuration within the Cryomodule. As can be seen in the results summary (Table 6) the blades in this position do not perform as well as the blades in the corners of the vessel, however, they still show a significant increase in performance over options 1 and 2.

1. Only coupler

2. Ø4mm Ti Rods

3. Two corner blades (2mm thick)

4. Blades in integration position
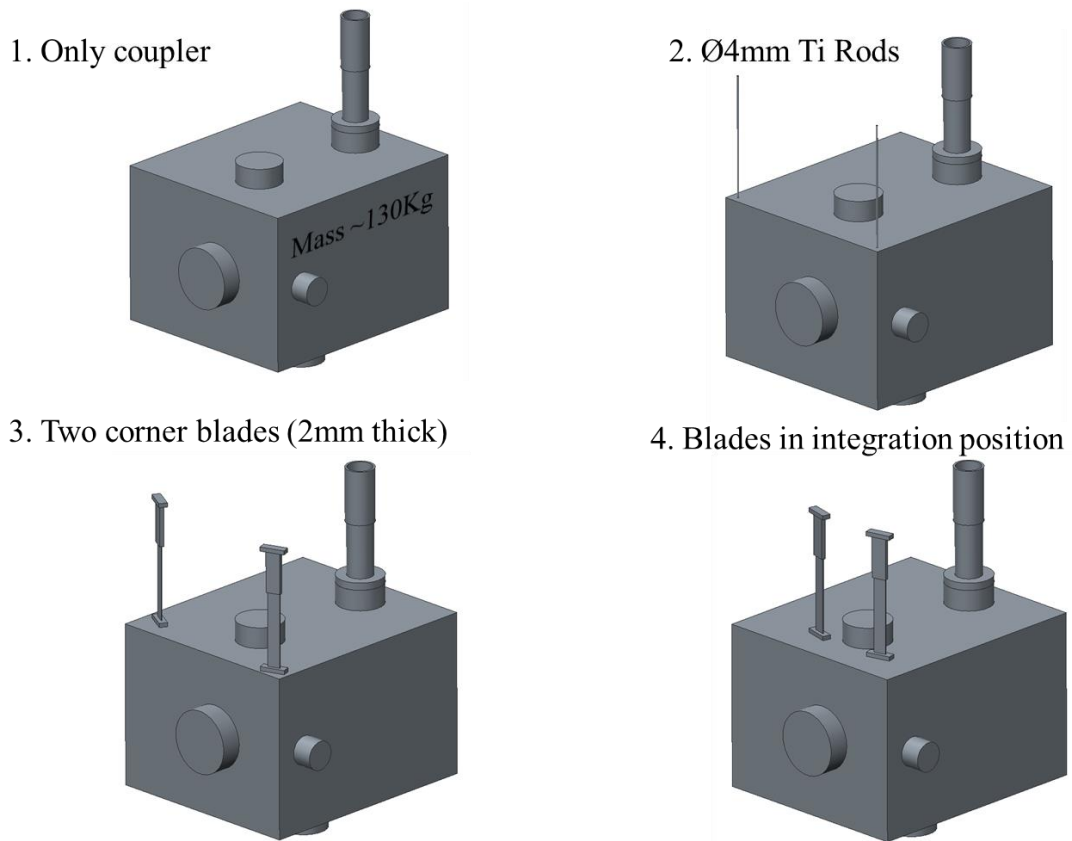
Figure 34. DQW cavity support options

Table 6. Summary of DQW support option results

Analysis	Max Static Deformation (mm)	Max von-Mises stress (MPa)	Mode 1 Frequency (Hz)	Mode 2 Frequency (Hz)	Mode 3 Frequency (Hz)	Mode 4 Frequency (Hz)
1	1.528	61.4	10.9	11.3	21	59.9
2	0.081	23.5	14.6	32	33.3	79.6
3	0.016	8.1	33.1	41.3	57.9	171.4
4	0.034	10.8	25.7	38.3	42.2	120.5

2.4. Studies using full engineering model

2.4.1. Preliminary design

As described in the previous section it was deemed necessary that a higher fidelity finite element model be created and assessed for mechanical stiffness and vibrational stability in order to identify problematic mechanical modes within the dressed cavity assembly. To assess the RF frequency response, the modal shapes would need to be analysed to assess the effect of each mode on the cavity shape. Transmission formulae, damping estimates and ground vibration acceleration spectral density data could then be used to predict deformation of the cavity. This can then be compared to parametric RF studies performed on the cavity shape in order to assess the effect on RF frequency. By incorporating the full dressed cavity into the model unforeseen issues were identified. The model was iterated several times, each design configuration is detailed within this thesis. The models were also assessed for; static deformation, cool down deformation from room temperature to 2K, and stresses under a transportation load of 1G in longitudinal direction (Department for Transport, 2002).
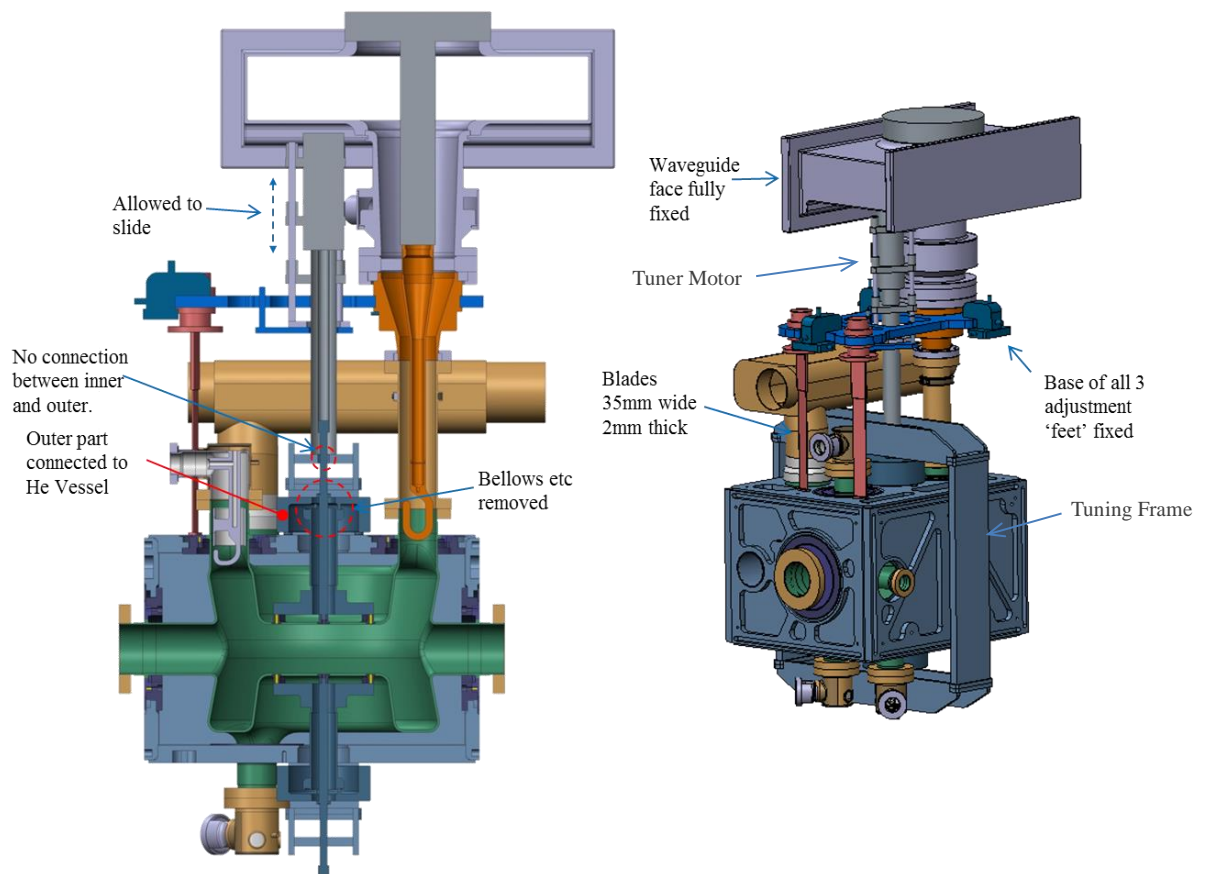
Figure 35. Full engineering model of dressed DQW cavity and support system

The design shown in Figure 35 was analysed in ANSYS Workbench for structural deformation due to the mass of the dressed cavity. The maximum rigid body deflection was 0.4mm for standard gravity conditions. The stresses in all structures were less than 20% of their yield. A Von-Mises stress of 8.5MPa was observed in the cavity, which was deemed acceptable. Using non-linear thermal expansion co-efficient values obtained from testing at Fermilab, (FERMILAB, 2013) a simulation of cavity cool-down from room temperature to 2K was also performed (Figure 36). These results showed no stresses above that of allowable limits. The main stresses under the thermal load are at the interfaces between the niobium cavity tubes and the stainless steel 316LN Conflat flanges. This is due to the significant difference in thermal contraction, however, the stress is below the allowable value of 400MPa for Niobium at 2K.
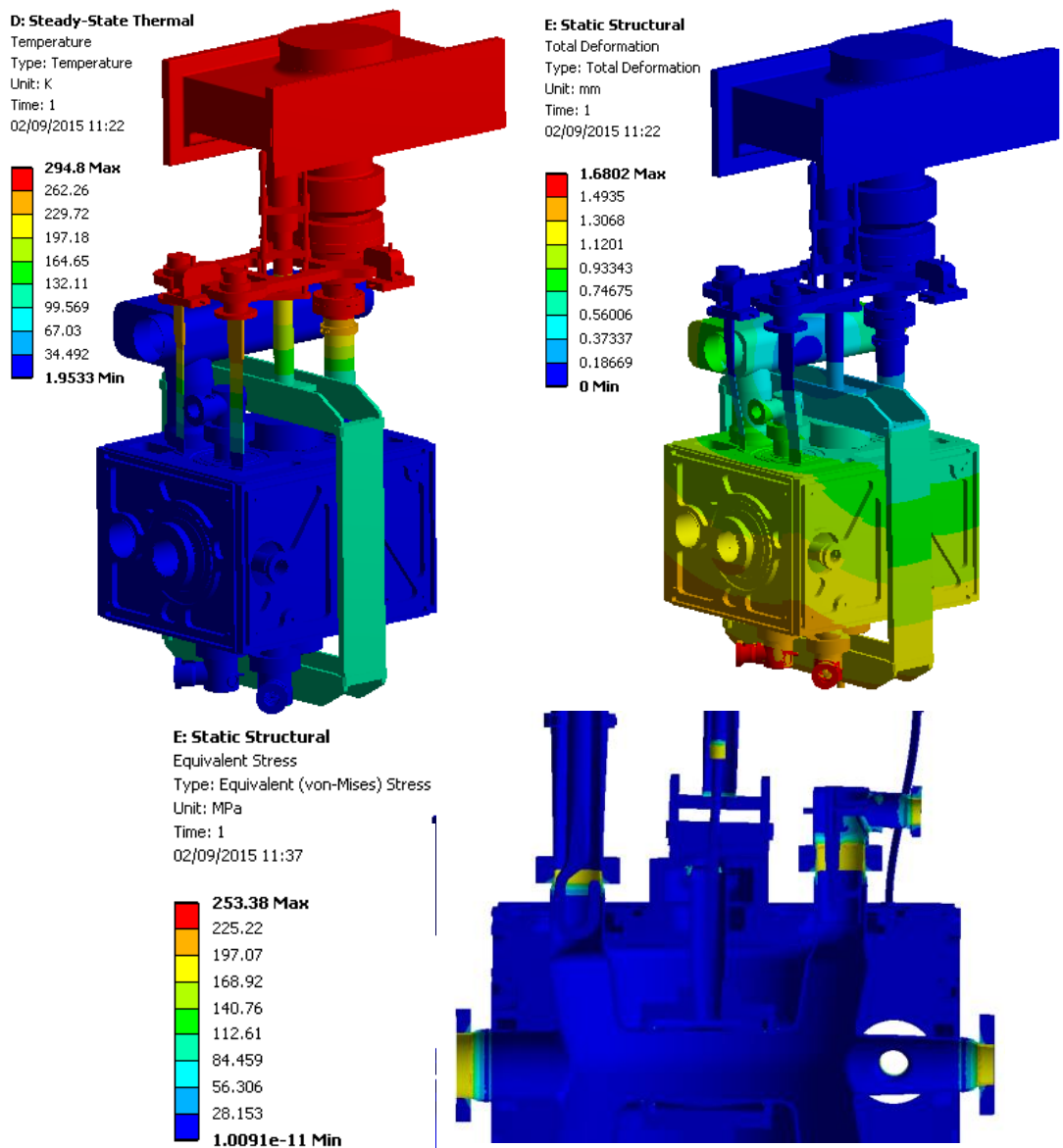
Figure 36. Cooled cavity temperature profile, deformation and stress

The model was also analysed using the ANSYS workbench modal solver in order to assess the first 10 mechanical vibration modes which are described in Table 7. One can see that the lowest modes are due to the cavity RF tuner mechanism 'rocking' both laterally and longitudinally. The fundamental modal shape is shown in Figure 37. It can be observed that tuner vibrations have a significant impact on the cavity shape and that the deformation is in one of the most sensitive regions of the cavity for RF stability. The deflection values shown on the left hand side of the image can be disregarded as in this modal analysis the driving frequencies and amplitudes have not been set. However, the relative values of deformations are valid and show that the cavity will deflect ~9-12% of maximum tuner amplitude in the tuning location. In order to assess the maximum deformation of the tuner, dressed cavity and other associated components, a transmissibility matrix was created in MS Excel based upon the following function (Sharma, 2005) modelling the system as a base excited single degree of freedom mass spring damper arrangement (more detail provided in Appendix A);

$$Transmissibility = \frac{Y}{X} = \sqrt{\frac{4\xi^2(\omega/\omega_n)^2 + 1}{[1 - (\omega/\omega_n)^2]^2 + 4\xi^2(\omega/\omega_n)^2}} \quad [Eq. 10]$$

Where; Y is displacement of the supported mass, X is displacement of the base of the support, ξ is the fraction of critical damping, ω/ω_n is the ratio of ground forcing frequency to the natural frequency of the supported mass.
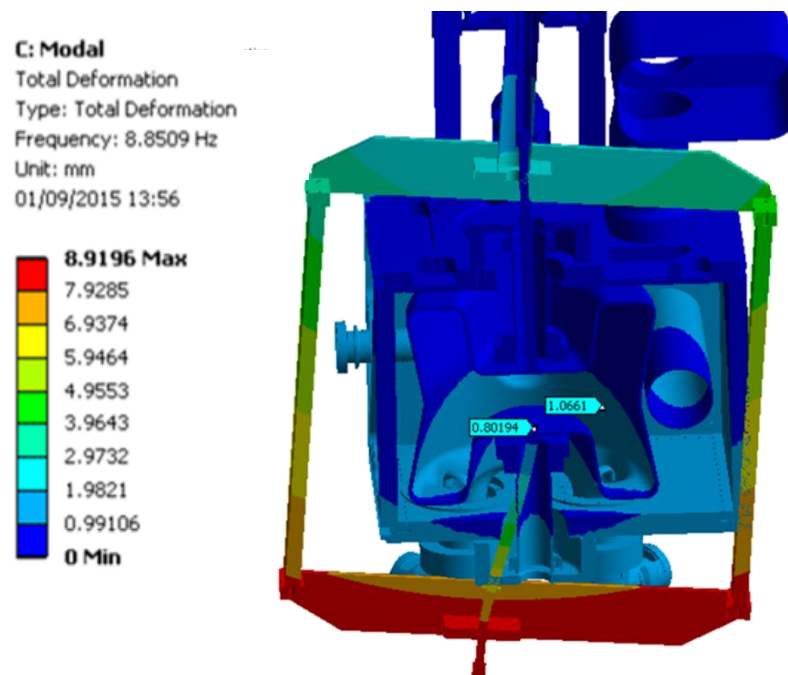
Figure 37. Relative cavity deflection due to 1st mode tuner movement

Table 7. Modal performance of 35mm wide flexures

Mode	Frequency (Hz)	Description
1	8.9	Tuner swinging laterally
2	9.9	Tuner swinging longitudinally
3	11.7	Tuner twisting about vertical axis
4	12.7	Cavity rotation about coupler
5	23.8	Cavity rotation about beam axis
6	26.7	Cavity and top plate twist
7	38.0	Tuner motor swinging laterally
8	38.7	Tuner motor swinging longitudinally
9	48.0	Helium reservoir swinging vertically
10	55.2	Tuner frame bending at corners

For each of the first 10 vibration modes of the cavity the transmissibility was calculated at each frequency band. This was then multiplied by the amount of ground movement at this frequency to give a plot of deformation vs frequency for each mode, shown in Figure 38 and Figure 39. There are often several peaks for each mode in close proximity (with regard to frequency), to capture the full displacement of the mode the contribution of each frequency band was combined using the root of the sum of the squares (RSS) method, also known as the integrated RMS value.

$$\text{Root of the Sum of the Squares (RSS)} = \sqrt{(Y_1{}^2 + Y_2{}^2 + \cdots + Y_n{}^2)} \qquad [\textit{Eq. 11}]$$

Where Y in this instance is the amplitude of ground vibration in nm for a given modal frequency (see Eq. 10) and within a given frequency band (or bin size).

Equation 11 provides an anticipated peak amplitude of each mode due to the given set of ground vibrations, shown in Table 8. As one can see the peak at the resonant frequency is normally the largest contribution to the RSS value, however, the width of peaks can vary, and modes can have several side bands that are periodically in phase with the central peak and would provide a larger detuning at the modal frequency in the cavity. Quote from Tom Power's presentation at SRF2017 "Random noise will come both in phase and out of phase with the vibration created at the mode of the structure and the microphonics will build up and down over time" (Powers, 2017). The RSS

value is used as it provides a realistic worst case maximum for each mode, i.e. when peaks and random noise are in phase.

As discussed previously lower modes are not excited by higher frequency vibrations when $\omega/\omega_n > \sqrt{2}$, and the transmissibility falls below that of the ground vibration at these frequencies. The integrated RMS values for individual modes do not necessarily add together, as the modal shapes are different, and affect different parts of the dressed cavity, for example the upper helium reservoir and the cavity tuner are not directly coupled mechanically, therefore will oscillate independently. There is, of course, the strong possibility of deflections due to the various vibration modes adding together which further supports the argument to reduce vibration levels to as low as reasonably practicable. The main focus of this work is to find problematic modes and suggest areas of the design that could be improved. This work does not consider forced vibrations whereby the driving forces act directly on the supported mass (the cavity in this instance). In reality this is a possibility as the cavity is also connected via the cryogenic system to both ground and potentially external vibration sources. The design of the cryogenic system is outside the scope of this work, however, it is understood that the pipework should be designed such that the cavity is decoupled from sources of vibration which would act directly on the cavity. These forced vibrations would appear as microphonics at the driving frequency, not the frequency of the mode excited.

Cavity deflections due to base excitation were calculated for both sets of data, 'Quite SPS' and 'DLS' in order to have a range of realistic scenarios. For all results a very conservative value of 0.001 for the fraction of critical damping, ξ, was used. The Ground Vibration input data used was measured in the vertical orientation, however, this motion was applied as a 'typical' driving frequency for all modes, regardless of direction. This was accepted as it provides a conservative estimate, with vertical ground vibration higher than either lateral or longitudinal in the case of the higher noise DLS data (Huang, 2006).
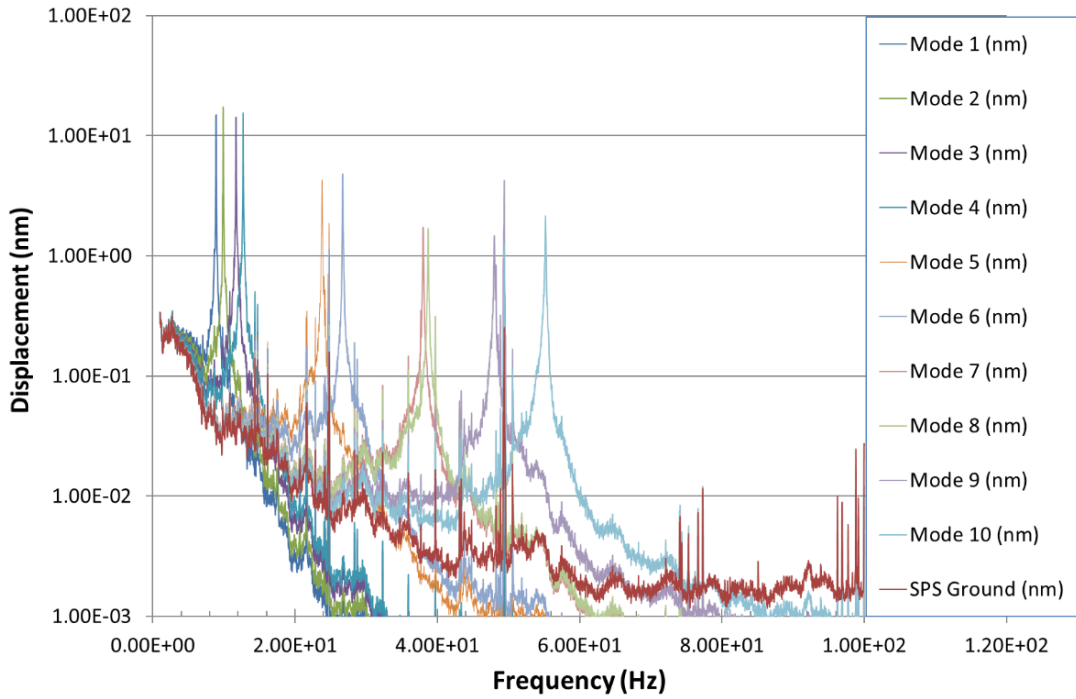
Figure 38. Preliminary Design: Ground and Cavity Modal displacement under quiet SPS ground conditions
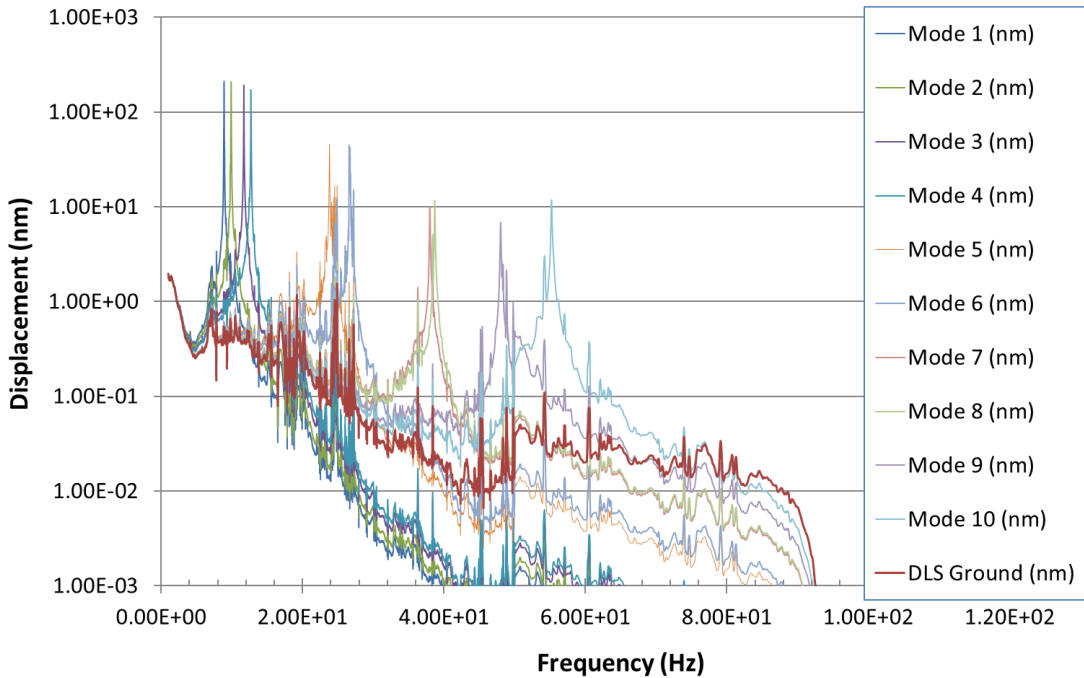
Figure 39. Preliminary Design: Ground and Cavity Modal displacement under DLS conditions

Natural frequencies ~10Hz involving tuner movement have been observed previously in the SRF community, for example, in the CEBAF 12GeV Upgrade Cryomodules (Davis, 2012). This study is of particular interest as it utilises a similar 'scissor' tuner design. In this case resonant frequencies were observed in the cavity string at 10.5Hz, 20-25Hz and 40-45Hz. Peak RF detuning was measured at 10.5Hz with an amplitude of RF frequency detuning of 21Hz, approaching the maximum allowable value of 25Hz (Davis, 2012), note RMS values are shown in Figure 40 not peak-peak. By stiffening the tuner mechanism engineers at CEBAF were able to reduce peak detuning by an average of 42%.
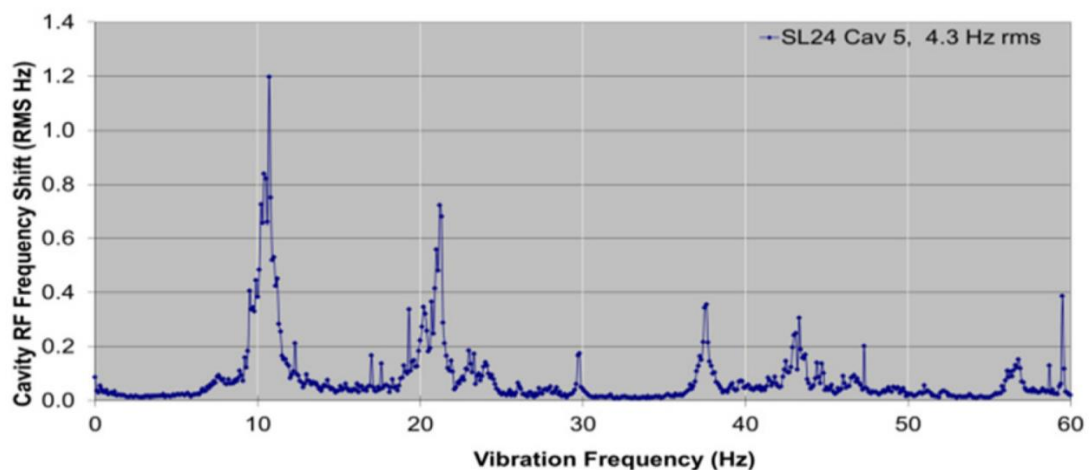
Figure 40. Mechanical Vibration contribution to RF Detuning (Davis, 2012)

From Table 8 we can anticipate a worst case tuner frame deformation of ~307nm RSS. As discussed previously, cavity deformation is 9-12% of the total tuner movement. In the central region of the cavity that is affected by the tuner it has been shown that cavity RF frequency sensitivity is 372kHz/mm (Verdu-Andres, 2015). If we assume 12% of total movement of 307nm, this gives deflection of the region of 36.84nm, which gives an RF detuning at a level of 13.7Hz for Mode 2. This is the detuning due to one mode only, deformations due to other modes would likely add to this giving a higher value, plus the effect of deformation of other regions of the cavity not considered in the calculation. Peak values of deformation due to seismic spikes in ground vibration may also be as high as 6x this value (Davis, 2012), therefore peak detuning would likely be out of the allowable 100Hz detuning range. Due to the relatively high values observed it was determined from this initial work that the first 4 cavity modes were too low and therefore additional stiffness was required in both the cavity support and tuner mechanism.

Table 8. Preliminary design: RSS displacement (nm) from 1Hz to 100Hz for the first 10 modes (35mm wide flexures used)

Facility	Ground	Mode									
		1	2	3	4	5	6	7	8	9	10
SPS	3.68	24.8	28.9	23.1	25.5	10.8	11.6	6.11	6.02	9.61	7.49
DLS	20.2	297	307	286	265	121	158	36.9	40.5	31.3	27.5

In addition to modal analysis, finite element studies were performed of the dressed cavity under a 1G longitudinal acceleration, with the aim of simulating a transportation shock load, such as a 'pot hole' or severe braking. The value of 1G static load is taken from The Department for Transport Safety of Loads on Vehicles, Code of Practise (Department for Transport, 2002). It is understood that dynamic loads during handling could be higher than this, and these would be assessed as part of future work outside the scope of this thesis. For transportation of the cryomodule whilst at CERN a 1G load limit in all directions was set and this was carefully monitored. The results (Figure 41) show that at 1G the tuner would be thrown forward relative to the helium vessel, inducing stresses in excess of the yield strength of the Niobium which is 70MPa. Due to these combined factors an improvement to the tuner design was developed and analysed as shown in Figure 42. This design incorporates flexures between the tuning frame and the helium vessel in order to minimise tuner movement.
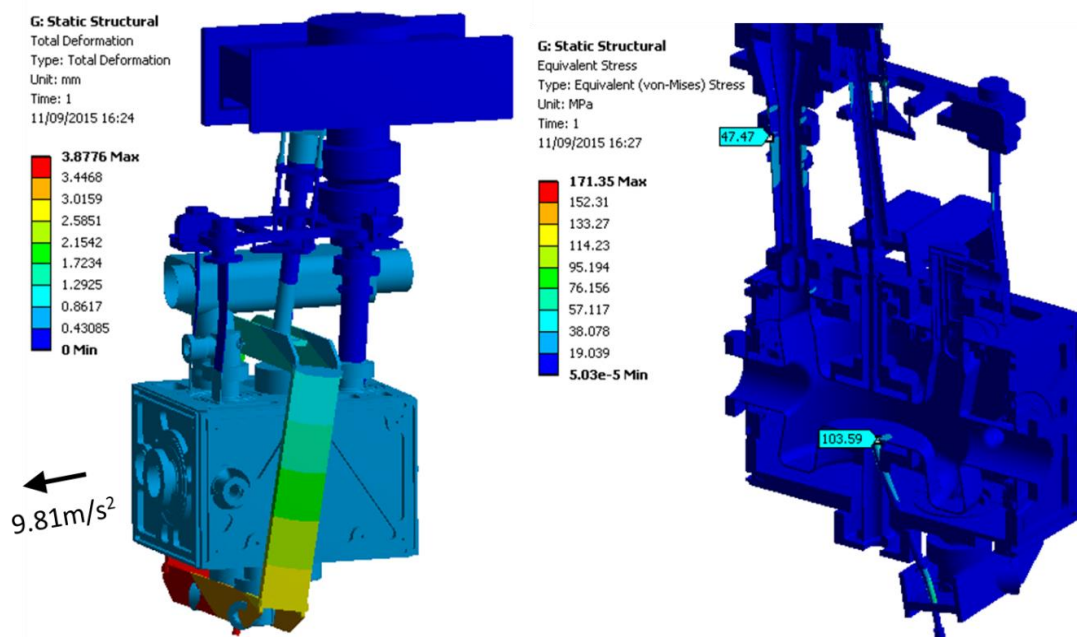
Figure 41. Cavity under 1G acceleration load, no tuner modifications
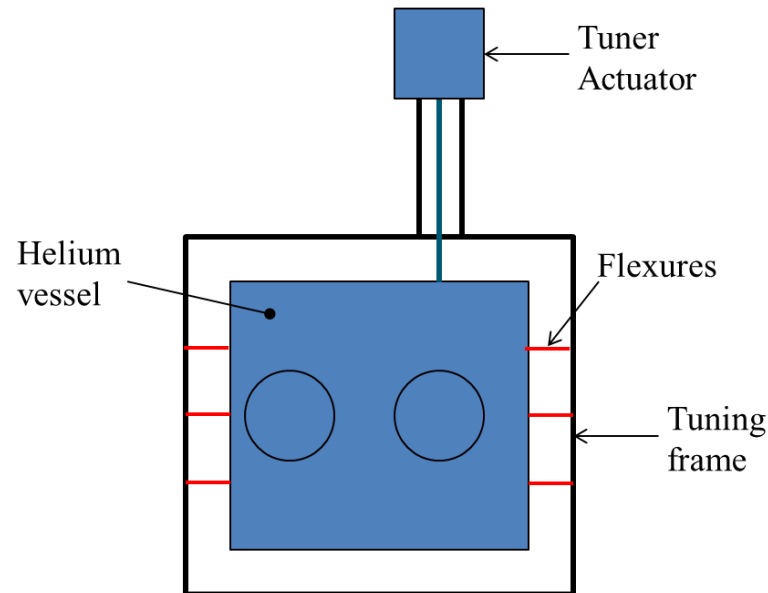
Figure 42. Proposed tuner improvement

An FE Modal analysis was performed with 3 x 4mm thick grade 2 titanium flexures per side between the frame and the helium vessel. The performance was vastly improved with the first two tuner vibration modes increased to 41.3Hz and 42.0Hz. The results were inputted into the transmissibility solver and gave the result spectrum shown in Figure 44. The integrated RMS value from 1Hz to 100Hz was reduced to 28.2nm for the 41.3Hz mode. Despite these promising results, it was believed that integration of flexures at this location may be problematic, in terms of assembly and may lead to additional heat leak to the helium vessel from the tuner frame. Therefore the mass of tuner frame was reduced and a flexure was added to the base of the tuner frame, linking the inner and outer actuators (Artoos K. , 2015b), shown in Figure 45. The implemented flexure allowed axial tuning but maintained lateral stiffness of $17x10^6$ N/m. However, there were still low modes (<15Hz) found for tuner rotation. Results for this revised design are shown in the next section, along with improvements to the cavity support flexures. Later in the project (in 2017) the design team at CERN returned to these analyses and decided to implement the tuner blades suggested here. This will be covered in the analysis of the final detailed dressed cavity design (Sub-Section 2.5).
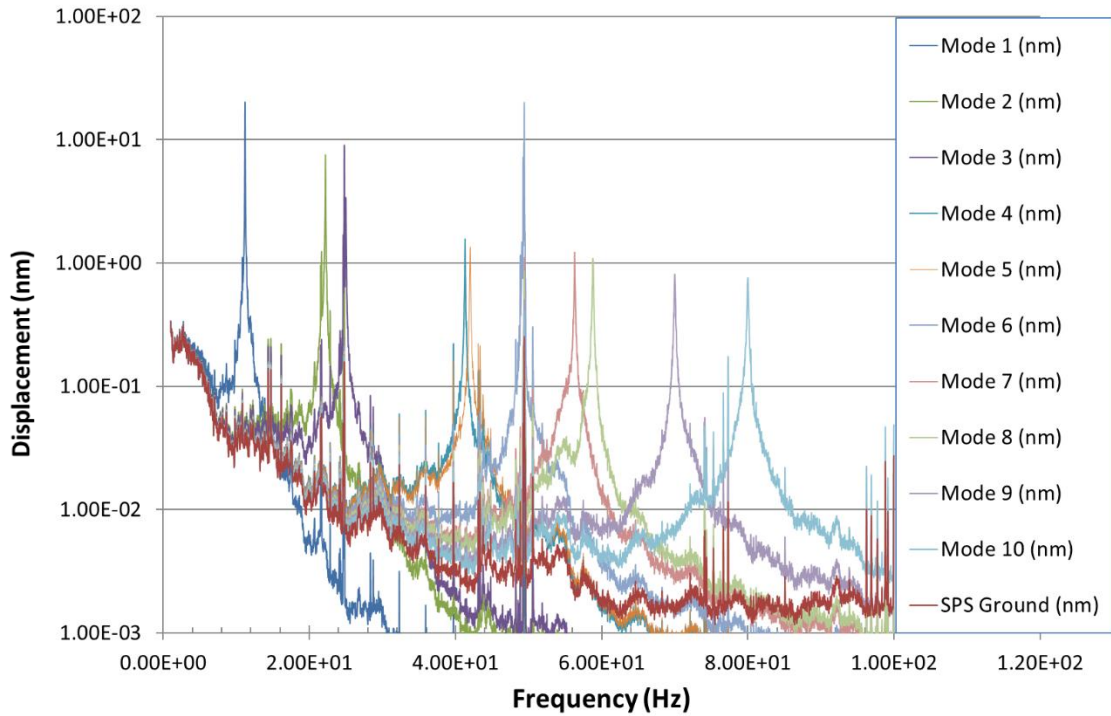
Figure 43. Tuner Flexure: Ground and Cavity Modal displacement under quiet SPS conditions
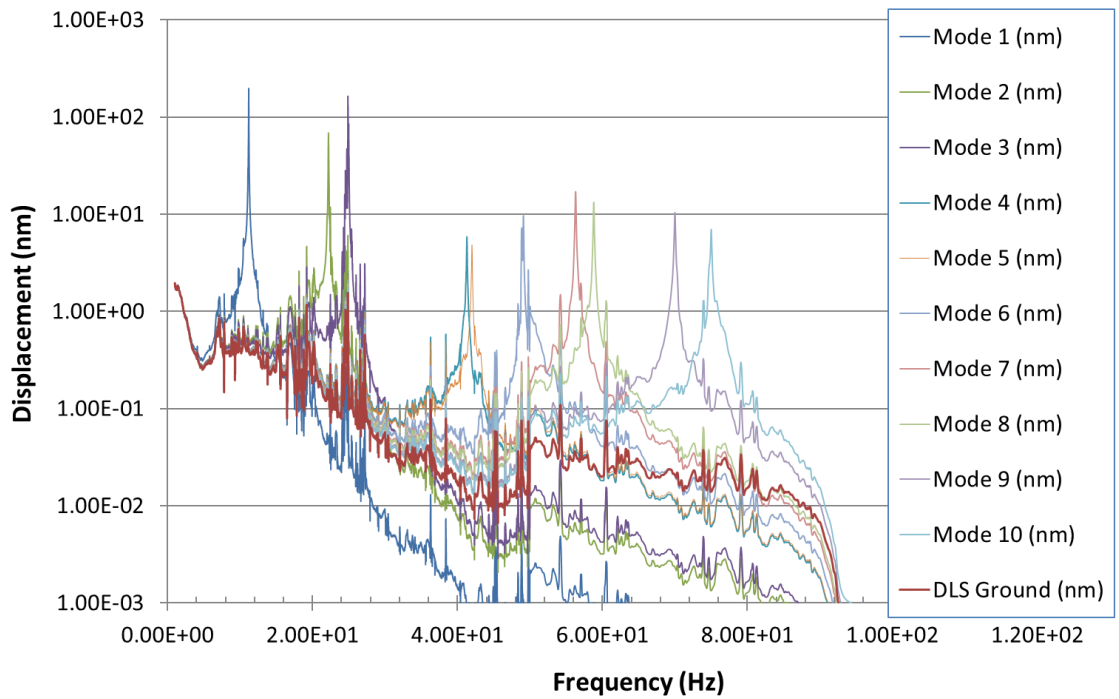
Figure 44. Tuner Flexures: Ground and Cavity Modal displacement under DLS ground conditions

2.4.2. Model for design review – 10/11/15

The design shown in the previous sub-section was reviewed internally, however, it was believed that for critical areas of the Crab Cavity Cryomodule a peer review was required with independent external reviewers. This was held at CERN on 10th November 2015. A revised model of the support structure was presented. This included the revised tuner design, and in addition the allowable heat leak for the flexure supports was increased to 1.2W in the cryogenic budget, allowing for 75mm wide, 2.5mm thick flexures. The design is shown in Figure 45.
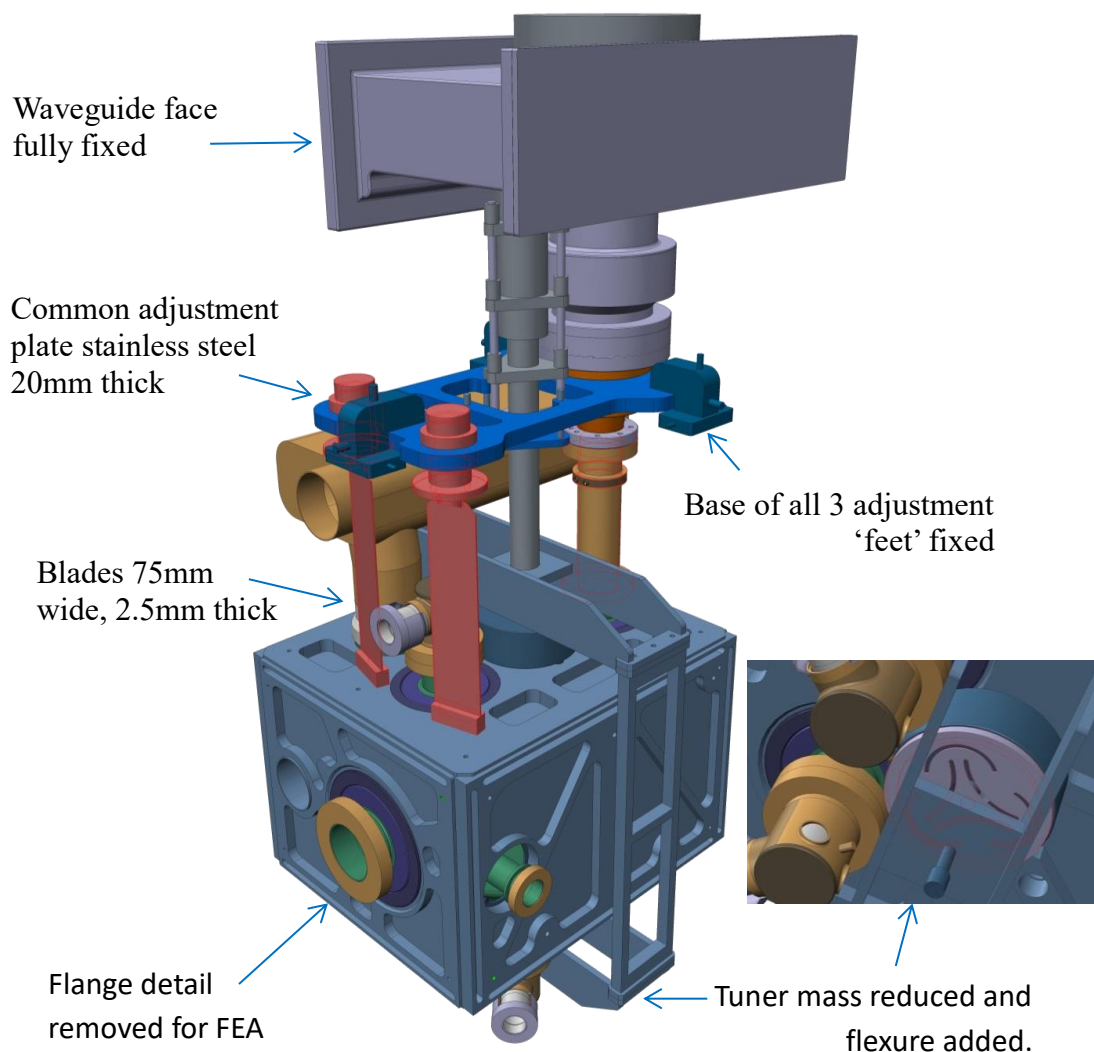
Figure 45. FEA model for external review November 2015
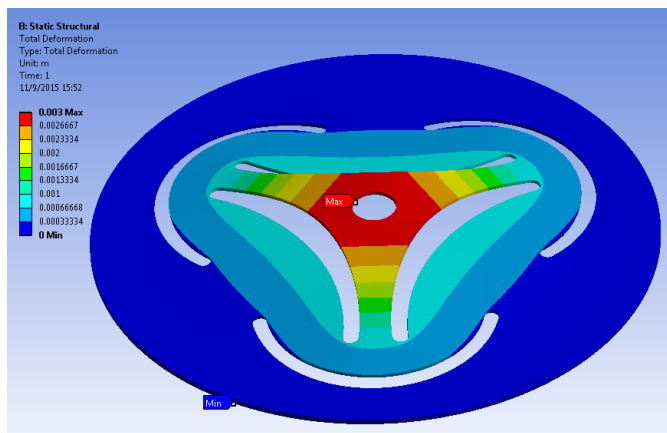
1mm thick Gr. 5 Titanium

+/-3 mm displacement

Axial stiffness 22 N/mm

Lateral stiffness 1.7 kN/mm

Torsional stiffness 0.1 mrad/Nm

Figure 46. CERN Tuner Flexure Design for review November 2015 (Artoos K. , 2015b)

Table 9. Modal performance of 75mm wide flexures

Mode	Frequency (Hz)	Description
1	12.649	Cavity and tuner swinging laterally
2	14.345	Tuner twist about central axis
3	23.028	Cavity and tuner swinging longitudinally
4	31.464	Cavity and tuner rotation about coupler axis
5	34.991	Tuner swinging longitudinally
6	35.683	Tuner swinging laterally
7	50.3	Tuner twist about central axis with frame twist
8	54.346	Helium reservoir tank motion
9	55.994	Helium reservoir tank motion
10	56.748	Tuner bending at corners

Table 10. Review model: RSS displacement (nm) 1Hz to 100Hz for the first 10 modes

Facility	Ground	Mode									
		1	2	3	4	5	6	7	8	9	10
SPS	3.68	25.8	73.0	10.9	8.8	7.6	8.7	14.0	8.5	5.9	5.6
DLS	20.2	265.2	202.6	125.5	48.0	51.1	54.0	36.4	44.4	29.9	29.1

The modal performance of the tuner is significantly improved in terms of lateral and longitudinal movements. These modes have increased from 9.9 and 8.9 to 35.0 and 35.7 respectively. The peak amplitude of the oscillations has decreased by a factor of 6 from ~300nm to ~50nm assuming the worst case floor loading. The tuner rotation mode is still fairly low at 14.3Hz, giving a worst case amplitude of 203nm, however, cavity deformation due to this is less than 1% of this value and therefore acceptable. The

performance under the 1G transportation load is improved and now within acceptable limits. As can be observed in Figure 48, the stress in the cavity is well below yield. The highest stresses are in the power coupler at ~50MPa but this again is far less than the yield strength of stainless steel 316L which is ~205MPa (Peckner, 1977). Thermal stresses due to cool down from room temperature to 2K were also identified and deemed acceptable. All results can be found in the design review presentation (Jones T. , 2015).
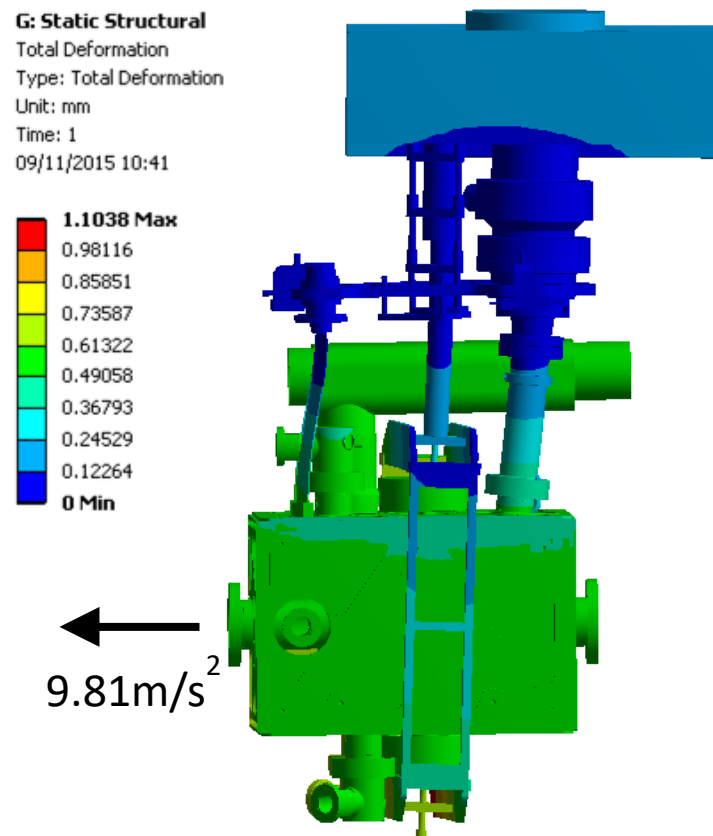
Figure 47. Dressed cavity deformation under 1G longitudinal transportation load
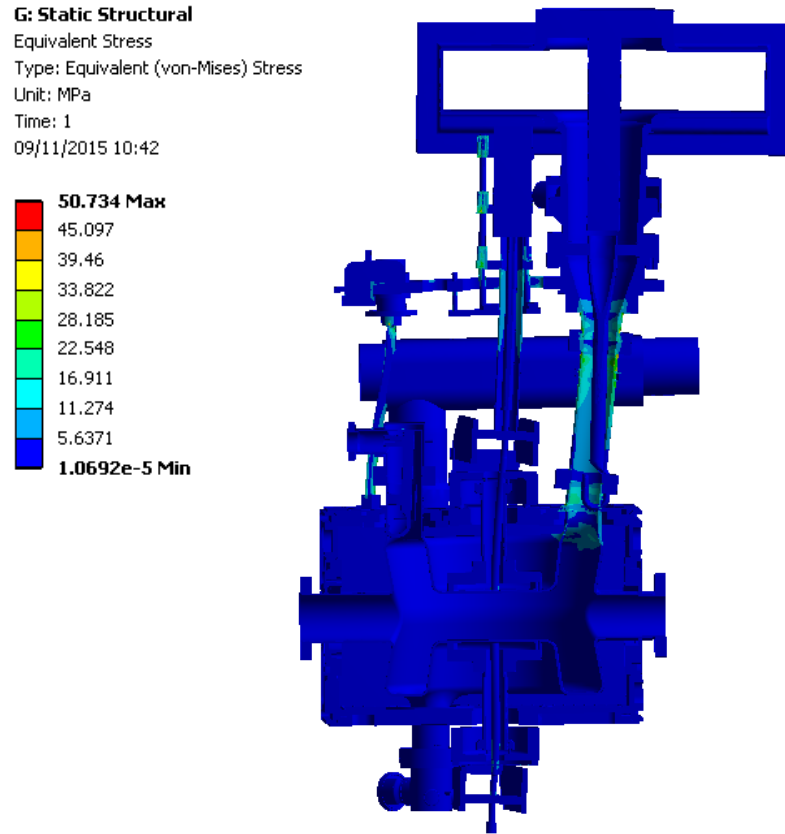
Figure 48. Dressed cavity stresses under 1G longitudinal transportation load
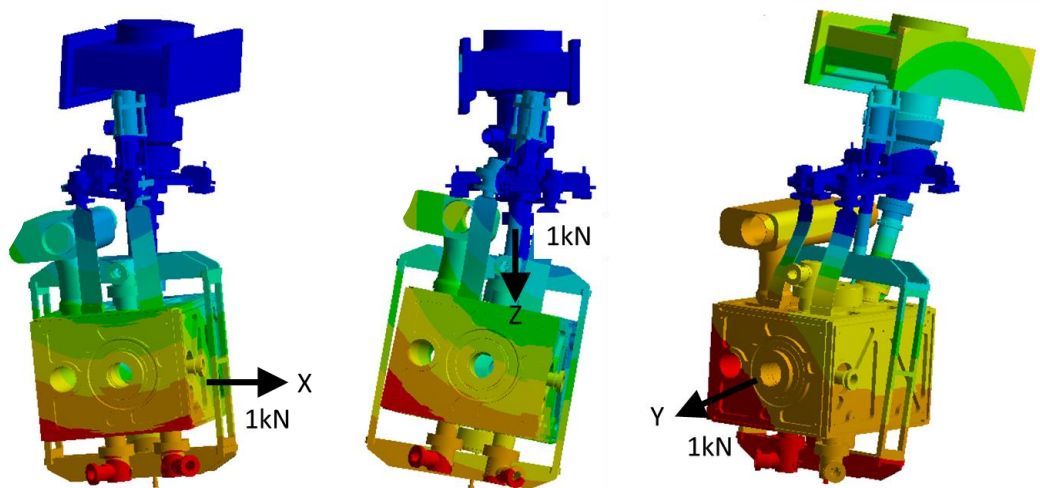
Figure 49. Amplified dressed cavity deformations under 1kN loading

Loads of 1kN were applied individually to each of the faces of the helium vessel as shown in Figure 49. The stiffness of the support system was then calculated using the inverse of the deformation result and these values are given in Table 11. Also in Table 11 are the values for the design described in the previous section for 35mm wide blades. One can see that the overall system stiffness in the X direction was not greatly

improved by the use of the wider blades as one might expect. This is also clear in the marginal improvements in the modal result for the cavity lateral swinging motion. The main recommendation of the review panel was to improve this stiffness to as high as reasonably practicable, within the thermal and geometrical boundary conditions. By analysing the fundamental modal shape (Figure 50) one can observe that the lack of stiffness in this direction is due to the rotation of the common top plate about the single support of the 3 point height and angle adjustment system. This was identified and corrected in the following design iteration (see section 2.4.3), and the stiffness results are also shown in Table 11.

Table 11. Directional stiffness of cavity support system options

Direction	Stiffness pre-review	Stiffness of review model	Stiffness post-review
X	0.62kN/mm	0.77kN/mm	1.83kN/mm
Y	1.58kN/mm	1.78kN/mm	1.70kN/mm
Z	6.87kN/mm	8.37kN/mm	25.79kN/mm
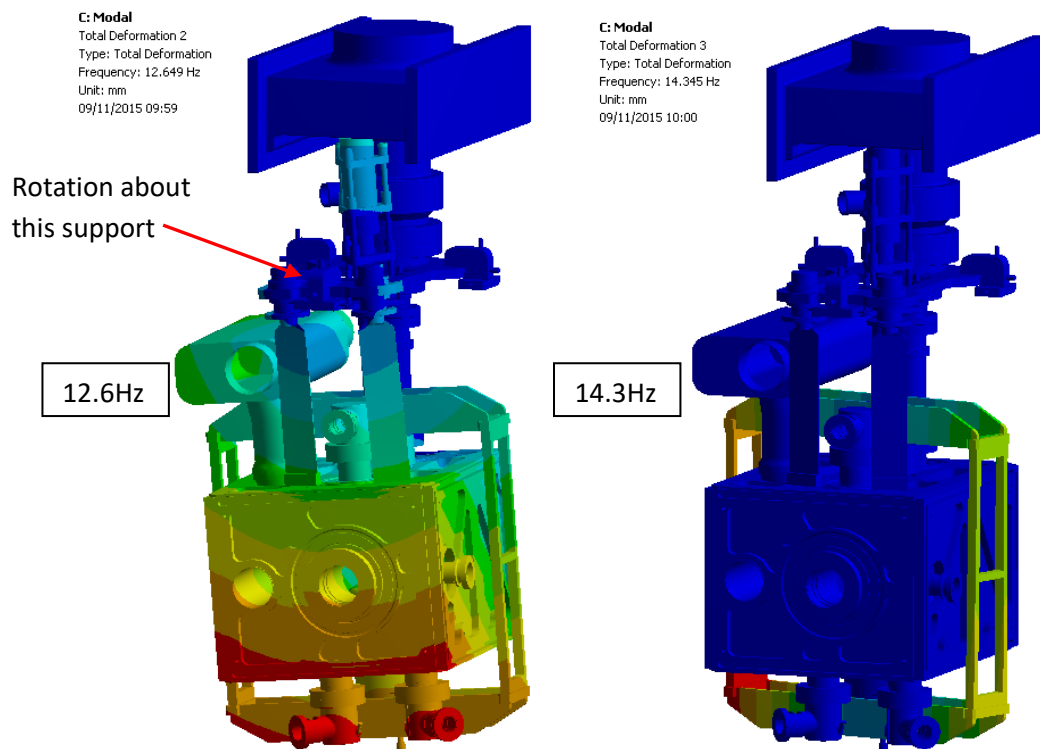
Figure 50. Lowest mechanical modes for design with 75mm flexures

2.4.3. Post review concept design

As previously discussed, improvements to the support structure were made following the design review at CERN in November 2015. The main design change was to the common support plate, altering the mounting technique from a common 3 point, cone, vee and flat type support, to a 5 point design with locking studs at each of the corners adjacent to the single point support end (Figure 51). This adds to the complexity of the cavity alignment methodology, which was the reason it was not implemented initially, however, the results show a significant improvement to the system stiffness, therefore, this was accepted by the survey and alignment group at CERN. One can see in Table 11 that the lateral stiffness improved by over a factor of 2. The vertical stiffness increased by over a factor of 3. Longitudinal stress is mainly reliant upon the stiffness of the outer conductor of the FPC and the configuration of the blades, which remained the same, therefore this stiffness was approximately the same.
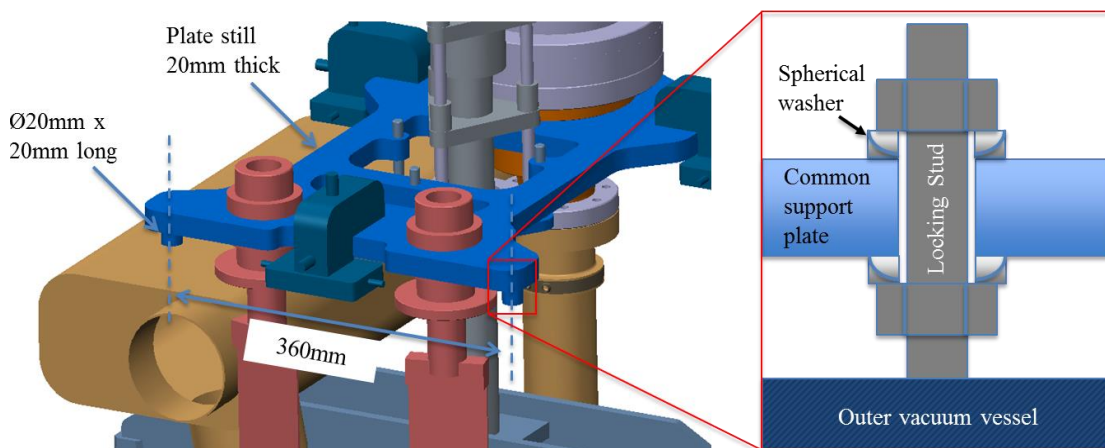
Figure 51. Post review common support plate adjustment system

Table 12. Modal performance of 5 point plate support

Mode	Frequency (Hz)	Description
1	14.258	Tuner twist about central axis
2	19.063	Cavity and tuner swinging laterally
3	22.93	Cavity and tuner swinging longitudinally
4	30.346	Cavity and tuner rotation about coupler axis
5	34.862	Tuner swinging longitudinally
6	35.582	Tuner swinging laterally
7	50.154	Tuner twist about central axis with frame twist
8	54.029	Helium reservoir tank motion
9	56.041	Helium reservoir tank motion
10	56.673	Tuner bending at corners

It can be observed in Table 12 that increasing to the 5 point mount has had a significant effect on the modal performance of the system. The cavity swinging mode has increased from 12.6Hz to 19.1Hz. This improvement has led to a reduction in vibration amplitude from 25.8nm to 14.7nm for the SPS ground vibration condition. Interestingly, there was a slight increase in the amplitude using the DLS ground data, which increased from 265.2nm to 301.4nm. This is due to the DLS facility having a local peak at 19.2Hz that the support structure is now coupling to. This peak is significantly greater than the amplitudes of the surrounding ground frequencies for example at 19.2Hz the amplitude is 1.2nm, at 19Hz it is 0.24nm. This highlights how critical having the correct vibration survey data for the area is. As the cavity will be installed on the SPS machine, it was deemed that the 5 point support should still be used, as it showed a significant improvement for the SPS ground vibration boundary conditions. Also as a general rule ground vibration amplitudes fall to the 4th power with increasing frequency, therefore stiffer structures are typically preferable. With any support structure one should aim to have no natural frequencies below 15Hz (Chao, 1999).

Table 13. Post Review: RSS displacement (nm) 1Hz to 100Hz for the first 10 modes

Facility	Ground	Mode									
		1	2	3	4	5	6	7	8	9	10
SPS	3.68	28.7	14.7	11.6	10.5	7.3	8.4	15.7	8.9	5.9	5.6
DLS	20.2	193.1	301.4	129.6	60.2	50.4	49.6	35.5	43.5	29.7	29.4
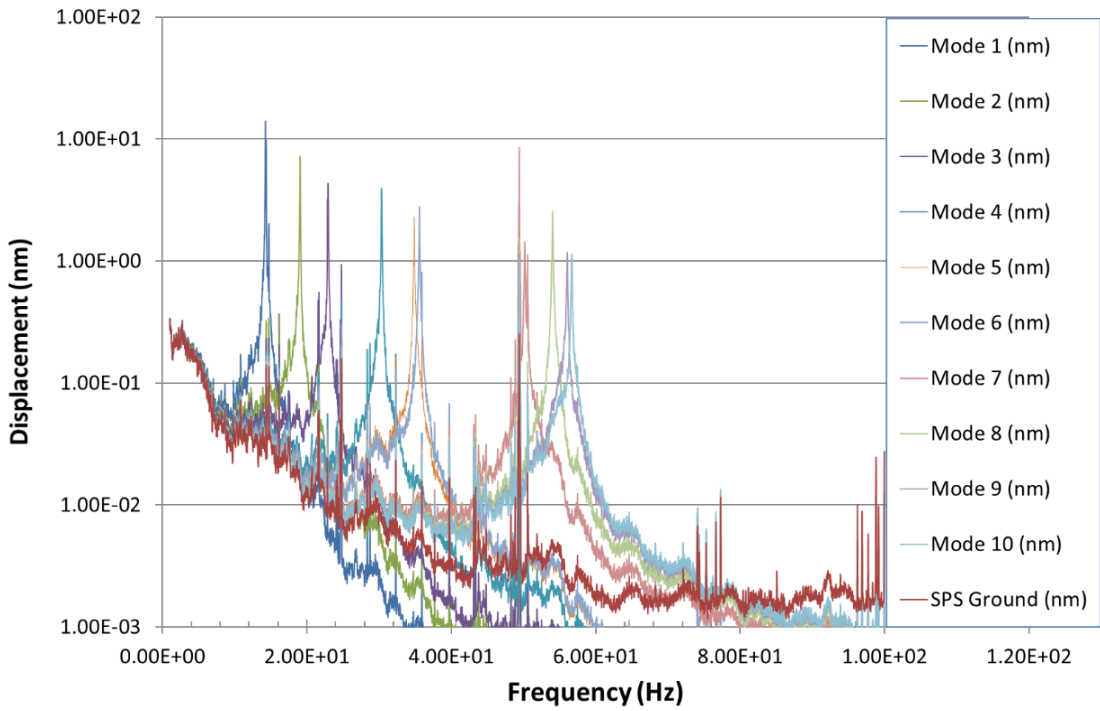
Figure 52. Post Review Design: Ground and Cavity Modal displacement under quiet SPS conditions
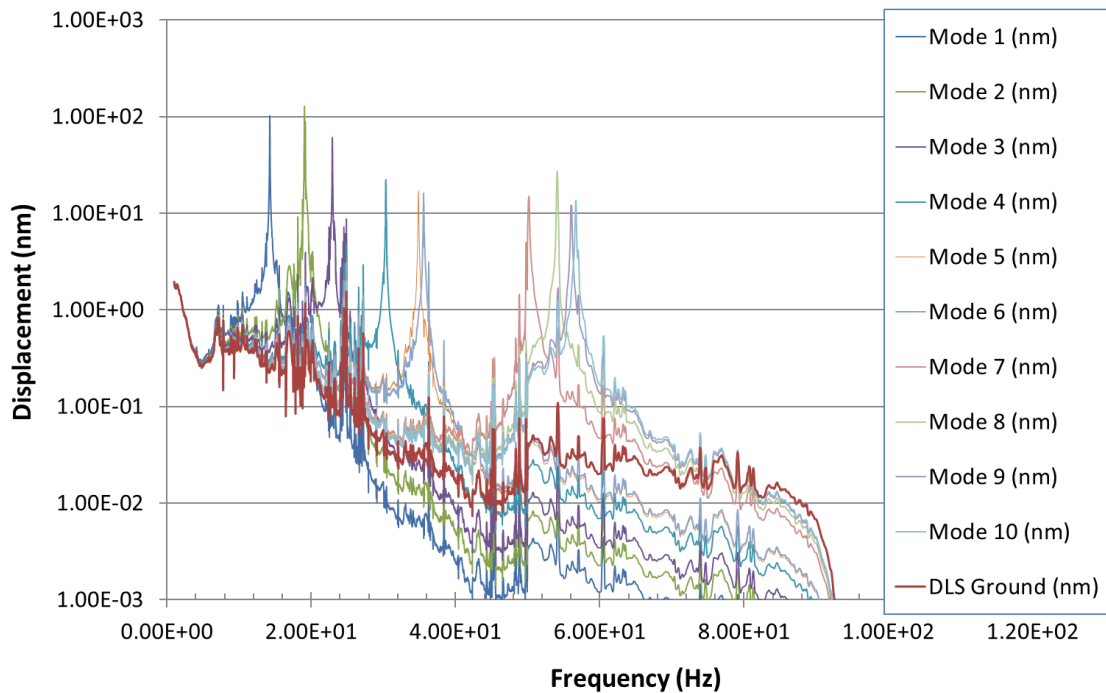
Figure 53. Post Review Design: Ground and Cavity Modal displacement under DLS ground conditions

2.5. Detailed Design of support system

As the design entered the detailed design stage in 2016 there were still concerns regarding the first mode of the tuner, which remained lower than 15Hz and therefore carried the potential to couple to high amplitude ground vibrations and detune the cavity. It was decided therefore to shift from the CERN designed lower tuner flexure to adding flexural blades to the tuner as proposed by the work of this thesis (shown in Figure 42). The detailed final design of the dressed cavity and associated support system is shown in Figure 54. The final tuner design is also shown, and this was reported in several conference proceedings (Artoos K. , 2015a) and (Artoos K. , 2019). Additional features were included within the blade design for ease of assembly and to allow accurate alignment, notably, screws at the top of the blade to allow the length to be adjusted and a locating dowel at the base to prevent vertical slip. Despite these features the blades still remain a simple 1 piece flexural mechanism, limiting the amount of components requiring analysis, specification, procurement, qualification and assembly. The thickness of the common support plate was increased from 20mm to 34mm and the thickness of the blades was increased from 2.5mm to 3mm, increasing the fundamental rigid body mode above 25Hz while remaining within the thermal budget.

A finite element model (shown in Figure 55) was generated for this design in order to assess the expected modes of vibration, transmission from ground vibration, system stiffness, thermal aspects and resilience to a 1G longitudinal transportation load. Complex parts such as the HOMs where replaced with single point masses in order to increase the speed of computation, modal analysis of these devices would be performed separately, outside the scope of this thesis. The colours of the model correspond to the material used, with values as per previous analyses (FERMILAB, 2013). The system was assigned a fully fixed boundary condition on the underside of each of the 5 point mounts which are themselves fixed to the common support plate. This boundary condition therefore assumes the vacuum vessel on which this system is mounted is infinitely stiff, which is not the case. For this assessment this was deemed an acceptable assumption. The vacuum vessel was structurally assessed separately and would be sufficiently stiff as to not dramatically affect the modal or any other performance of the cavity support system. Appropriate masses A through E were assigned to each of the mounting ports on the cavity. This was to minimise computation time as each of these components was analysed separately to the support system analysis.
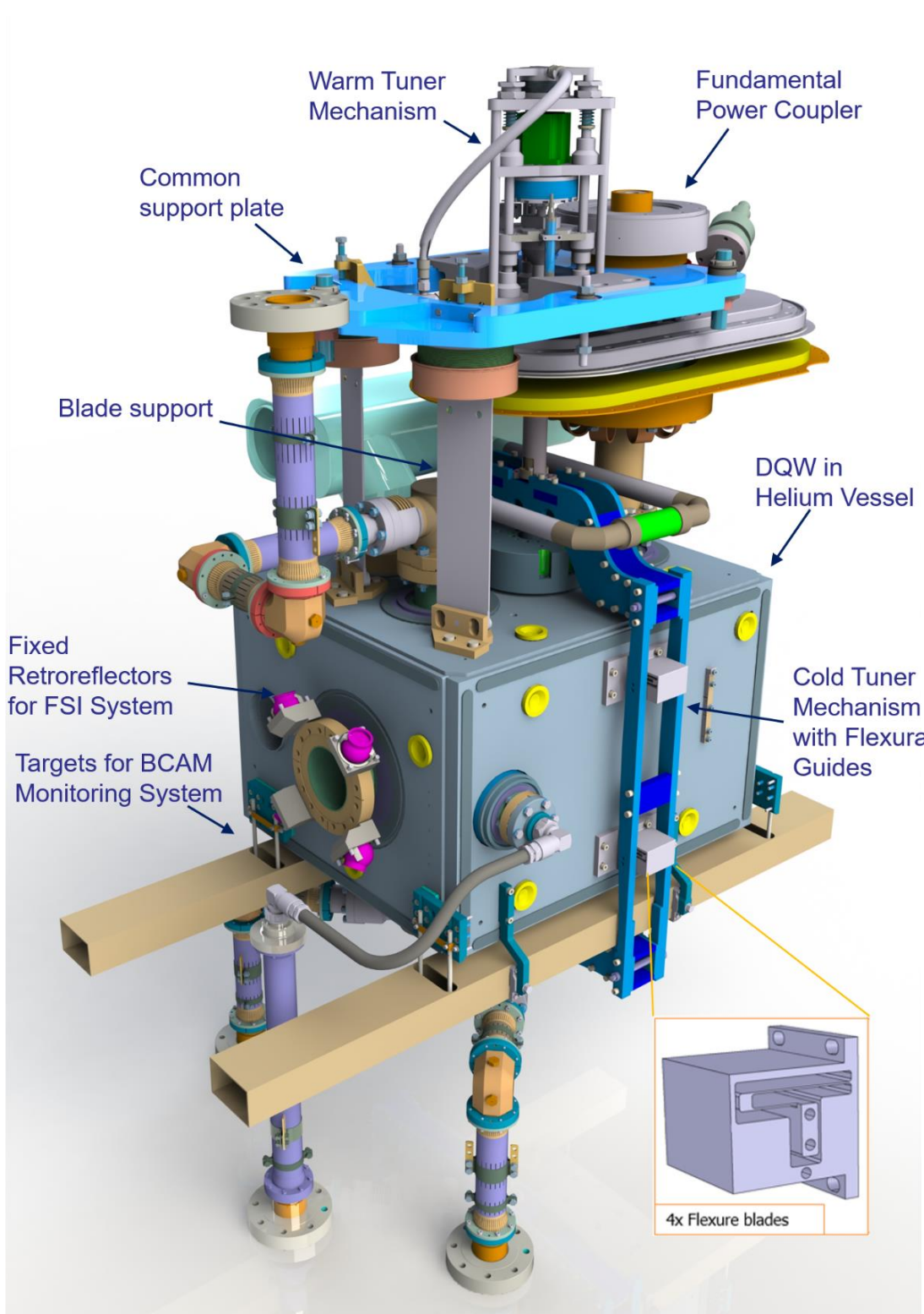
Figure 54. Crab Cavity Support System Detailed Design
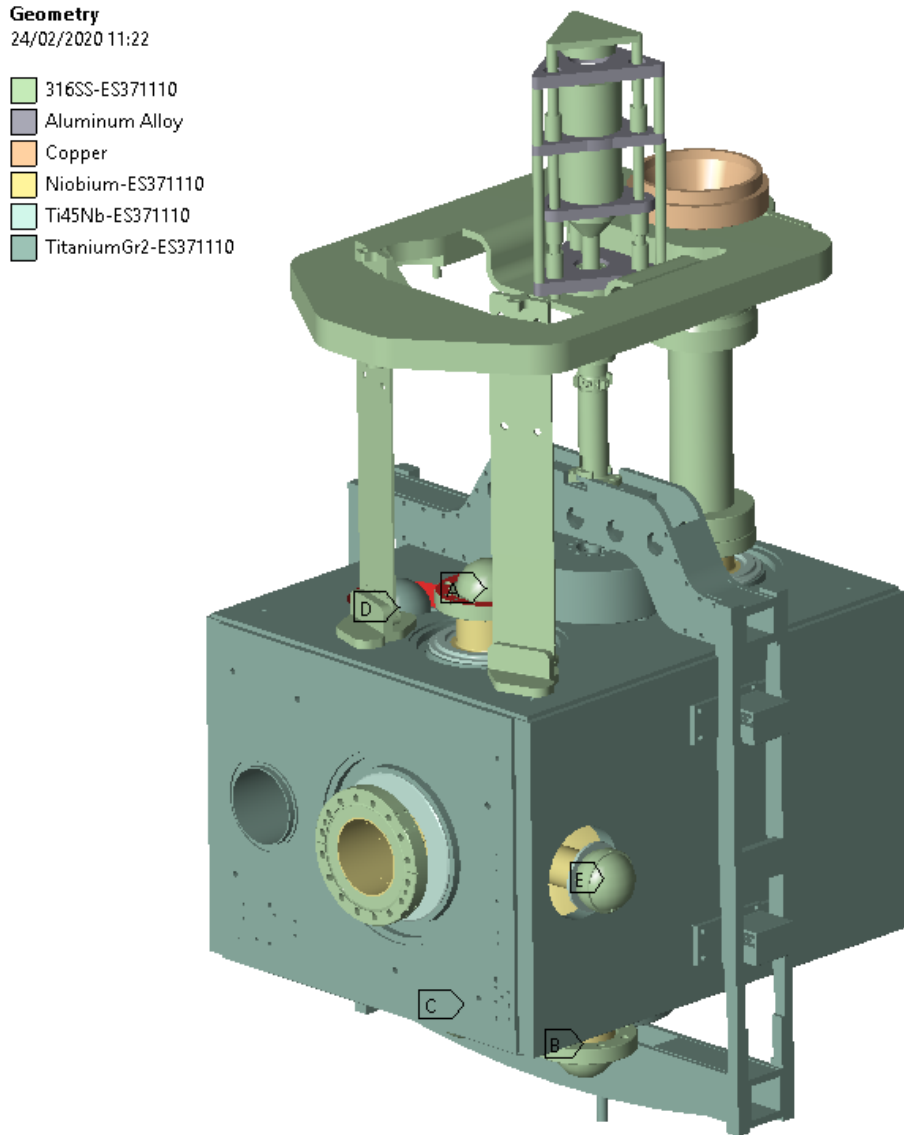
Figure 55. Final Support System Finite Element Model

2.5.1. Vibration studies and system stiffness

The first 10 modal shapes of the system are shown in Figure 56 and Table 14 summarises the mode frequencies. It can be observed that all modes are now above 15Hz. Comparing Figure 38 with Figure 57 one can observe a significant reduction in the number of modes with individual frequency displacement contributions above 1nm (from 12 to 3). The final design has no individual frequency displacement contributions >10nm for the quiet SPS data. For the relatively noisy DLS ground vibration spectrum shown in Figure 58 there are a number of displacement peaks in the 10-100Hz range but none above 100nm, compared to the preliminary design which had 4 peaks above 100nm. The significant improvement in performance can also be observed by

comparing the RSS displacements calculated for each mode of the final design (Table 15) against the previous design (Table 13).
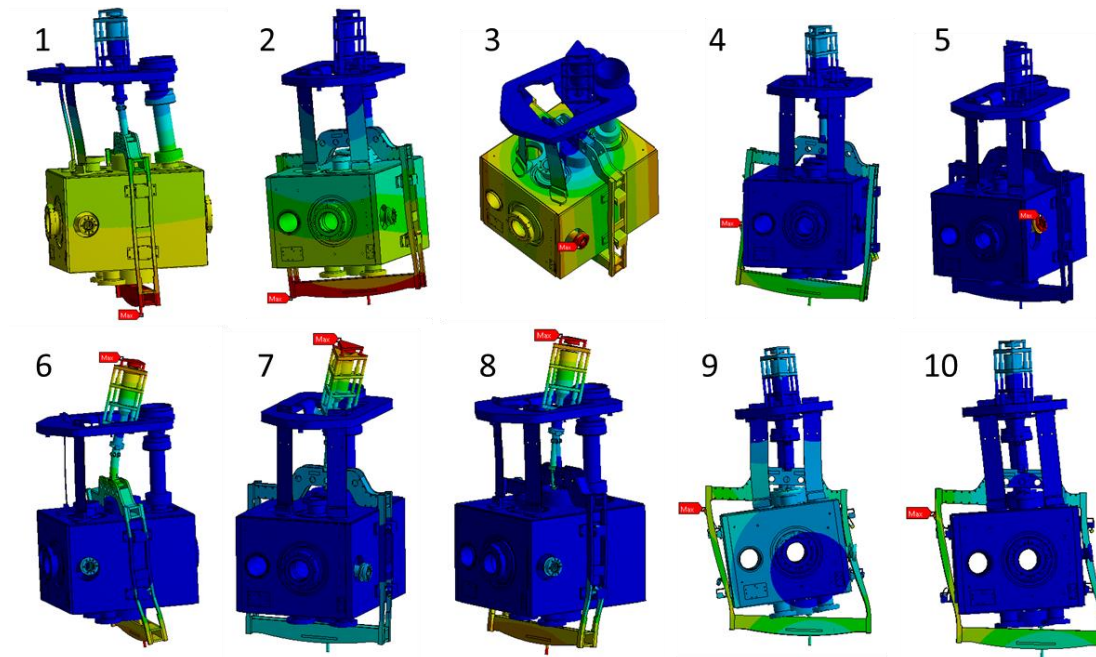
Figure 56. Final Cavity Support System Modes

Table 14. First 10 Modes of final detailed design

Mode	Frequency (Hz)	Description
1	25.5	Rigid body longitudinal swing
2	26.8	Rigid body lateral swing
3	56.1	Rigid body twist about tuner axis
4	67.1	Tuner Frame lateral swing
5	83.5	RF Probe port vertical
6	86.1	Tuner Frame Longitudinal
7	88.4	Tuner motor assembly lateral
8	102.1	Tuner motor assembly longitudinal
9	102.9	Rigid body roll about Cavity Axis
10	107.6	Tuner frame corner skew

Table 15. Final Design: RSS displacement (nm) 1Hz to 100Hz for the first 10 modes

Facility	Ground	Mode									
		1	2	3	4	5	6	7	8	9	10
SPS	3.7	9.2	11.6	5.8	4.8	5.0	4.9	5.1	4.0	3.9	3.7
DLS	20.2	173.1	160.5	30.9	25.9	23.9	23.1	22.0	20.5	20.5	20.4
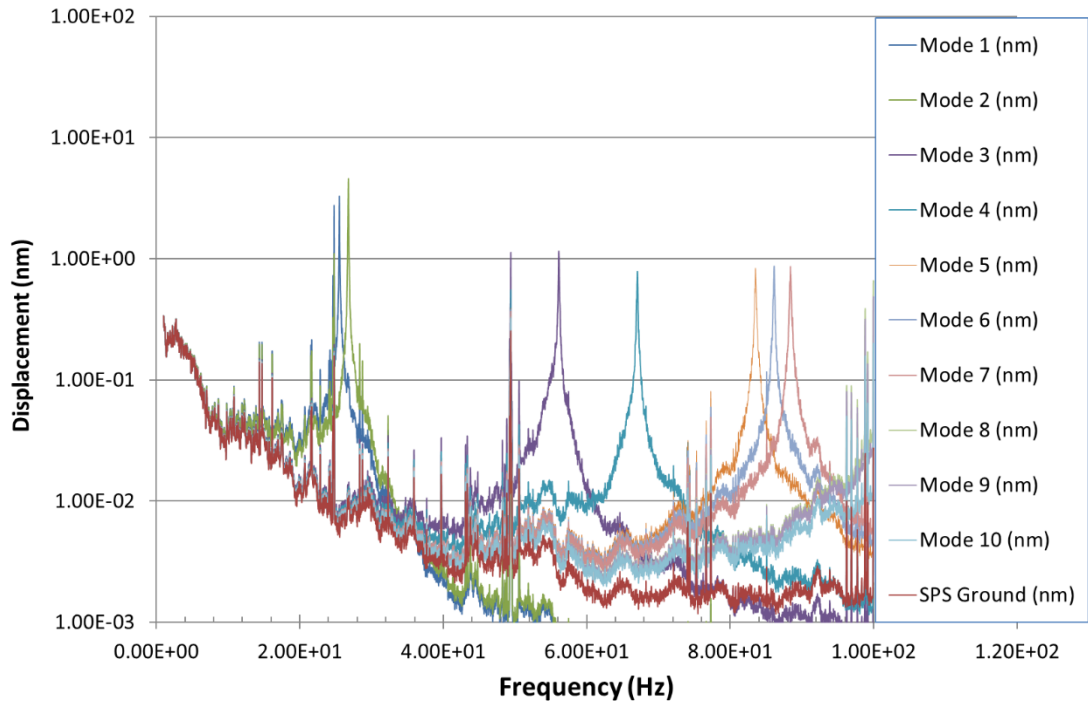
Figure 57. Final Detailed Design: Ground and Cavity Modal displacement under quiet SPS conditions
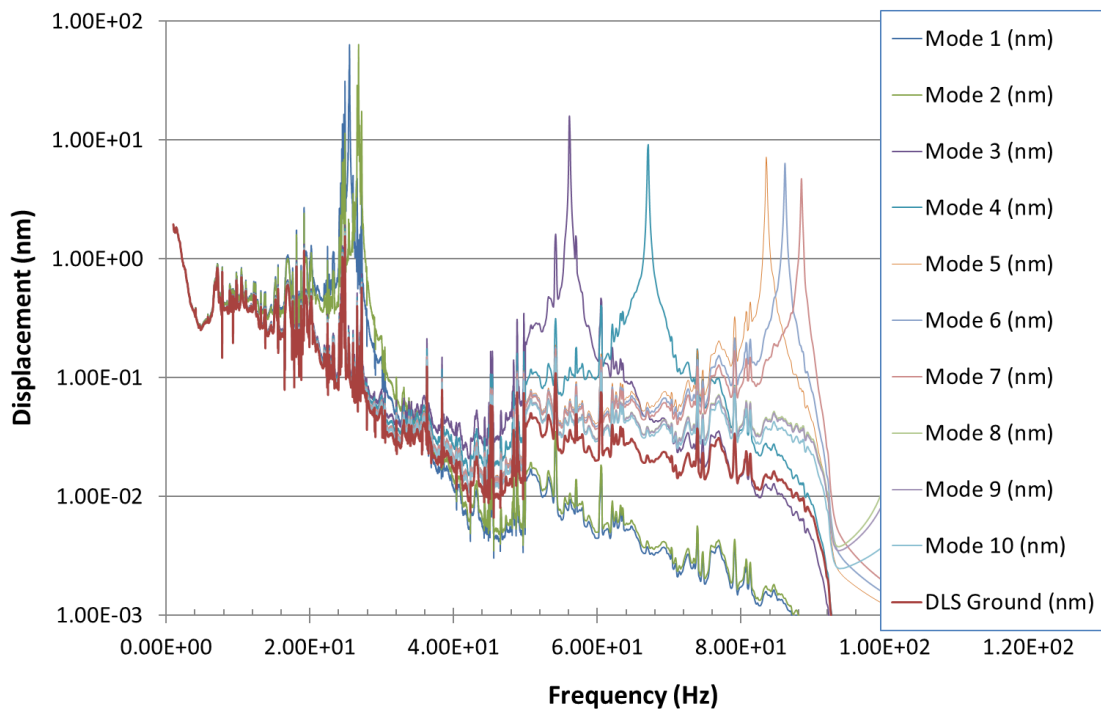
Figure 58. Final Detailed Design: Ground and Cavity Modal displacement under DLS conditions
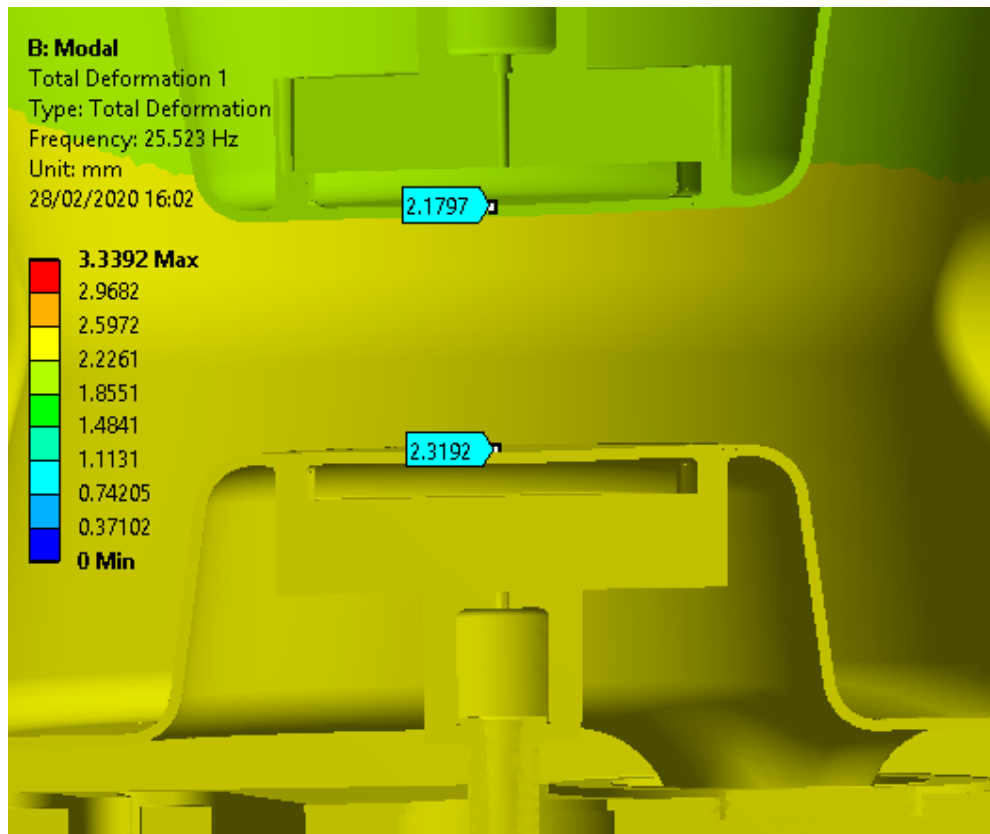
Figure 59. Final Design: Displacement of central tuning region in Mode 1
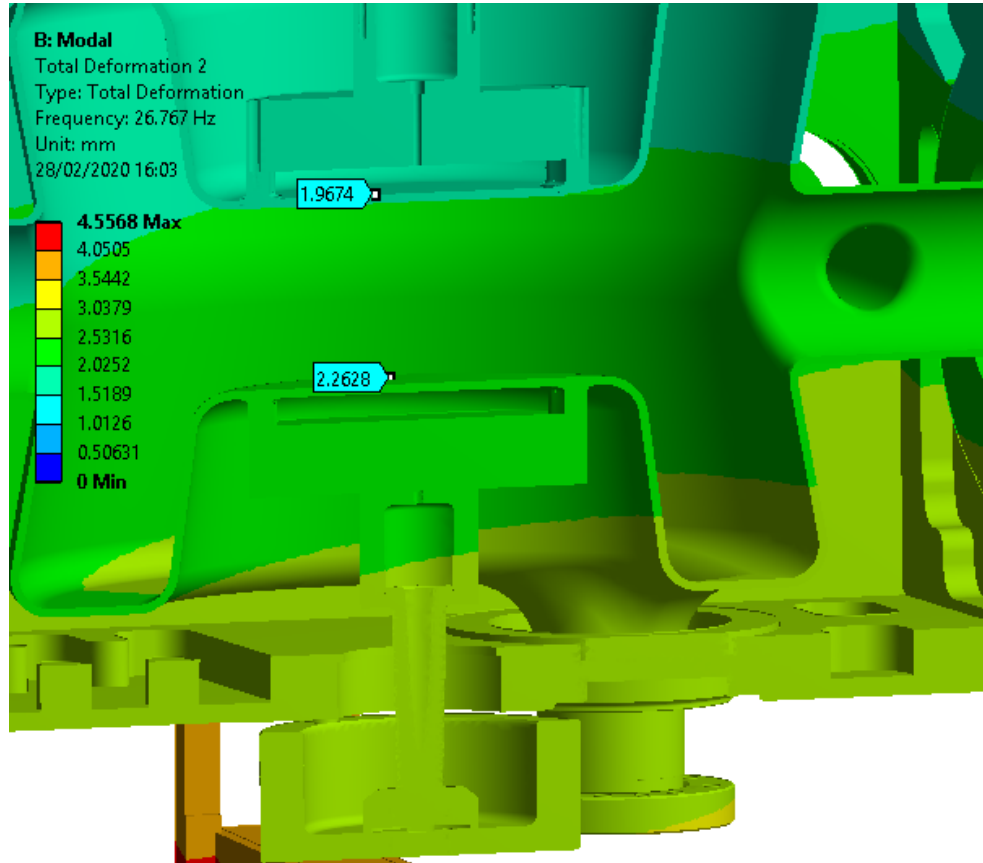
Figure 60. Final Design: Displacement of central tuning region in Mode 2

In Figure 59 and Figure 60 one can see the displacement of the central tuning region under modal deformation, i.e. the movement when the full system deforms as per Mode 1. In this movement the central tuning plates will deform relatively to each other which causes a detuning of the cavity. The sensitivity of the RF frequency due to this is 372kHz/mm of relative displacement of the plates (Verdu-Andres, 2015). Calculating the relative displacement as a fraction of the total movement we get for Mode 1 a relative displacement fraction of 0.042 ((2.32-2.18)/3.34) and for Mode 2 0.065 ((2.26-1.97)/4.56). If we multiply the DLS RSS displacement (peak movement taken from Table 15) of each mode by these factors we have for Mode 1 a relative movement of 7.3nm and for Mode 2 10.4nm. This equates to RF detuning of ~2.7Hz for Mode 1 and 3.9Hz for Mode 2. As these modes are close together in frequency, and act on the same region of the cavity, when in phase the detuning is likely to be as high as 4.7Hz (the RSS of the two figures). Deformation of other areas of the cavity in addition to deformation due to higher modes may also combine with this, providing a higher detuning value, however, this is expected to be ~10Hz, therefore well within the 100Hz maximum allowable.

The system stiffness was assessed in all 3 directions using the same method as previously employed. This being to apply a uniform 1kN load to each face normal to the direction of stiffness to be calculated and using maximum deflection values to assess and compare directional stiffness with previous designs shown in Table 16. The increase in stiffness compared to the pre-review design is considerable.

Table 16. Evolution of support system stiffness

Direction	Stiffness Pre-Review	Stiffness Review Model	Stiffness Post-Review	Stiffness Final Design
X (Lateral)	0.62kN/mm	0.77kN/mm	1.83kN/mm	3.44kN/mm
Y (Longitudinal)	1.58kN/mm	1.78kN/mm	1.70kN/mm	3.68kN/mm
Z (Vertical)	6.87kN/mm	8.37kN/mm	25.79kN/mm	34.48kN/mm

2.5.2. Thermal assessment

A reassessment of the thermal aspects of the design was required due to the increased thickness of the blades and the potential impact on heat leak to the 2K system. An assessment of the position of the thermal intercept on the blades was also required with regards to the thermal contraction of the assembly.

Using Equation 7 (Sub-section 2.2) one can calculate that for 75mm wide, 3mm thick flexures and 340mm overall length, an 80K intercept at 100mm from room temperature provides 6.17W of heat to the 80K cooling system and 0.30W to the 2K system per blade. This has been validated using FEA, where the average heat flux in the blades to the 2K system was shown to be 1277.6W/m^2, the cross sectional area of the blade is 2.25×10^{-4} m^2 therefore total heat leak to the 2K system calculated from the FE model is 0.29W per blade. A total of 1.16W to 2K for the 4 cavity support blades. The temperature profile is shown in Figure 61 alongside the vertical displacement (mm) of the supported cavity. As the temperature profile of the support blade, tuner and fundamental power coupler is not identical when they contract the cavity axis does not remain level. With a difference of ~0.32mm in thermal contraction of the blades and power coupler. This difference causes no unacceptable stresses in the power coupler as can be observed in Figure 62 (highlighted in the green box). The high stresses observed are at the intersections of dissimilar materials, as discussed previously in this thesis the Niobium to Stainless Steel brazed joint has been pre-qualified by CERN and is acceptable. There were high stresses between the Stainless Steel base bracket of the flexure and the Grade 2 Titanium helium vessel, again this were deemed acceptable as the real bolted joint will allow for some movement of the surfaces relative to each other, reducing the stress level observed.
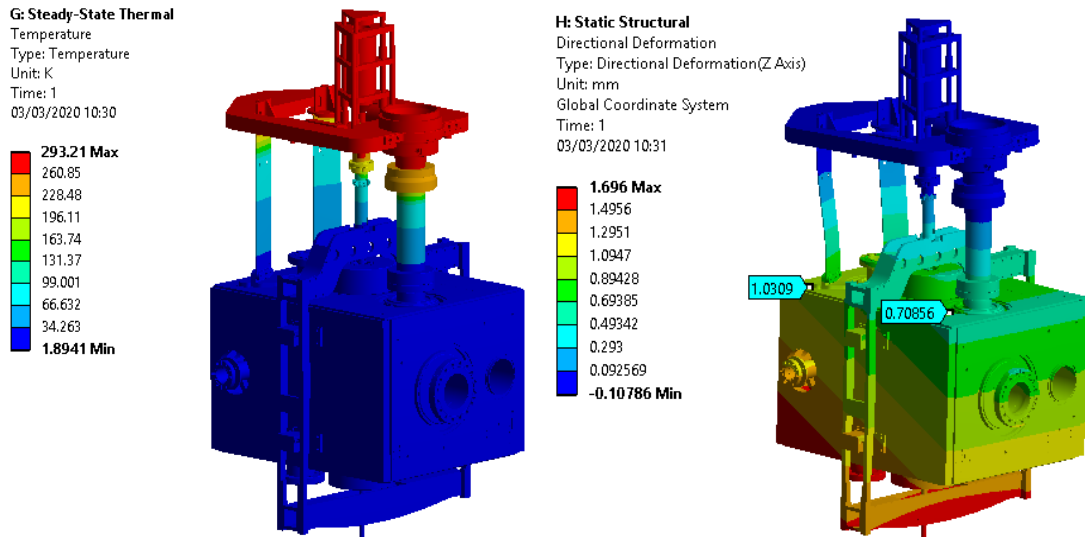
Figure 61. Final Design: Cavity support system temperature profile (left) and vertical displacement (right)
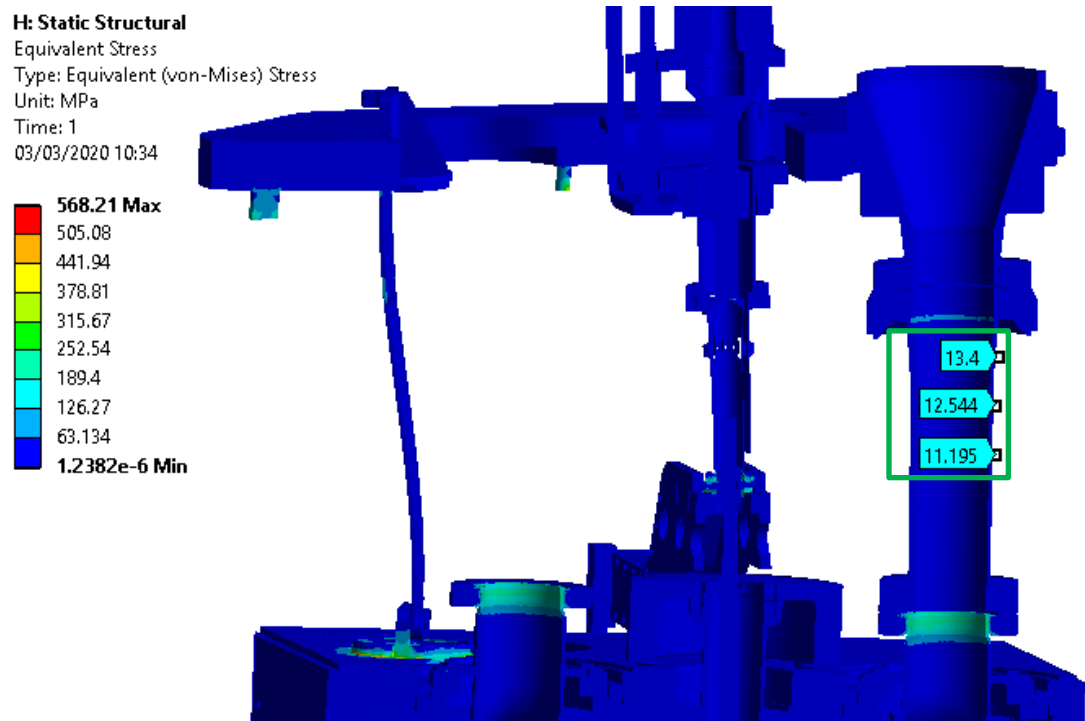
Figure 62. Final Design: Cool-down stresses

In the real system the difference in vertical contraction rates was measured on first cool-down and then adjusted for in the alignment system, so that when the cavity was at 2K it was in the correct position. One recommendation of this report is to lower the thermal intercept on the blades whilst remaining within allowable heat load limits of the 2K system to allow a more level cool-down and to ensure no angular mis-

alignment is introduced with any dynamic thermal loads on the system (for example when RF is turned on in the coupler).

In order to optimise the intercept position, heat leak to 2K was calculated at varying intercept positions on a single blade using Equation 7 to generate Figure 64. The FEA model was used to generate Figure 65. At 285mm thermal intercept position the cavity is level upon cool-down, however, the heat leak to the 2K system for the full support system is outside of the 2W allowable limit at a value of 5.2W for the 4 support blades. This shows that a level cool-down is not possible with the current system. With the blade intercept at 200mm from the room temperature connection the heat leak to 2K will be 0.5W per blade, bringing the total to 2W. At this value the difference in vertical displacement will be halved to 0.15mm shown in Figure 63. For the LHC Cryomodule an additional 4K-20K gas Helium intercept will be introduced to the FPC, if this could be passively linked to the blades it may allow further optimisation of the cool-down contractions.
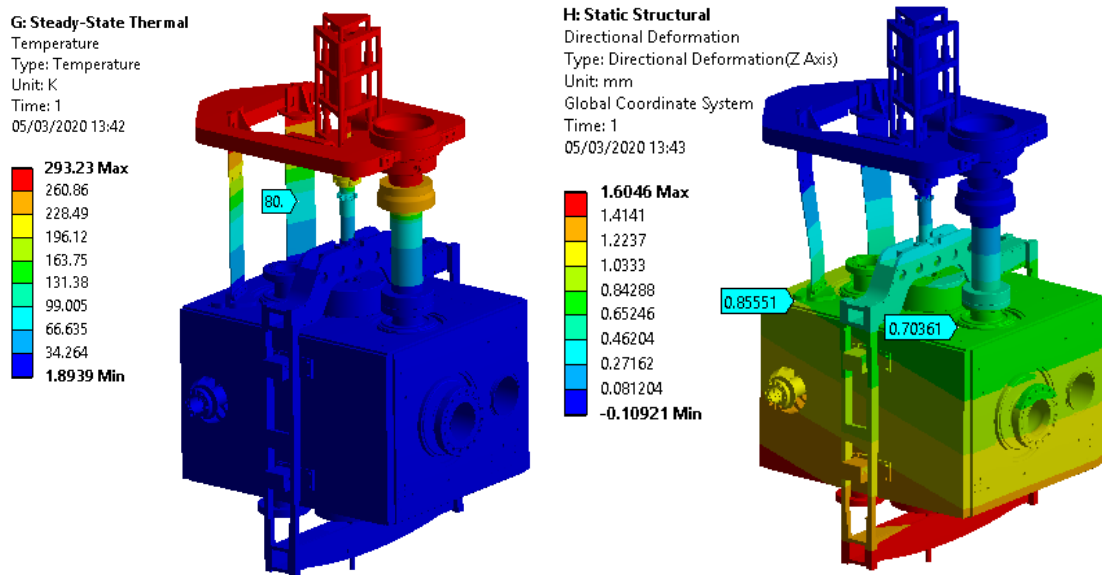
Figure 63. Final Design (Option): Temperature profile (left) and vertical displacement (right) with 80K intercept at 200mm from room temperature
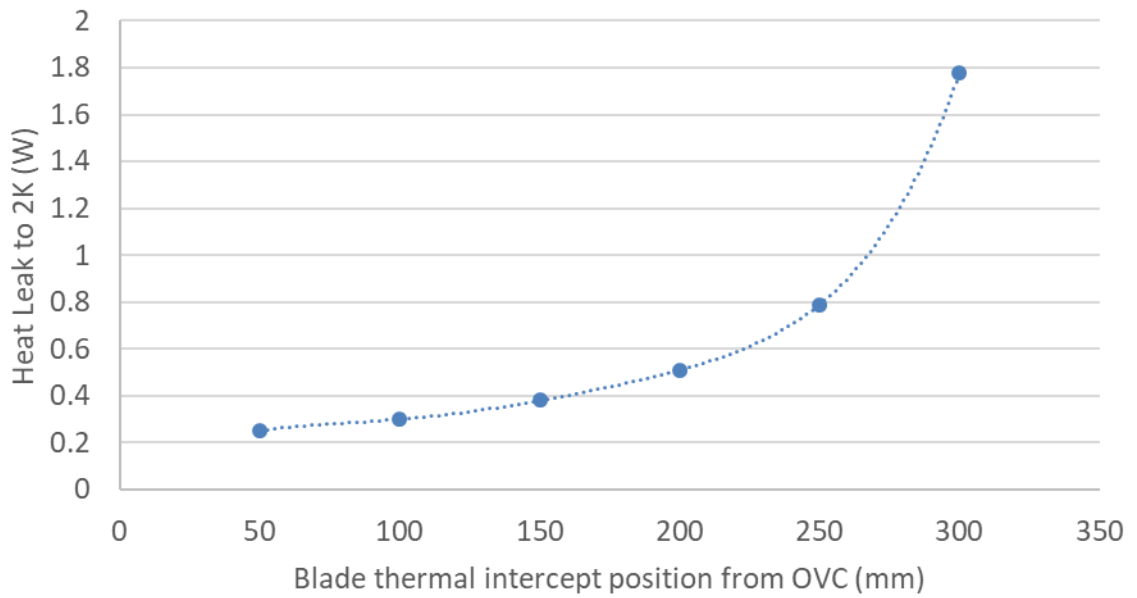
Figure 64. Heat Leak to 2K vs. Thermal Intercept position from OVC Top Plate
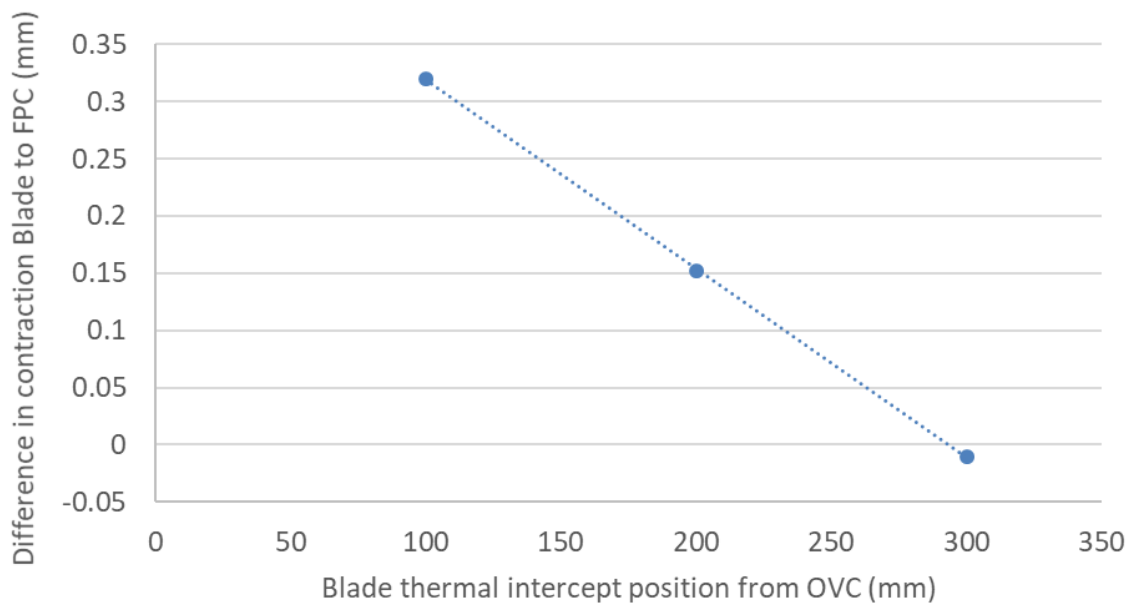
Figure 65. Difference in contraction Blade to FPC vs. Thermal Intercept position from OVC Top Plate

2.5.3. Transportation load assessment

The 1G longitudinal transportation load (Department for Transport, 2002) was also assessed for the final design. Displacement and stresses were all within acceptable limits for the materials used. This analysis showed there would be no need for temporary internal support structures to be installed for transport of the Cryomodule from the assembly area to the test bunker or to the final installation. This helped to simplify the Cryomodule design, with no additional penetrations required through the outer vacuum chamber, outer magnetic shield and thermal shield. In future iterations of the Cryomodule, which will be built off the CERN site and require international transportation, temporary internal supports may be required, in addition to a suitable Cryomodule Transportation Frame fitted with wire rope isolators.
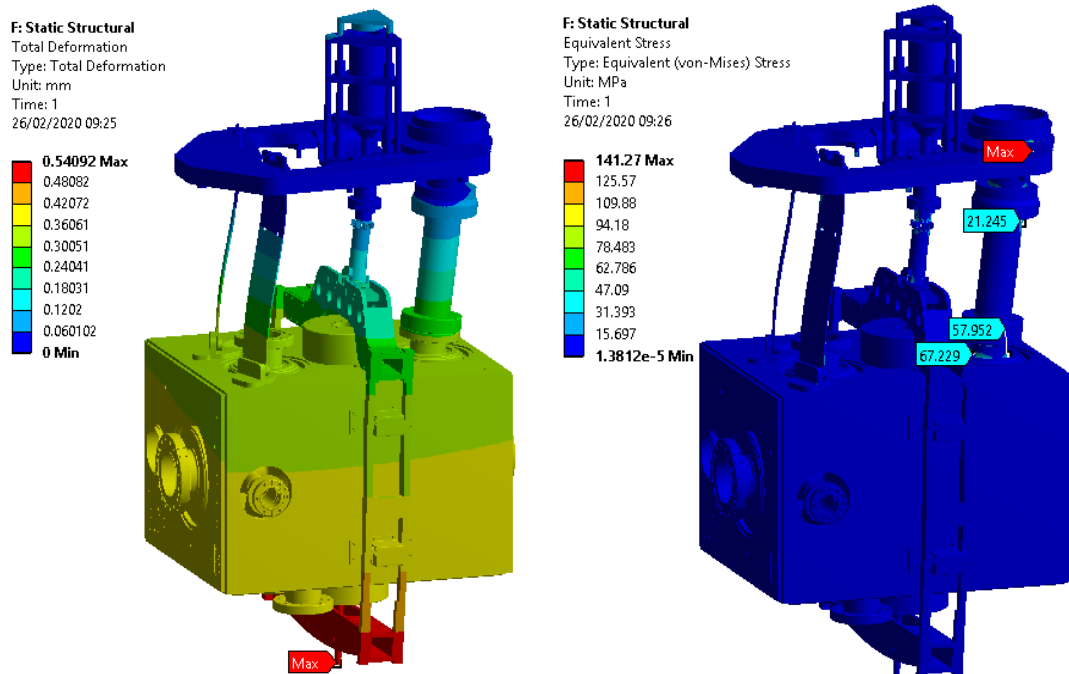
Figure 66. Final Design: 1G Longitudinal acceleration (transport load). Total deformation (left), von-Mises stress (right)

2.6. Section 2 Comments

This chapter described the process by which the novel cavity support system for the SRF DQW Crab Cavities was developed from initial ideas through to a final detailed design including the iterations performed and the reasoning behind each change. It also outlined the process in which amplitudes of cavity vibration modes were calculated using a transmission matrix. These calculations were primarily used to identify problematic modes in the Dressed Cavity assembly. This allowed for an improved tuner design to be developed as well as providing justification for a more robust 5 point cavity support plate height and levelling adjustment system. The calculations were also used to predict an estimated level of approximately 10Hz detuning per mode RF detuning due to microphonics based upon available ground vibration data and considering base excitation only.

The intervention on the tuner design was seen as an important contribution to the project, if this issue was not identified prior to installation there would have been a real possibility that the cavity could not be powered. The novel support concept, using flexural blades to support the cavity in addition to a fixed power coupler, has been shown through calculation, analysis and subsequent operation to perform well, Figure 67 shows the blades installed on the Cryomodule outer vacuum vessel top plate. The limited number of components meant that the cost of manufacture was relatively low and assembly was straight forward compared to more complex support assemblies. Cavity positioning, survey and alignment was also markedly successful due to the use of the common support plate.

Figure 67. Support blades installed on the Crab Cavity Cryomodule

3. Bare Cavity Modal Analysis and Testing

3.1. Bare Cavity Finite Element Modal Analysis

The first bare DQW cavity manufactured is shown on a modal test bench in Figure 68. As validation for the work provided previously the Project Leader requested that Finite Element Modal predictions be made for the bare DQW and compared to that of the experimental modal testing. The work was conducted independently, i.e. the staff involved did not know each other's results until both had compiled their data. The reasoning for this was to test the robustness of each process, and investigate the effect of any human influence i.e. in defining boundary conditions etc.

Figure 68. Bare DQW Cavity Modal Experiment Setup

To reflect the 'real-world' boundary conditions of the bare cavity on test the FE model was setup as shown in Figure 69. To represent the simply supported 'V' block configuration of the testing setup it was deemed inappropriate to fully fix the cavity beam port flanges as per the final cavity configuration (i.e. the cavity collars adjacent to the flanges are ultimately bolted to the rigid Helium Vessel). Therefore a single fully fixed point on one of the cavity beam port flanges was used plus additional points fixed on height and lateral movement at appropriate locations on the cavity flanges. The body is coloured as per material applied, i.e. the body is Niobium, port collars are Nb-Ti, and Conflat flanges assigned 316LN Stainless Steel. A 1mm mesh was used to give at least

2 elements through the thickness of the cavity in all locations Figure 70. ANSYS Workbench Modal solver was used to identify the first 5 modes for the cavity, these are summarised in Table 17 and the modal shapes can be observed in Figure 71 to Figure 75. Notes points B and D in Figure 69 are on the Cavity flange on the opposite face to points A and C.
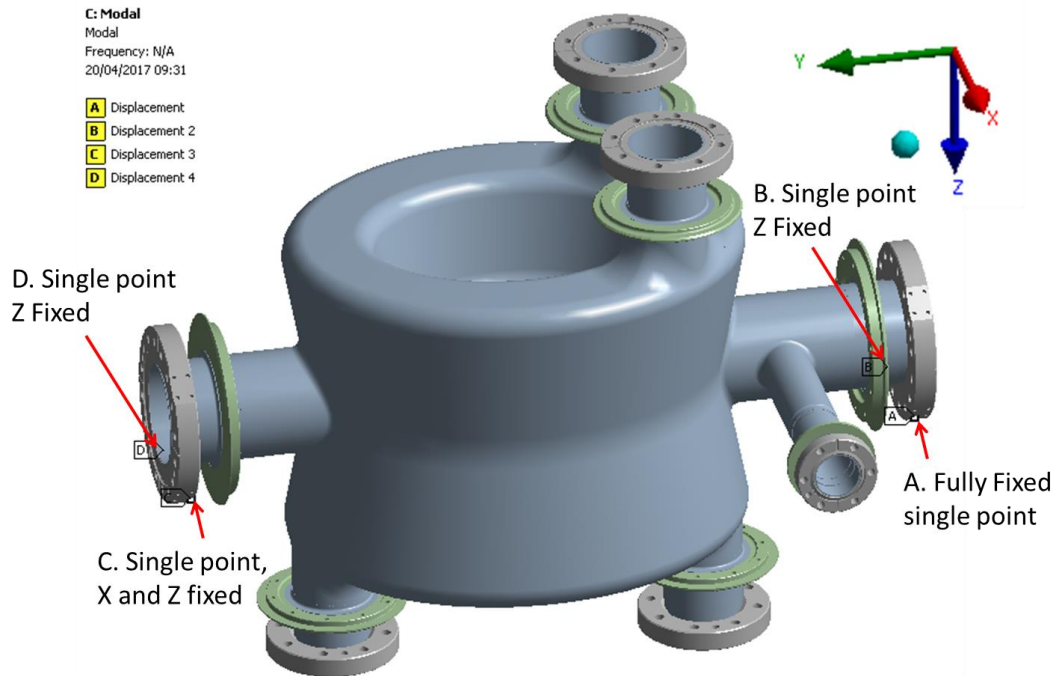
Figure 69. Bare Cavity FE Model Setup
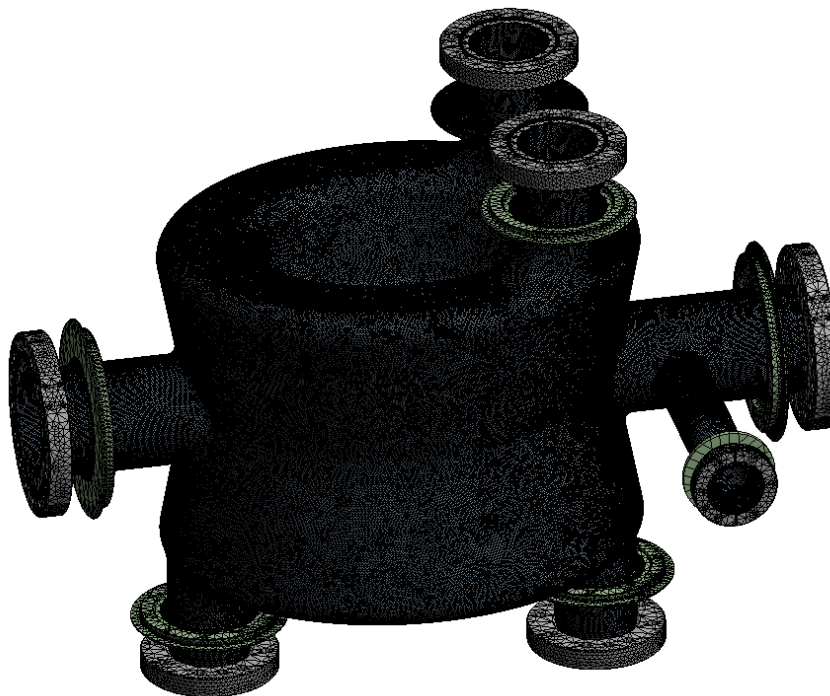
Figure 70. Bare Cavity Mesh for Modal Analysis

Table 17. FEM modal testing results

Mode	FEM Frequency (Hz)
1	39.9
2	84.3
3	104.6
4	115.1
5	136.5
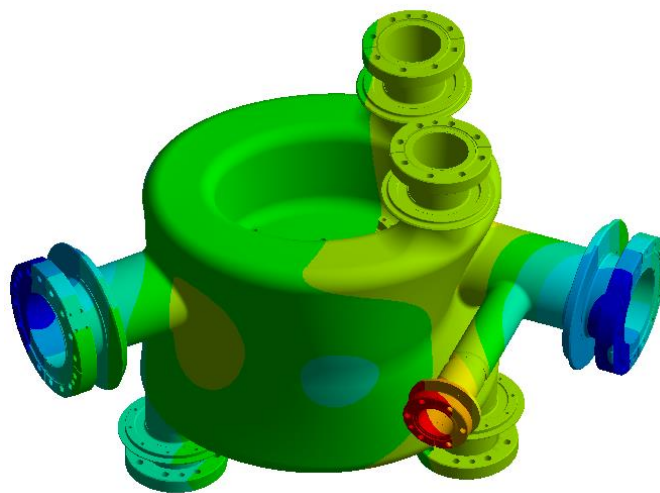
Figure 71. Bare Cavity Mode 1 – 39.9 Hz
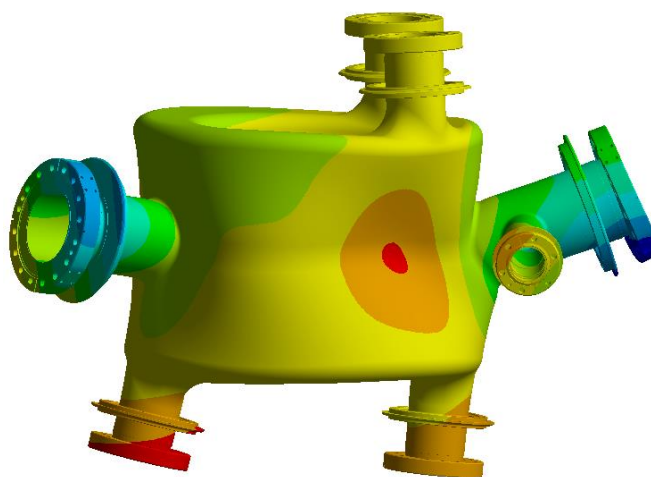
Figure 72. Bare Cavity Mode 2 – 84.3Hz
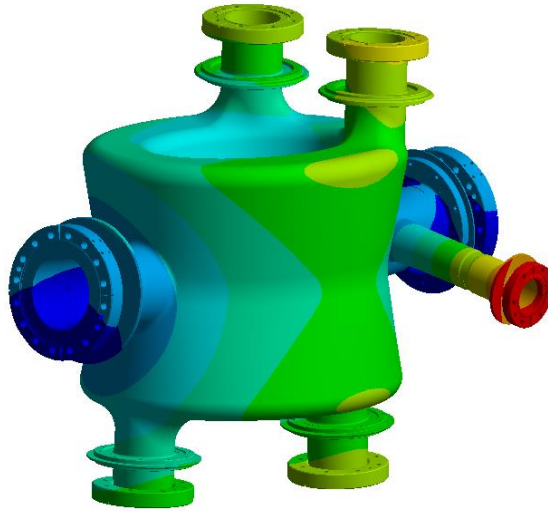
Figure 73. Bare Cavity Mode 3 – 104.6Hz
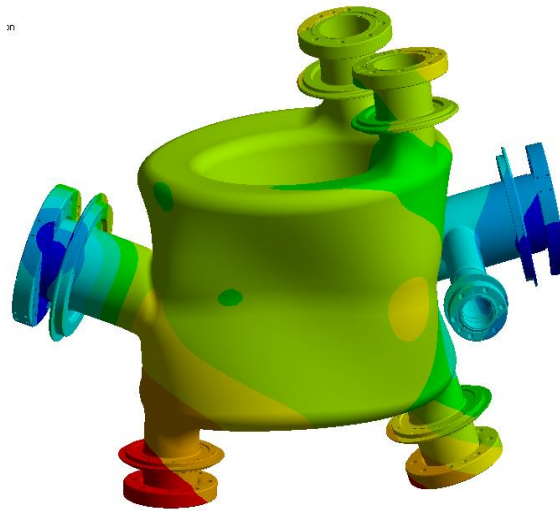
Figure 74. Bare Cavity Mode 4 – 115.1 Hz
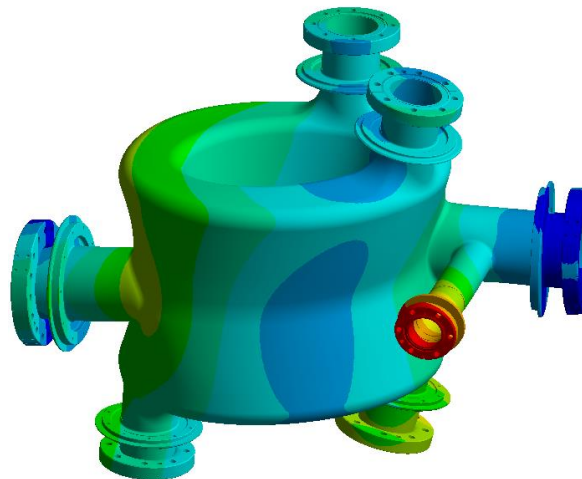
Figure 75. Bare Cavity Mode 5 – 136.5Hz

3.2. Bare Cavity Experimental Mode Acquisition

Full details of the bare cavity experimental modal testing can be found on the CERN Engineering Data Management System (EDMS), Report number 1771639 (Lacny, 2017). For the experiment the cavity was setup on the test bench as can be seen in Figure 68, i.e. the cavity was simply supported in a precision 'V' block and rotation was prevented with a scissor jack elevated to support one of the lower HOM ports. From experience these scissor jacks are fairly soft, and not pre-loaded therefore have clearances which allow movement over the small range of these vibration amplitudes. The stiffness of the scissor jack was therefore not included in calculations. The process of identifying the modes of the structure involves tapping the cavity with a calibrated hammer and measuring the dynamic response, this is known as a 'bump' test. The 'bump' ideally should excite all modes in the system, therefore peaks are observed in the transfer function plot at the natural frequencies. To measure the dynamic response of the system and assess the modal shapes 5 accelerometers were attached to the cavity in various locations which were not detailed but can be observed in Figure 68. Details of the accelerometers used are given in Table 18. Prior to the experiment each accelerometer was calibrated using a handheld shaker which supplied an acceleration of 9.81m/s^2 at 159.2Hz (Lacny, 2017). The acquisition system which records and post processes the data from the accelerometers is a Müller-BBM MKII (Müller-BBM GmbH, 2019). The hammer used to excite the cavity was a PCB 086D05 with a sensitivity of 0.23 mV/N (PCB Piezotronics, 2019).

Table 18. Cavity Modal Testing Accelerometers (Lacny, 2017)

	Type	Sensitivity	Frequency Range
A1	356A33	$1.02 \text{ mV/(m/s}^2)$	2 Hz – 7kHz
A2	356A33	$1.02 \text{ mV/(m/s}^2)$	2 Hz – 7kHz
A3	356A15	$10.2 \text{ mV/(m/s}^2)$	2 Hz – 5 kHz
A4	356B08	$10.2 \text{ mV/(m/s}^2)$	0.5 Hz – 5kHz
A5	356B08	$10.2 \text{ mV/(m/s}^2)$	0.5 Hz – 5kHz

"ME'scopeVES® software (Vibrant, 2019) was used to obtain the modal parameters (modal frequencies, modal shapes) from the transfer functions acquired from PAK® Software (Müller-BBM GmbH, 2019). It also allows graphical presentation of the test structure and animation of the motion." (Lacny, 2017). To identify the modal shapes of the cavity a virtual topology of the cavity was generated

in the software, which contains the accelerometer positions (Figure 76). Figure 77 shows the transfer function results for all tests overlaid on one plot. Table 19 details the modes identified by the software. Videos of the modal shapes were also generated and distributed to the project team.
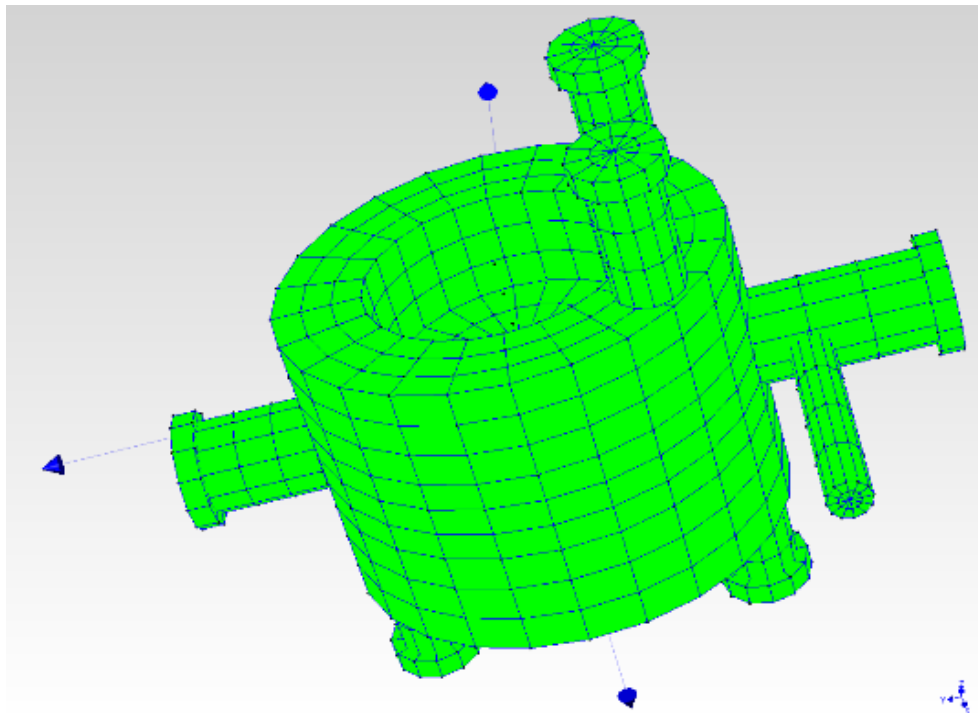
Figure 76. Crab Cavity model used in ME'Scope Software (Lacny, 2017)
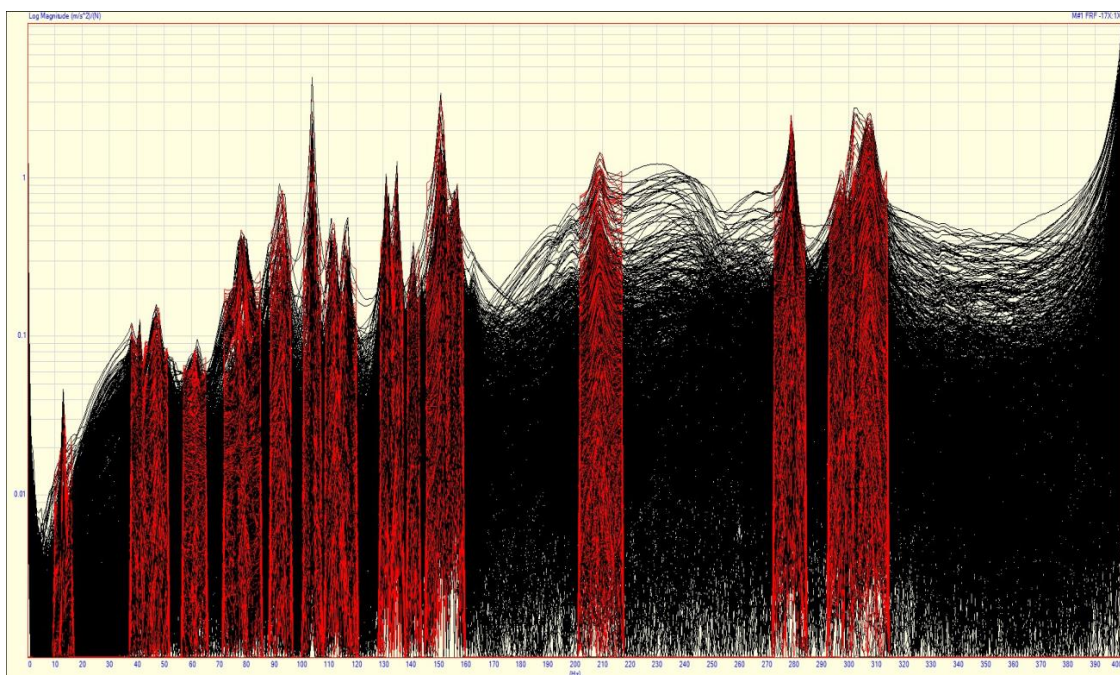
Figure 77. Bare Crab Cavity transfer functions (Lacny, 2017)

Table 19. Experimental Modal Analysis results (Lacny, 2017)

	Frequency [Hz]	Damping [%]	Mode Shape
1	12.8	0.450	Lateral Rigid Body Motion
2	40.8	0.496	Lateral Bending
3	47.7	1.770	Longitudinal Rigid Body Motion
4	61.4	0.742	Vertical Rigid Body Motion
5	78.5	0.805	Vertical Bending
6	92.9	1.420	Upper Pipes
7	104	0.312	Side Pipe
8	112	0.702	
9	115	0.300	Bending
10	132	0.201	
11	135	0.233	
12	141	0.369	
13	151	0.407	Lateral
14	157	0.535	
15	209	0.780	
16	279	0.243	Circumferential
17	298	0.480	
18	308	0.544	

3.3. Comparison between Bare Cavity FE and Experimental Results

As remarked by CERN staff in the EMA report, the results were positive. The FE model and experimental testing agree, and on average the agreement is ~3% (Table 20). This clearly demonstrates the accuracy of both methods. From video output it was shown that the modes identified at 12.8Hz, 47.7Hz and 61.4Hz were all rigid body modes of the cavity moving in its temporary supports, therefore functions of the experimental setup that would not be identified by the FE solver which will not converge if unconstrained in any direction. Figure 78 shows both an outputted image from the EMA software and the corresponding modal shape from the FE solver. One can clearly see the similarity between the modal shapes. The strong correlation between FE modelling and physical modal testing indicated the fidelity of the FE approach used for the more complex system.

Table 20. Comparison of FE and Experimental Mode Results

Mode	FEM Frequency (Hz)	EMA Frequency [Hz]	Agreement (%)
1	39.9	40.8	2.23
2	84.3	78.5	7.13
3	104.6	104.0	0.58
4	115.1	115.0	0.09
5	136.5	135.0	1.10
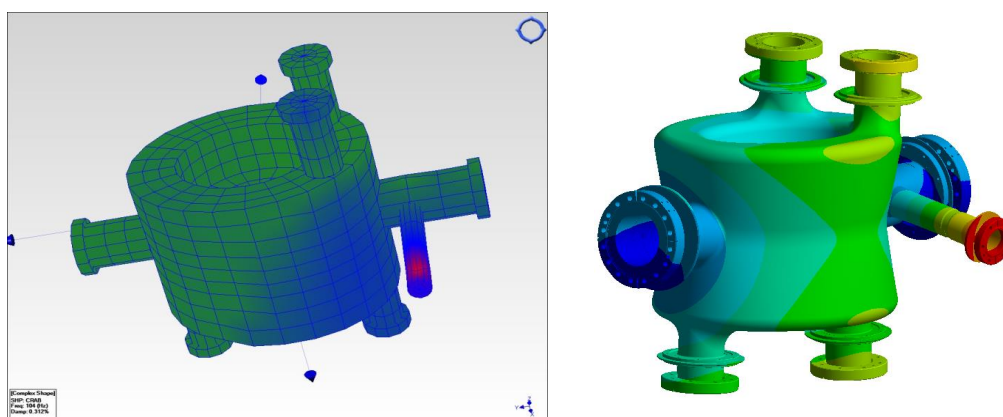
Figure 78. Comparison of mode shapes at 104Hz (Lacny, 2017)

4. Crab Cavity Support System in Operation

4.1. Microphonic Detuning

Crab Cavity microphonic detuning was measured in the cryomodule installed on the SPS on 30th November 2018 without beam (Yamakawa, 2019). In general the amplitude of detuning is comparable to the levels predicted in this thesis by using the Diamond Light Source ground vibration spectrum, rather than the quiet SPS data. As previously discussed the SPS ground vibration spectrum was measured prior to the installation of local services required for the module, such as cryogenic and vacuum pumping systems which can increase base excitation and introduce forced vibration onto the supported mass through the cryogenic pipelines (known as Cryolines). Cryogenic pumps operate in the 20Hz to 30Hz region, coupling to the fundamental modes of the Crab Cavity support system (Yamakawa, 2019). The level of detuning at 21Hz is within acceptable limits, however, was periodically higher than the predicted value of 10Hz. Various values were observed ranging from as high as 18Hz detuning at 21Hz shown in Figure 79 to a lower value of 11Hz detuning at 21Hz as shown in

Figure 83. The periodic nature combined with the frequency point to pumps as the cause of the detuning. The mounting of the local pumps to the ground and connections of the vacuum/gas lines to the cryomodule should therefore be assessed for the final installation in LHC with the aim of minimising this level further. In Figure 80 an undamped vacuum cart is highlighted by the red box, isolators under the base of pumping units (Postek M. T., 1991), and damped flexible hoses (National Electrostatics Corp., 2019) would act to significantly improve the microphonic performance of the system. At 49Hz the source is likely the High Voltage supply to the RF power units (Klystrons) (Yamakawa, 2019).

It is likely that both 49Hz and 60Hz peaks are ground coupling to the same mode. Simulations predict a twisting mode of the cavity at 56.1Hz (Mode 3), in the Final Design transmissibility plot for the SPS ground spectrum (Figure 57) two peaks can be observed for Mode 3, one at the base excitation frequency of 49Hz and one at the natural frequency. Figure 81 shows the same data but over the range of 40Hz to 70Hz for clarity, and for a range of viscous damping levels. It can be observed that the peak at the driven frequency remains the same despite the changing damping. The peak at the natural frequency falls with increased damping. From this data one can estimate a viscous damping co-efficient of 0.002 to 0.003 for the supported dressed cavity system by calculating the relative height of the two peaks in Figure 79 and comparing with the data in Figure 81 .
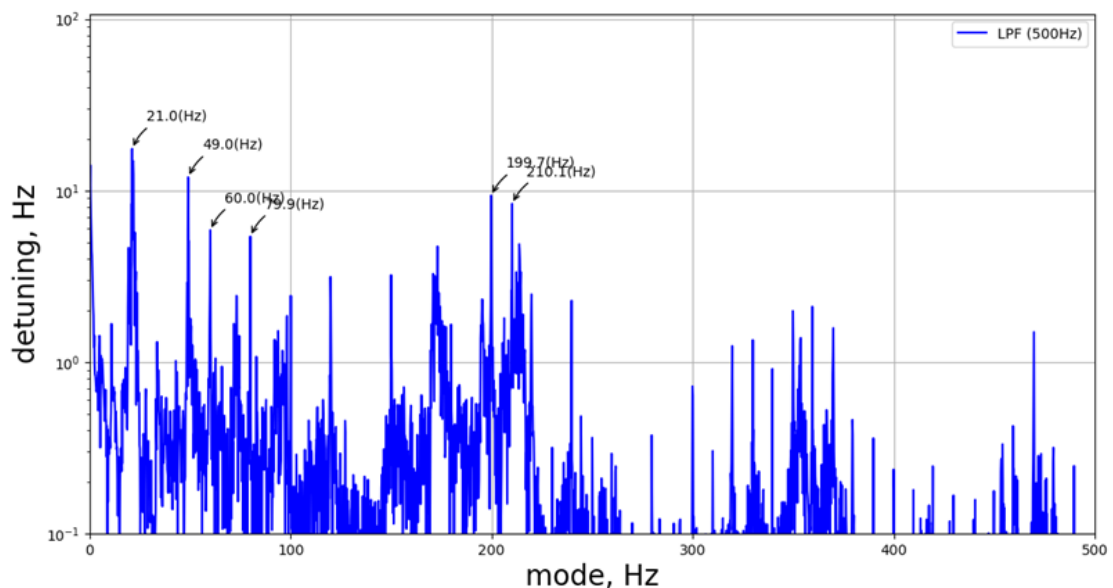
Figure 79. Crab Cavity detuning due to microphonics measured on the SPS, 30th November 2018 (Yamakawa, 2019)

Figure 80. DQW Crab Cavity Cryomodule installed on the SPS
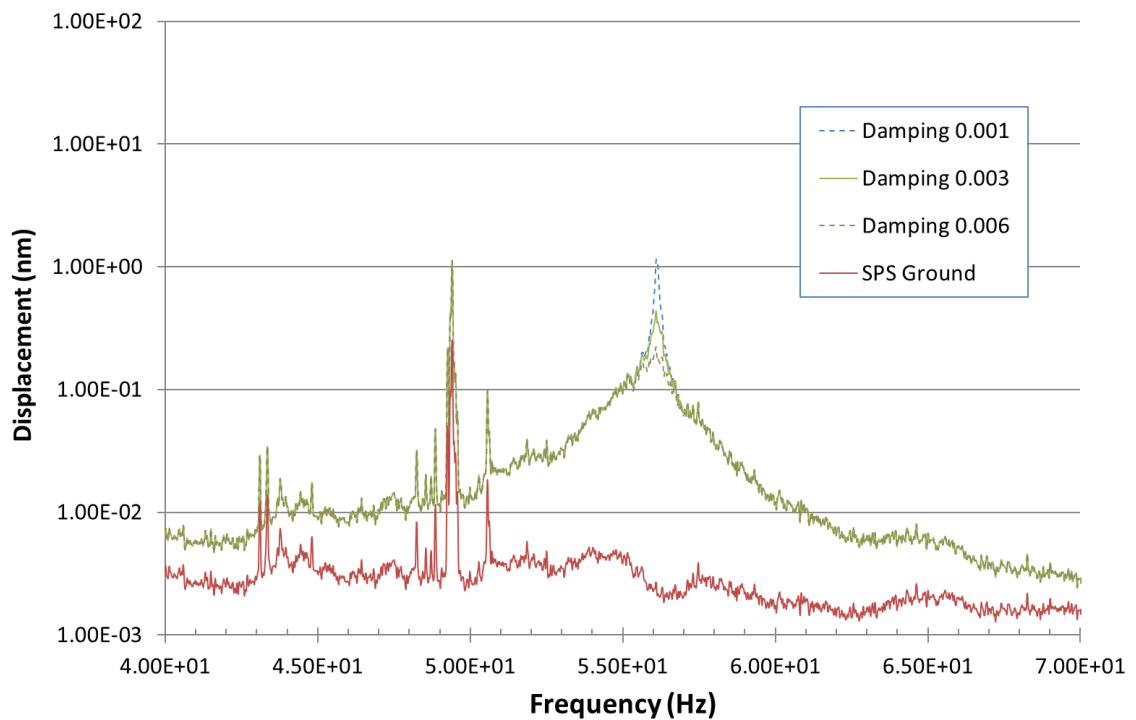
Figure 81. Displacement of Dressed Cavity Mode 3 (56.1Hz) under SPS ground conditions, in the range 40Hz to 70Hz. Shown with varying Damping co-efficient.

4.2. Ponderomotive Instability

Tests performed in October 2018 with the Crab Cavities driven without feedback and with voltage >1MV "revealed severe instabilities" (Yamakawa, 2019) in the control of the Cavity RF frequency. Levels of detuning exceeding the cavity half bandwidth of 400Hz were observed at ~218Hz. The problem was identified as Ponderomotive Instability (Delayen, 2005) which is an effect whereby changing electromagnetic forces induced by changes to the RF power level couple to a mechanical mode of the system. The electromagnetic force is known as Lorentz Force, the Lorentz pressure, P, is calculated using Equation 12.

$$P = \frac{1}{4}(\varepsilon_0 E^2 - \mu_0 H^2) \quad [Eq.\ 12]$$

Where, ε_0 is the permittivity of free space, E is the electric field amplitude, μ_0 is the permeability of free space and H is the magnetic field intensity amplitude. The profile of E and H field varies across the cavity, with the E field the main contributing factor. Figure 82 shows the profile of the Lorentz Forces in the cavity, note they are highest in the region of the central tuning plates. This force is in steady state until there is a desired change to the cavity voltage. Ponderomotive Instability, is where the time required to change the cavity voltage and therefore the profile of changing Lorentz Forces couple to a mechanical mode which itself causes detuning oscillating at the frequency of the particular mechanical mode which matches the cavity power change profile giving an amplifying effect leading to instability. The issue is solvable by using the Low Level RF feedback to lock the driving frequency at low power, and a carefully planned procedure for ramping up the voltage, however, it was requested that the mechanical mode coupling to the Lorentz Forces be investigated as part of this work.
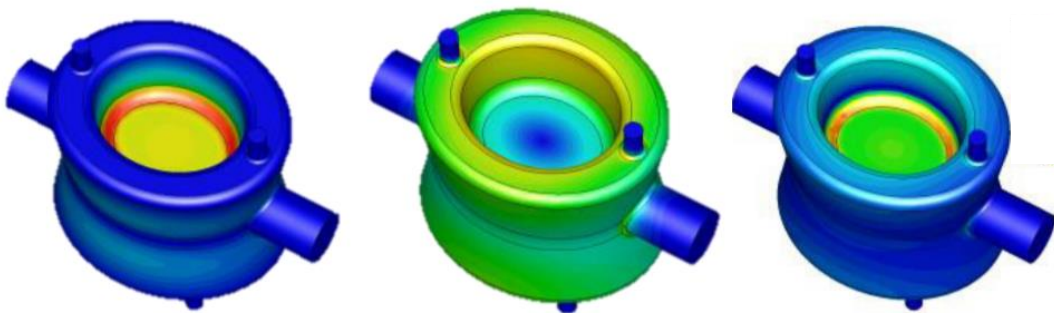
Figure 82. Profile of DQW E field (Left) H Field (Centre) and Lorentz Pressure (Right) (Verdú-Andrés S. , 2015)
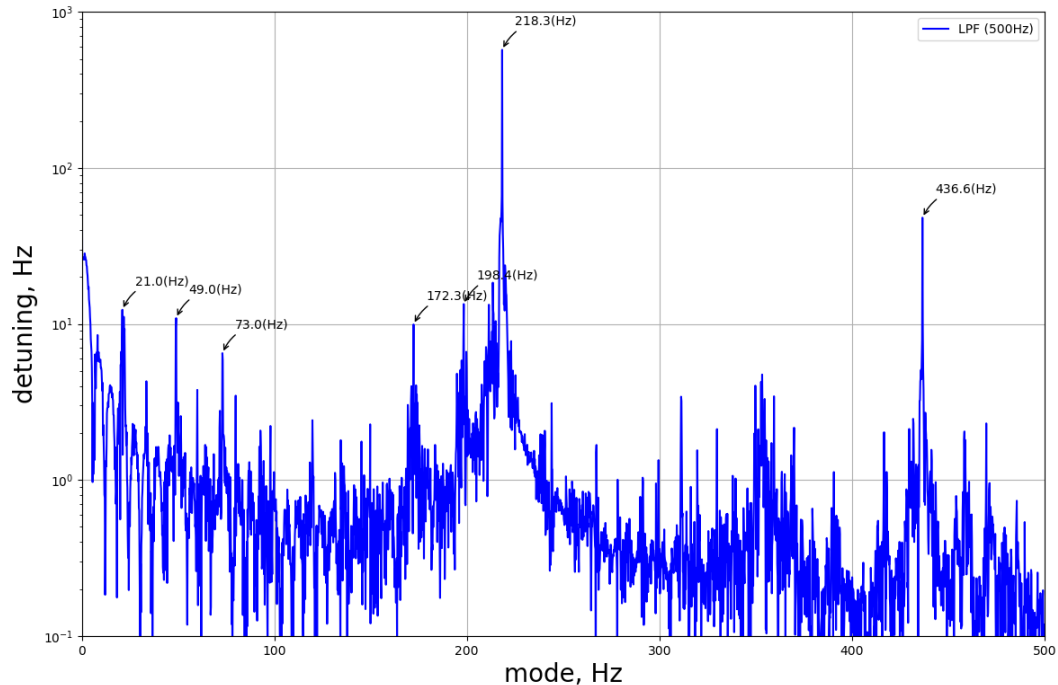
Figure 83. Ponderomotive Instability in SPS Crab Cavity when driven open loop at voltage >1MV

A modal analysis was performed on the 'Final Design' model from Sub-Section 2.5 in the range 180Hz to 240Hz. Three modes were identified, one being oscillation of the RF Field Probe (shown in Figure 84) and two modes of the inner shaft of the Tuner (shown in Figure 85). As the Lorentz force acts directly on the central plates of the cavity to which the inner shaft of the Tuner is attached this is the prime candidate for the source of the instability. An additional proposal is that as the modes of the probe and tuner are so close in frequency, should the oscillations in the field probe at ~200Hz provide a signal oscillation at the same frequency this would then drive Lorentz Force oscillations at the ~200Hz frequency, and therefore couple to the modes of the Tuner. Following this work it was suggested to the Crab Cavity Project Leader to include pre-loaded bearings between the inner and outer shafts of the tuner in order to mitigate against Ponderomotive Instabilities in future iterations of the design. A full study of Tuner modes in the range 0 to 500Hz would also be recommended.
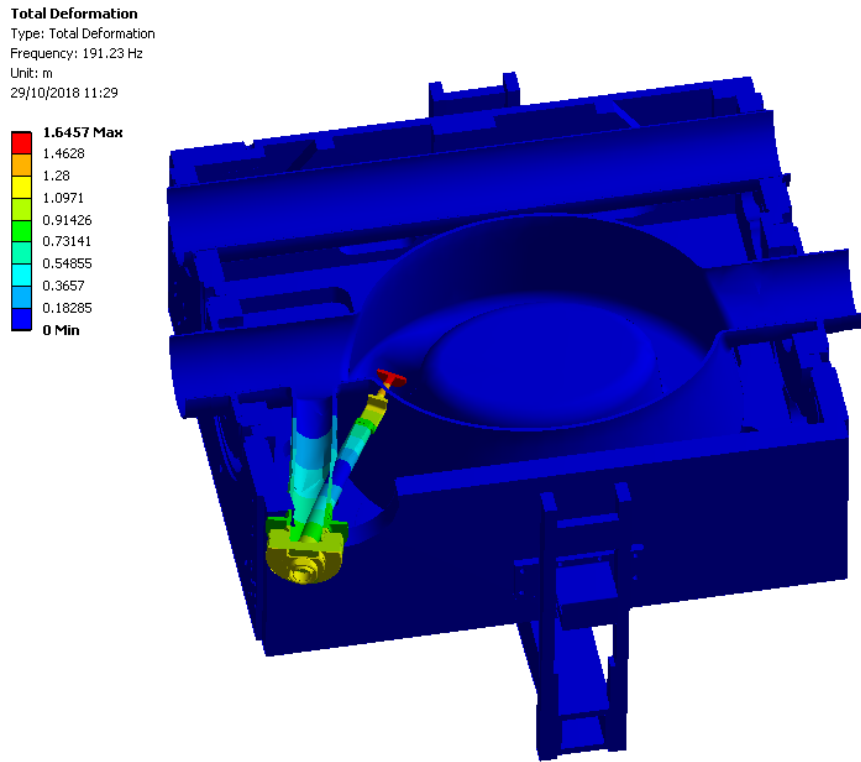
Figure 84. Cavity RF Field Probe oscillation mode at 191.2Hz.
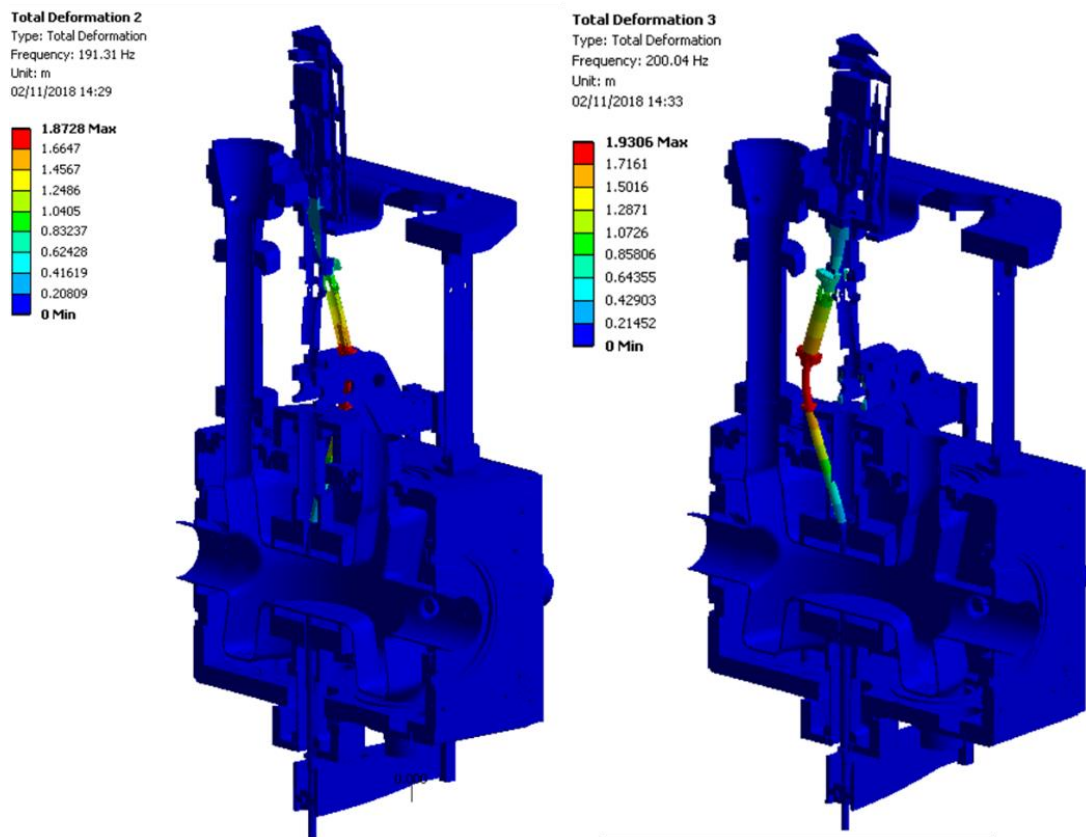
Figure 85. Tuner Inner Shaft modes at 191.3Hz (left) and 200.0Hz (right)

4.3. Crab Cavity Alignment

It was noted that cavity alignment was straight forward thanks to the common support plate and the rigidity of the support system. On initial cool-down the angular misalignment of the cavities as shown in simulations was observed, this was adjusted for in the support system and the final positioning of the cavities was well within specification, as can be observed in Figure 86. The cavity centre lines were within a cylindrical tolerance zone of Ø0.26mm compared to the specification of Ø0.5mm. As mentioned previously in the thesis, it is believed that lowering the thermal intercepts on the flexural blades would be beneficial, providing a more level initial thermal contraction and lowering stress in the system.
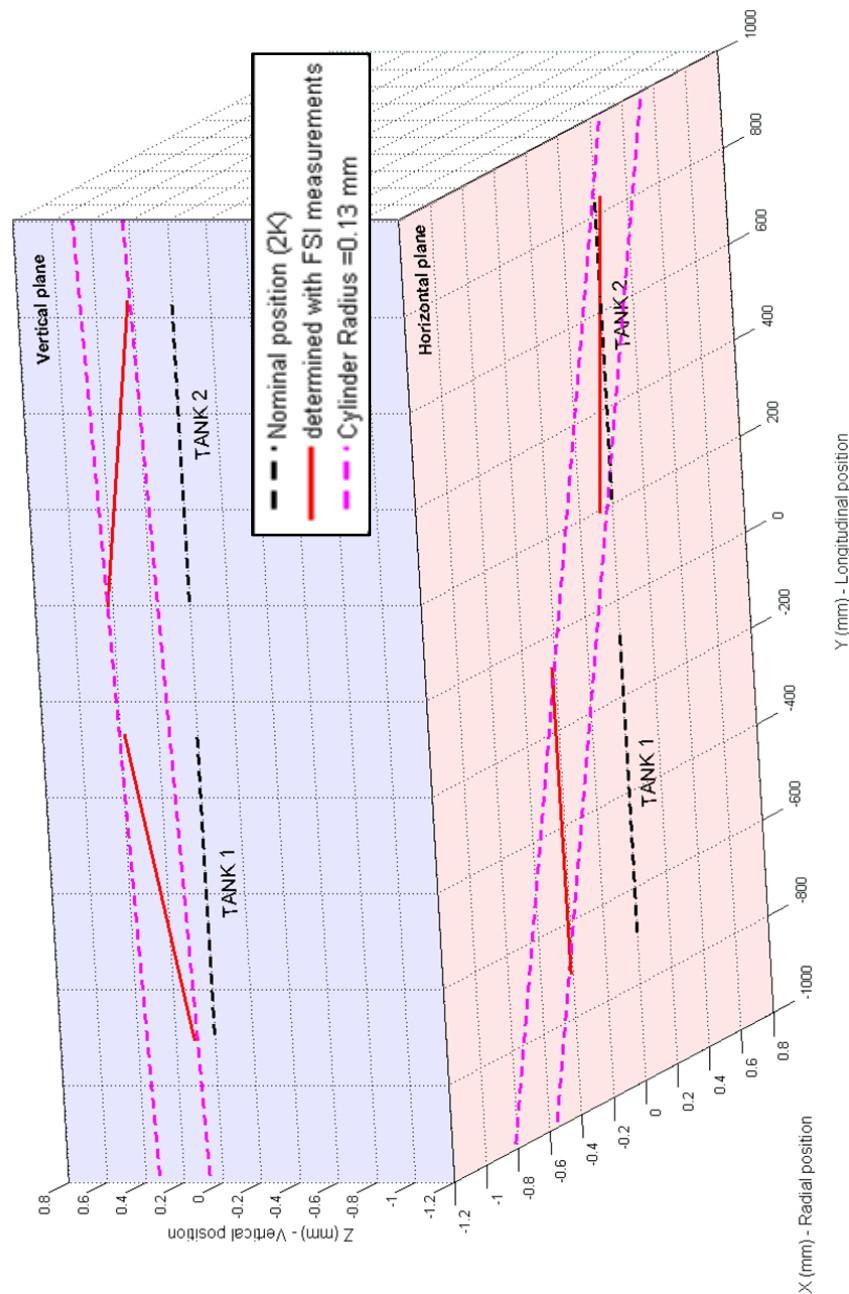
Figure 86. DQW Crab Cavity in SPS, final alignment position (Calaga, 2018)

4.4. Heat Leak to 2K

Unfortunately no thermometry was available on the blade supports to provide a directly measured temperature profile. The total heat leak observed for all supports other than the Power Coupler (which was fitted with thermometry) was 2.1W, which is just above the specification of 2W. The 2.1W includes 2 additional supports which were required to support the Helium gas return line off the Outer Vacuum Chamber. The total heat leak of these supports is estimated via FEA to be ~0.4W, see Figure 87, which implies a heat leak due to the blade supports higher than the predicted value. It can be observed in Table 21, however, that in general the static heat loads to 2K were higher than specification and heat leak to 80K lower than specified. For components with thermal intercepts the values are typically 1.4x specification additional to 2K. If one assumes 1.4x the predicted values, the additional support heat leak to 2K is 0.56W leaving 1.54W contribution of the blades. The predicted value for the 4 blades was 1.16W, 1.4x this is 1.6W therefore in line with all other components. The 80K intermediate temperature is a target for the thermal strap design. As the thermal shield operates at 50K-70K, the value of 80K allows for 10K to 30K thermal gradient across the braided straps used to passively link each sub-system to the thermal shield. The value of 1.4x heat load to the 2K circuit suggest the intercept positions on the blades were ~100K not 80K (from Equation 7). The thermal straps therefore were providing too high a thermal resistance to the intermediate cooling system. This could be improved in future by using shorter, higher cross sectional area straps, using more fasteners and/or higher tightening torque to connect them to components in order to lower thermal contact resistance and ensure good contact (i.e. forcing the mating faces flat to each other).

Table 21. Static Heat Load Specification and Measured* values in SPS Testing (Pleite , 2018)

Static loads	Specification		Measured*	
	2 K	80 K	2 K	80 K
Radiation	3.4	30	3.3	8
CWT	0.2	10	0.1	28
Supports	2	40	2.1	21
RF/FPC	4	100	5.3	72
Instrumentation	2.3	10	2.4	8
HOM/Pickup	3.9	40	5.5	15
Tuner	1	10	1.4	15
Total static	16.8	240	20.1	167

*Some values measured directly, others estimated from indirect measurements

Type: Temperature
Unit: K
Time: 1
12/10/2018 18:20

300.02 Max
266.69
233.35
200.01
166.68
133.34
100
66.665
33.328
-0.0089661 Min

T_{room}

T_{cold}

$T_{intermediate}$

T_{room}

T_{cold}

$T_{intermediate}$

- **0.3 W** to the 2 K bath
- **3.8 W** to the intercepts

- **0.1 W** to the 2 K bath
- **1.3 W** to the intercepts
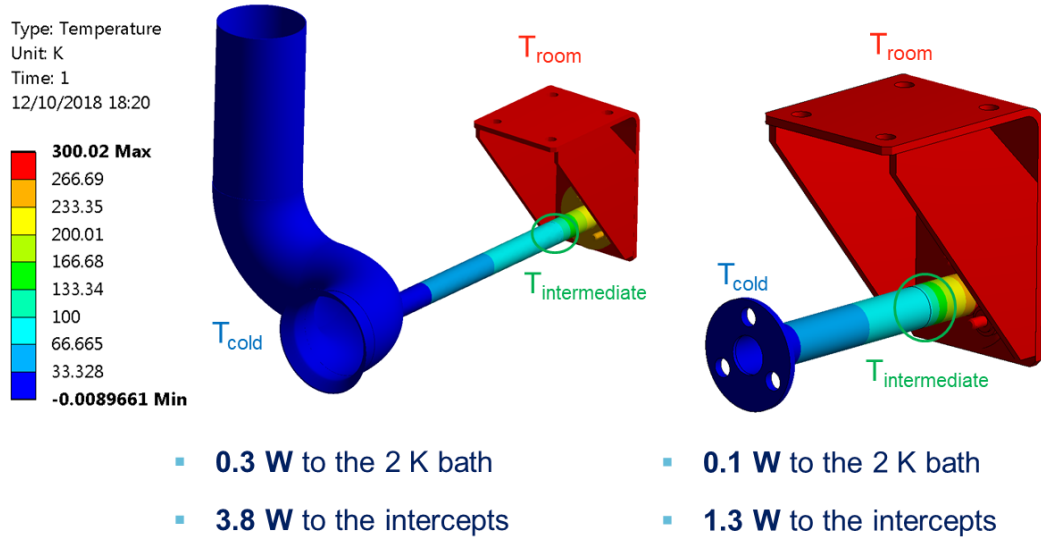
Figure 87. FEA of additional supports for Helium 2-Phase Line showing predicted heat leak to 2K and intermediate temperature (Pleite , 2018)

4.5. Crab Cavity Transportation

The completed cryomodule was carefully transported from the assembly area to the SPS tunnel. A specification of 1G peak maximum allowable acceleration (in addition to gravity) in all directions was set. No acceleration higher than 0.3G was observed. Vibration was monitored in real time and verbal direction provided from the engineering team to the rigging technicians (Figure 88). There was no damage to the cryomodule during any transport or handling operation and no misalignment of the cavities.

Figure 88. Crab Cavity Cryomodule Transportation and Vibration Monitoring

5. Summary, Recommendations and Conclusion

5.1. Thesis Summary

A working support system for the HL-LHC Crab Cavities is imperative for their operation and therefore contributing in part to the overall success of the HL-LHC Project. This thesis has described the work performed to ensure the Cavity Support System design was robust, fit for purpose, cost effective and straight forward to assemble and operate. The adaption of a technique used in a space science application for use in a cryomodule shows the benefits of working across a multidisciplinary organisation such as STFC. The Flexural Blade concept has been shown through both analysis and operation to perform well and the technique will be employed for the series production of cryomodules for use within the LHC. It is hoped that by showing each iteration of the design the thesis shows the level of scrutiny under which the design was placed. Also the work displays what one would consider a 'typical' design cycle, or initiation, concept design, detailed design and implementation.

Throughout the development of the hardware, expertise was gained in vibration analysis which led to significant improvements not only to the support system of the cavity but the Cavity Tuning System. The expertise gained has subsequently been called upon to assist in solving issues in operation of the cavities such as Ponderomotive Instabilities, and it is envisaged this consultation will continue as the project progresses, for example in vibration considerations for international transportation of a cryomodule. In general the measurements available on the installed cavities verifies the values calculated as part of the design process, for example the Finite Element Modal Analyses of the Bare Cavity being in agreement with Modal testing. In some areas discrepancies were found between predictions and reality, offering opportunities for further investigation and recommendations for improvements to the cryomodule. An example of this is higher than anticipated conductive heat transfer to the 2 Kelvin helium circuit, this suggests the thermalisation of the blades (and in fact all of the Cryomodule intercepted components) can be improved. A photograph of the author alongside CERN colleagues and the Cryomodule itself as installed on the SPS is shown in Figure 89. In summary, the design and implementation process was fairly long, over a period of 3 years, however, the result was a significant contribution to the world's first crabbing of a proton beam, which was achieved on 23rd May 2018 (CERN, 2018c).

Figure 89. Crab Cavity Cryomodule team adjacent to module installed on SPS

5.2. Recommendations

Work will continue in this area with the development of the support system for the RFD Pre-Series Cryomodule, which will be assembled at Daresbury Laboratory from October 2020. There are several recommendations from this report which should be investigated further and potentially implemented in the Pre-Series and Series Cryomodules for HL-LHC. These are;

1. That the stiffness of the support system should be as high as reasonably practicable within thermal budget and whilst still minimising thermal contraction induced stresses. This was a recommendation of an external review, and the finding of this thesis. To achieve this the support blades should be positioned as far from the coupler and as far into the corners of the helium vessel as integration allows.

2. It is recommended that modes for the RFD Cavity Support Structure, Dressed Cavity and ancillaries be assessed for the final detailed design, and the

transmissibility matrix applied to predict problematic modes when coupling to ground vibration. This would at a minimum be in the region of 0-100Hz, above this range computation times and hardware utilisation increase significantly, therefore it may beneficial to analyse components individually above 100Hz.

3. The design of the Tuner needs to be assessed to ensure no issues with Ponderomotive instabilities. This may include the inclusion of a set of pre-loaded bearings between the inner and outer actuators to raise the inner actuator fundamental modes above that of the forcing frequency. It is recommended that modal frequencies for the Tuner are assessed from 0-500Hz.

4. If possible a ground vibration survey of the SPS installation site with all services installed and running should be performed to identify the real conditions of the area in order to provide both accurate detuning assessment and to ensure high amplitude ground frequencies can be avoided by mechanical modes.

5. Failing the availability of current SPS installation area data one should consider the use of a background source with a higher integrated RMS displacement value than the relatively quiet data available for the machine. For example the Diamond Light Source data was used for this work and provided a suitable level of background random vibration.

6. All pumps in the area of the Cryomodule should be on suitably designed isolation mounts, and connections to the Cryomodule should be via damped flexible hoses/connections.

7. Thermal intercepts within the Cryomodule in general are not performing as anticipated. It is recommended that the number of fasteners per end of the braids used be increased from one to at least two fasteners per end of each thermal strap.

8. The thermal interface position on the blade supports could be adjusted to provide a more level cool-down of the structure and lower stress within the coupler to negligible levels.

5.3. Conclusion

- A support system design was required for the Superconducting Crab Cavities which are a key component of the High Luminosity Upgrade of the Large Hadron Collider.

- The support system was to be supplementary to a rigid power coupler design which would be the main support for the cavity and be the central point of thermal contraction.

- The support would be fixed from the cavity helium vessel to a common support plate outside of the Outer Vacuum Chamber. This would be used to adjust the power coupler and supplementary support in parallel.

- A novel concept of flexural blade supports was developed by the author which provided rigidity to the system whilst minimising cool-down stresses and heat conducted to the cavity which operates at 2 Kelvin.

- The concept was iterated into a detailed design, having been reviewed by an international panel.

- Vibration issues with the cavity tuner were identified and a solution proposed by the author, which was implemented in the final design.

- The final design was manufactured and assembled into the Double Quarter Wave Crab Cavity Cryomodule which was installed on the Super Proton Synchrotron at CERN.

- The cryomodule was operated successfully, a world first demonstration of the crabbing of a proton beam.

- The cavity support system was shown to work well in operation and will be used in all subsequent crab cavity cryomodule designs.

- A number of recommendations were found by the work of this thesis which have been communicated to the project team, with the aim of implementing them in future iterations of the design.

Appendix A – Ground Vibration Transmission Calculator

First 10 Mechanical Vibration Modes (ω_n) found using FEA

Calculate ratio of ω/ω_n for each mode (ω_n) to find transmissibility at all driving frequencies (ω) from 1 to 100Hz, in steps of 0.02Hz (Bin size). ξ taken as 0.001.

$$Transmissibility = \frac{Y}{X} = \sqrt{\frac{4\xi^2(\omega/\omega_n)^2+1}{[1-(\omega/\omega_n)^2]^2+4\xi^2(\omega/\omega_n)^2}}$$

Multiply ground displacement (X) at frequency by transmissibility to obtain modal displacement (Y) at specific frequency

$$X \times Transmissibility = Y$$

Ground displacement data. Frequency in steps of 0.02Hz Bin size with associated ground displacement in nm (X)

Use Root Sum of the Squares (RSS) method to combine displacements of all frequencies and obtain peak displacement of each mode.

From modal shape identify ratio of total mode displacement to level of displacement of the central tuning plates. Use ratio to estimate tuning plate deformation under ground conditions and therefore RF detuning (from RF sensitivity study)

$x(t) = X\sin(\omega t)$

Stiffness

Damping

$Y = X \times Z$

Figure 90. Ground Vibration Transmission Calculation Flow Chart

RSS for all displacements from 1Hz to 100Hz

RSS 1 to 100Hz (nm)	20.2	173.1	160.5	30.9	25.9	23.9	23.1	22.0	20.5	20.5	20.4	
Frequency [Hz]	DLS Ground (nm)	Mode 1 (nm)	Mode 2 (nm)	Mode 3 (nm)	Mode 4 (nm)	Mode 5 (nm)	Mode 6 (nm)	Mode 7 (nm)	Mode 8 (nm)	Mode 9 (nm)	Mode 10 (nm)	<- Displacement
1.00E+00	1.955581755	1.96E+00	1.96E+00	1.96E+00	1.96E+00	1.96E+00	1.96E+00	1.96E+00	1.96E+00	1.96E+00	1.96E+00	
1.02E+00	1.915358974	1.92E+00	1.92E+00	1.92E+00	1.92E+00	1.92E+00	1.92E+00	1.92E+00	1.92E+00	1.92E+00	1.92E+00	
1.03E+00	1.861518198	1.86E+00	1.86E+00	1.86E+00	1.86E+00	1.86E+00	1.86E+00	1.86E+00	1.86E+00	1.86E+00	1.86E+00	
1.05E+00	1.776597872	1.78E+00	1.78E+00	1.78E+00	1.78E+00	1.78E+00	1.78E+00	1.78E+00	1.78E+00	1.78E+00	1.78E+00	
1.07E+00	1.782946999	1.79E+00	1.79E+00	1.78E+00	1.78E+00	1.78E+00	1.78E+00	1.78E+00	1.78E+00	1.78E+00	1.78E+00	
1.08E+00	1.767172883	1.77E+00	1.77E+00	1.77E+00	1.77E+00	1.77E+00	1.77E+00	1.77E+00	1.77E+00	1.77E+00	1.77E+00	
1.10E+00	1.719273102	1.72E+00	1.72E+00	1.72E+00	1.72E+00	1.72E+00	1.72E+00	1.72E+00	1.72E+00	1.72E+00	1.72E+00	
1.12E+00	1.699529347	1.70E+00	1.70E+00	1.70E+00	1.70E+00	1.70E+00	1.70E+00	1.70E+00	1.70E+00	1.70E+00	1.70E+00	
1.13E+00	1.687409257	1.69E+00	1.69E+00	1.69E+00	1.69E+00	1.69E+00	1.69E+00	1.69E+00	1.69E+00	1.69E+00	1.69E+00	
1.15E+00	1.711972547	1.72E+00	1.72E+00	1.71E+00	1.71E+00	1.71E+00	1.71E+00	1.71E+00	1.71E+00	1.71E+00	1.71E+00	
1.17E+00	1.711695066	1.72E+00	1.71E+00	1.71E+00	1.71E+00	1.71E+00	1.71E+00	1.71E+00	1.71E+00	1.71E+00	1.71E+00	
1.18E+00	1.719273102	1.72E+00	1.72E+00	1.72E+00	1.72E+00	1.72E+00	1.72E+00	1.72E+00	1.72E+00	1.72E+00	1.72E+00	
1.20E+00	1.738591384	1.74E+00	1.74E+00	1.74E+00	1.74E+00	1.74E+00	1.74E+00	1.74E+00	1.74E+00	1.74E+00	1.74E+00	
1.22E+00	1.721365737	1.73E+00	1.72E+00	1.72E+00	1.72E+00	1.72E+00	1.72E+00	1.72E+00	1.72E+00	1.72E+00	1.72E+00	
1.23E+00	1.689881653	1.69E+00	1.69E+00	1.69E+00	1.69E+00	1.69E+00	1.69E+00	1.69E+00	1.69E+00	1.69E+00	1.69E+00	
1.25E+00	1.657452865	1.66E+00	1.66E+00	1.66E+00	1.66E+00	1.66E+00	1.66E+00	1.66E+00	1.66E+00	1.66E+00	1.66E+00	
1.27E+00	1.66	1.66E+00	1.66E+00	1.66E+00	1.66E+00	1.66E+00	1.66E+00	1.66E+00	1.66E+00	1.66E+00	1.66E+00	
1.28E+00	1.689881653	1.69E+00	1.69E+00	1.69E+00	1.69E+00	1.69E+00	1.69E+00	1.69E+00	1.69E+00	1.69E+00	1.69E+00	
1.30E+00	1.731372288	1.74E+00	1.74E+00	1.73E+00	1.73E+00	1.73E+00	1.73E+00	1.73E+00	1.73E+00	1.73E+00	1.73E+00	
1.32E+00	1.794547297	1.80E+00	1.80E+00	1.80E+00	1.80E+00	1.79E+00	1.79E+00	1.79E+00	1.79E+00	1.79E+00	1.79E+00	
1.33E+00	1.820700415	1.83E+00	1.83E+00	1.82E+00	1.82E+00	1.82E+00	1.82E+00	1.82E+00	1.82E+00	1.82E+00	1.82E+00	
1.35E+00	1.818405895	1.82E+00	1.82E+00	1.82E+00	1.82E+00	1.82E+00	1.82E+00	1.82E+00	1.82E+00	1.82E+00	1.82E+00	
1.37E+00	1.824362902	1.83E+00	1.83E+00	1.83E+00	1.83E+00	1.82E+00	1.82E+00	1.82E+00	1.83E+00	1.83E+00	1.82E+00	
1.38E+00	1.834407261	1.84E+00	1.84E+00	1.84E+00	1.84E+00	1.83E+00	1.83E+00	1.83E+00	1.83E+00	1.83E+00	1.83E+00	
1.40E+00	1.845751879	1.85E+00	1.85E+00	1.85E+00	1.85E+00	1.85E+00	1.85E+00	1.85E+00	1.85E+00	1.85E+00	1.85E+00	
1.42E+00	1.842471167	1.85E+00	1.85E+00	1.84E+00	1.84E+00	1.84E+00	1.84E+00	1.84E+00	1.84E+00	1.84E+00	1.84E+00	
1.43E+00	1.820700415	1.83E+00	1.83E+00	1.82E+00	1.82E+00	1.82E+00	1.82E+00	1.82E+00	1.82E+00	1.82E+00	1.81E+00	
1.45E+00	1.809198718	1.82E+00	1.81E+00	1.81E+00	1.81E+00	1.81E+00	1.81E+00	1.81E+00	1.81E+00	1.81E+00	1.81E+00	
1.47E+00	1.799166474	1.81E+00	1.80E+00	1.80E+00	1.80E+00	1.80E+00	1.80E+00	1.80E+00	1.80E+00	1.80E+00	1.80E+00	
1.48E+00	1.790642343	1.80E+00	1.80E+00	1.79E+00	1.79E+00	1.79E+00	1.79E+00	1.79E+00	1.79E+00	1.79E+00	1.79E+00	
1.50E+00	1.790642343	1.80E+00	1.80E+00	1.79E+00	1.79E+00	1.79E+00	1.79E+00	1.79E+00	1.79E+00	1.79E+00	1.79E+00	

Modal Frequencies (Hz) and Damping Co-efficient

Damping co-efficient =	0.001
Mode 1 =	25.523
Mode 2 =	26.767
Mode 3 =	56.127
Mode 4 =	67.059
Mode 5 =	83.533
Mode 6 =	86.121
Mode 7 =	88.409
Mode 8 =	102.11
Mode 9 =	102.91
Mode 10 =	107.59

Frequency increasing in steps of 0.02Hz to 100Hz

Ground displacement at Frequency

Modal displacement at Frequency

Figure 91. Annotated extract from Ground Vibration Calculation Spreadsheet showing 1 to 1.5Hz. The rows extend to 100Hz in the full spreadsheet.

References

Arkan, T. (2018). LCLS-II CRYOMODULES PRODUCTION AT FERMILAB. *IPAC2018 - WEPMK010* (pp. 2652 - 2655). Vancouver: Jacow.

Artoos, K. (2015a). Development of SRF Cavity Tuners For CERN. *SRF2015 - THPB060*, (p. 1247 to 1251). Whistler.

Artoos, K. (2015b, November). Crab Cavity Cryomodule review - Tuner. Geneva, Switzerland: EDMS, CERN.

Artoos, K. (2019). Status of the HL-LHC Crab Cavity Tuner. *SRF2019 - TUP081* (pp. 648 - 653). Dresden: JACoW.

Ballarino, A. (2014). Development of superconducting links. *Supercond.Sci.Technol. 27 (2014) 044024*, 1-7.

Barron, R. F. (1985). *Cryogenic Systems Second Edition.* Oxford University Press.

Baudrenghien, P. (2013). *Functional Specifications of the LHC Prototype Crab Cavity System.* Geneva: CERN.

Berry, S. N. (2016). ASSEMBLY OF XFEL CRYOMODULES: LESSONS AND RESULTS. *LINAC2016 - WE1A02* (pp. 646 - 650). East Lansing: JACoW.

Brett, D. (2014). Accurate crab cavity modeling for the high luminosity Large Hadron Collider. *PHYSICAL REVIEW ACCELERATORS AND BEAMS 17*, Article 104001.

Buhler, S. (93). ACTIVITIES ON CRYOSTATS AND SRF CAVITIES AT THE IPN ORSAY LABORATORY. *SRF93I42* (pp. 1002 - 1013). Newport News: JACoW.

Burt, G. (2019). *RF Linear accelerators Lecture 3: Coupling to Standing Wave Cavities.* Retrieved from sas.stfc.ac.uk: https://sas.stfc.ac.uk/vportal/fileUploads/prod/A-89f6891a-4670-455f-b36d-43eb095c3839-b81ab137-4d71-45d6-b956-0310df8978c1_lecture3coupling.pdf

Calaga, R. (2018, October 16). Crab Cavities - SPS MDs, Design Advancement, Plan for Production. *Presentation for 8th HL-LHC Collaboration Meeting.* Geneva, Switzerland.

Capatina, O. (2014, October 1). *Crab cavities design choices & interfaces overview.* Retrieved May 29, 2017, from indico.cern.ch: https://indico.cern.ch/event/334041/contributions/1721995/attachments/651947/896432/Cavity_interfaces.pdf

Carra, F. (2015). Crab Cavity and Cryomodule Development for HL-LHC. *SRF 2015.* Whistler: SRF 2015.

Carra, F. (2017). Assessment of thermal loads in the CERN SPS crab cavities cryomodule. *IOP Conf. Series: Journal of Physics: Conf. Series 874 (2017) 012005* (pp. 1 - 7). Copenhagen: IOP Publishing.

CERN. (2008, October 16). *CERN Releases Analysis of LHC Incident.* Retrieved May 28, 2017, from press.cern: https://press.cern/press-releases/2008/10/cern-releases-analysis-lhc-incident

CERN. (2010). *LHC P Collisions - Taking a closer look at LHC.* Retrieved May 28, 2017, from LHC-Closer: https://www.lhc-closer.es/taking_a_closer_look_at_lhc/0.lhc_p_collisions

CERN. (2015). EDMS - 1578808. *Measurements Procedure For SPS Crab-Cavities Cryomodule Prototype.* Geneva.

CERN. (2016a). *CERN Annual Report 2015.* Geneva: CERN Education, Communicatins and Outreach Group.

CERN. (2016b). *The HL-LHC Project.* Retrieved May 29, 2017, from hilumilhc.web.cern.ch: http://hilumilhc.web.cern.ch/

CERN. (2017a). *https://home.cern/about.* Retrieved May 25, 2017a

CERN. (2017b). *Budget Overview.* Retrieved May 28, 2017b, from press.cern: https://press.cern/facts-and-figures/budget-overview

CERN. (2017c). *Member States Contributions.* Retrieved May 28, 2017c, from fap-dep.web.cern: https://fap-dep.web.cern.ch/rpc/member-states-contributions

CERN. (2017d). *Facts and Figures.* Retrieved May 28, 2017d, from press.cern: https://press.cern/backgrounders/facts-figures

CERN. (2017e). *Processing: What to Record?* Retrieved May 28, 2017e, from home.cern: https://home.cern/about/computing/processing-what-record

CERN. (2018a). EDMS - 1389669. *Engineering Specification - Dressed Bulk Niobium Radio-Frequency Crab Cavities.*

CERN. (2018b). EDMS - 2043014. *Engineering Specification - Cryomodules for Crab Cavities.* Geneva.

CERN. (2018c, May 29). *World's first crabbing of a proton beam*. Retrieved from home.cern: https://home.cern/news/news/engineering/worlds-first-crabbing-proton-beam

Chao, A. W. (1999). *Handbook of Accelerator Physics and Engineering.* Stanford, California: World Scientific Publishing Co. Pte. Ltd.

Coupard, J. (2016). LHC INJECTORS UPGRADE (LIU) PROJECT AT CERN. *IPAC2016 - MOPOY059.* Busan, Korea.

Cryogenic Society of America. (2018, March 6th). *Liquefied Natural Gas (LNG).* Retrieved from cryogenicsociety.org:
https://cryogenicsociety.org/resources/defining_cryogenics/liquefied_natural_gas_lng/

Davis, K. (2012). Vibration response testing of the CEBAF 12GeV upgrade Cryomodules. *LINAC 2012 - MOPB031.* Tel-Aviv, Israel.

Davis, K. (2012). Vibration Response Testing of the CEBAF 12GeV Upgrade Cryomodules . *LINAC 2012.* Tel-Aviv: LINAC 2012.

Delayen, J. R. (2005). Ponderomotive Instabilities And Microphonics. *SRF2005 - SUP01*, (p. 35 to 39). Ithaca.

Department for Transport. (2002). CODE OF RACTICE: . *Safet of Loads on Vehicles, Third Edition.* London, United Kingdom: Crown Copyright.

Doolittle, L. (1989). Tuners, Microphonics, and Control Systems in Superconducting Accelerating Structures . *SRF89E01* (pp. 341 - 350). Tsukuba: JACoW.

Edwards, D. A. (1995). *TESLA Test Facility Linac Design Report.* Hamburg: DESY.

FERMILAB. (2013, May 01). Material Properties for engineering analyses of SRF Cavities. *Fermilab Specification ED0371110 Issue A*. Batavia, Illinois, USA.

Galayda, J. N. (2018). The LCLS-II: A HIGH POWER UPGRADE TO THE LCLS. *IPAC2018 - MOYGB2* (pp. 18 - 23). Vancouver: JACoW.

Huang, H. (2006). Vibration Measurement at Diamond and the Storage Ring. *THPLS027.* Edinburgh.

Huque, N. (2019). Improvements to LCLS-II Cryomodule Transportation. *SRF2019 - TUP094* (pp. 686-691). Dresden: JACoW.

Jones, R. (2015). *Beam Instrumentation and Diagnostics for HL-LHC.* Retrieved May 29, 2017, from acelconf.web.cern: http://accelconf.web.cern.ch/AccelConf/IPAC2015/talks/tuac1_talk.pdf

Jones, T. (2013). *RFS-1017-FEA-002-V3-Interface plate thermal analysis.* STFC.

Jones, T. (2015, November). *tdl-1165-meng-prs-0024-Crab Cavity support system*. Geneva, Switzerland: CERN.

Jones, T. (2017). Determining BCP Etch Rate and Uniformity In High Luminosity LHC Crab Cavities. *SRF2017 - TUPB100* (pp. 635 - 639). Lanzhou: JACoW.

Krzewicki, M. (2014, October 23). *HL-LHC Computing*. Retrieved May 29, 2017, from indico.cern.ch: https://indico.cern.ch/event/315626/contributions/729452/attachments/605642/833484/ECFA-HLLHC-Aix-Les-Bains-Computing-Krzewicki.pdf

Lacny, L. (2017). *Experimental modal analysis of CRAB Cavity cell.* Geneva: CERN - EDMS.

Medjidzade, V. (2005). DESIGN OF THE CW CORNELL ERL INJECTOR CRYOMODULE. *PAC2005* (pp. 4290 - 4292). Knoxville: JACoW.

Mitsunobu, S. (1989). Cryostat For TRISTAN Superconducting Cavity. *SRF89G29* (pp. 805 - 819). Tsukuba: JACoW.

Müller-BBM GmbH. (2019). *Brochures.* Retrieved from www.pakbymbbm.com: https://www.pakbymbbm.com/brochures/

Müller-BBM GmbH. (2019). *PAK Software.* Retrieved from www.pakbymbbm.com: https://www.pakbymbbm.com/home/data-acquisition-products/pak-software/

National Electrostatics Corp. (2019, March). *Vibration Isolator Model VI-1.* Retrieved from Pelletron.com: https://www.pelletron.com/wp-content/uploads/2017/02/VIB-ISO-I-v2.pdf

Parma, V. B. (2013). Status of the Superconducting Proton Linac (SPL) Cryomodule. *SRF2013.*

PCB Piezotronics. (2019). *MODEL: 086D05.* Retrieved from www.pcb.com: https://www.pcb.com/products?model=086D05

Peckner, D. (1977). *Handbook of Stainless Steels.* New York, NY: McGraw-Hill Book Company.

Petersen, B. (2008). Industrialization of Superconducting Accelerator Module Production. *EPAC08 - WEIM03*, (pp. 1964-1966). Genoa.

Peterson, T. J. (2000). *TESLA & ILC Cryomodules.* Batavia: FERMILAB Research Alliance.

Pleite , E. C. (2018, October 16). Thermal studies & measurements for SPS-DQW. *Presentation - 8th HL-LHC Collaboration Meeting*. Geneva, Switzerland.

Popielarski, L. (2013). Testing Of Copper Plating Quality On Rea3 Coupler Bellows And Approach To Improved Plating For FRIB Production. *SRF 2013.* Paris: SRF 2013.

Postek M. T., K. W. (1991). Cryopump Vibration Isolation System for an SEM. *SCANNING Vol.13*, 404-409.

Powers, T. (2017). Control of Microphonics for Narrow Control Bandwidth Cavities. *FRXBA04*, (p. Invited Talk). Lanzhou.

Raynova, I. (2017, March 29). *First tests of crab cavities promise a luminous future*. Retrieved May 29, 2017, from home.cern: https://home.cern/cern-people/updates/2017/03/first-tests-crab-cavities-promise-luminous-future

Sharma, S. (2005, July). *Design of Accelerator Girder System for Vibration Suppression.* Retrieved from www.yumpu.com: https://www.yumpu.com/en/document/view/7944587/design-of-accelerator-girder-system-for-vibration-suppression

Sitko, M. A.-T. (2018). Towards the Implementation of Laser Engineered Surface Structures for Electron Cloud Mitigation. *IPAC 2018 - TUZGBE3.* Vancouver: CC-BY-3.0.

Sosin, M. (2016). Position Monitoring System For HL-LHC Crab Cavities. *IPAC2016 - WEPOR018* (p. 2704 to 2706). Busan: CC-BY-3.0.

Vallgren, C. Y. (2011). Amorphous Carbon Coatings for the Mitigation of Electron Cloud in the CERN SPS. *Review of Modern Physics 14*, 2033-2035.

Verdú-Andrés, S. (2013). Optimization of the Double Quarter Wave Crab Cavity. *Proceedings of SRF2013.* Paris.

Verdu-Andres, S. (2015). DESIGN AND PROTOTYPING OF HL-LHC DOUBLE QUARTER WAVE. *MOBD2.* Richmond, VA, USA.

Verdú-Andrés, S. (2015). Lorentz Detuning For A Double-Quarter Wave Cavity. *SRF2015 - THPB051* (pp. 1215 - 1218). Whistler: CC-BY-3.0.

Vibrant. (2019). *Visual Engineering*. Retrieved from /www.vibetech.com: https://www.vibetech.com/solutions/visual/

Willering, B. B. (2019). Nb3Sn 11 T Dipole for the High Luminosity LHC (CERN). *Nb3Sn Accelerator Magnets*, 223-258.

Xiao, B. P. (2013). Design and Vertical Test of Double Quarter Wave Crab Cavity for LHC Luminosity Upgrade. *Proceedings of SRF2013.* Paris.

Yamakawa, E. (2019). *HL-LHC UK Participation Project - Deliverable report D2.11.*

Ziemiański, D. (2014). *EDMS no.: 1391859. Ground Motion Measurements in the LSS4 cavern – CRAB cavity project.* Geneva: CERN.

Ziemianski, D. (2014). *Ground Motion Measurements in the LSS4 cavern – CRAB cavity project.* CERN.